Hedgehog Signaling in Joubert syndrome

Arianna Ericka Gómez

A dissertation
submitted in partial fulfillment of the
requirements for the degree of

Doctor of Philosophy

University of Washington
2022

Reading Committee:
Daniel Doherty, Chair
Mark Majesky
Kathleen Millen

Program Authorized to Offer Degree:
Laboratory Medicine and Pathology

University of Washington

Abstract

Hedgehog Signaling in Joubert syndrome

Arianna Ericka Gómez

Chair of the Supervisory Committee:
Daniel Doherty
Department of Pediatrics

Joubert syndrome (JS) is a mostly recessive, neurodevelopmental condition diagnosed by the molar tooth sign (MTS) on axial brain imaging. Currently, >40 genes are associated with JS, all of which encode proteins that function in and around the primary cilium, a microtubule-based signaling organelle. The association of >40 cilium-related JS genes with the JS-specific brain malformation suggests a unifying cilium-related disease mechanism across genetic causes; however, the mechanistic details remain unknown. Aberrant Hedgehog (Hh) signaling has been implicated in model systems representing more than half of the JS genes, but specific alterations in the Hh signaling cascade have not been characterized across genetic causes of JS in a single model system. To determine whether a consistent disruption in Hh signaling underlies JS, we evaluated Hh signaling using standard assays for two key steps in a single model system. Using the CRISPR-Cas9 system in hTERT RPE-1 cells, I engineered biallelic frameshift variants in 9 representative JS-associated genes encoding ciliary proteins that localize to each of the major sub-compartments of the cilium: tip, cilium-

proper, transition zone, and basal body. Transition zone mutants displayed fewer cilia, and multiple mutants exhibited abnormal cilium length; however, these defects were not uniformly present across mutants. Similarly, relocalization of the key Hh pathway component SMO in response to pathway stimulation was blunted in several mutants across compartments, most severely in the one transition zone mutant that made enough cilia to be tested. Finally, induction of the Hh target gene *GLI1* was blunted in cilium-proper and transition zone mutants, but not in tip and basal body mutants. My work indicates that blunted Hh signaling is a key mechanistic feature associated with JS gene dysfunction, potentially identifying a target for pharmacologic treatments. Future work will focus on determining whether JS gene dysfunction impacts the dynamic range, timing, and other aspects of Hh signal transduction, or if we need to look beyond Hh to identify a unifying mechanism underlying JS.

Dedication

*To my parents, Rosa and Francisco Gómez***.**

To my community. Lo hicimos.

Acknowledgements

I want to thank everyone who was part of this journey. This work was the result of many people coming together to guide and support me through this endeavor.

I want to thank my thesis advisor, Dr. Dan Doherty, and our lab postdoc, Dr. Julie Van De Weghe, for their mentorship throughout the years. Our discussions made a significant impact on my scientific work and career development. I also want to thank my committee members, Dr. Kathleen Millen, Dr. Mark Majesky, Dr. John Neumaier, and Dr. Hannah Tully, for our wonderful discussions and for providing input as my projects progressed.

A special thanks to everyone in the Doherty lab and our former lab neighbors, the Mefford lab. Thank you, Dr. Heather Mefford, for always providing feedback on my talks and projects (and for letting me bother Edith between experiments!). To all of the past and present members of both labs, you made the RR wing a great place to work! I am lucky to call many of you my friends. Thank you for the input and support, big or small, that you provided throughout the years. I could not have gotten through my projects without the help of all the research scientists who were part of the lab throughout the years: Ian, Megan, Caitlin, Hailey, and Angela. Thank you, Jen, for your kindness throughout the years.

To my UW/Seattle friends and mentors, thank you for always being there and for having my back on this journey. There were many people who I could rely on for advice when this journey got tough: Dr. Carolyn Jackson, Anthony Salazar, Dr. Bill Mahoney, Steve Berard, Megan Barker, Dr. TK Francis, Dr. Todd Sperry, Dr. Amanda Bradley, Lauren Bedson, Erin Kirshner, Maia Low, and Kyle Shea. You all taught me invaluable

lessons that helped shape who I have become. Thanks to all of the SACNAS and GO-MAP/GSEE friends I made throughout the years. You all taught me how to bring my culture and science together! When I wasn't in the lab or on campus, I was with my volleyball friends who helped me forget about the stress of grad school and who have been part of some great memories in Seattle! A HUGE shoutout to my GO-MAP writing group: Dr. Natalie Gasca, Dr. Juandalyn Burke, Dr. Elizabeth Ramirez Arreola, and Dr. Antonio Olivas-Martinez. We spent long days and nights together working to achieve our dreams. From our lengthy discussions to our nights out celebrating each other's wins, I am so glad to call you my friends and family.

Finally, to my family. You have been there with me from the beginning. You taught me to be an independent, intelligent person who will not be pushed around. You taught me to be proud of my culture and where I came from, reminding me that our community would always be there to catch me if I fall. My endless gratitude to my parents, who were my biggest supporters. While my dad isn't here to see me finish, this work is dedicated to my mom and dad. Tu hija lo hizo. Ella es Doctora!

Table of Contents

List of Figures

List of Tables

Chapter 1: Introduction

Authors: Arianna Gómez[1], Dan Doherty[1]
[1]Department of Pediatrics, University of Washington

Overview

Our ability to identify the genetic causes of rare diseases, such as Joubert syndrome (JS), has quickened with improved sequencing technologies and bioinformatics approaches. With the identification of over 40 JS-associated genes, we are now tasked with understanding the cellular biology underlying the condition. By understanding what cellular characteristics are perturbed in individuals with JS, we can improve healthcare guidance and identify potential therapeutic targets. Currently, several mechanisms are proposed to underly JS, but few studies have looked across multiple causes of JS, in the same system, and with the same assays. Thus, there remains the need to understand the mechanism underlying Joubert syndrome across genetic causes of the condition.

My thesis focuses on determining whether Hedgehog signaling (Hh) is perturbed across genetic causes of JS. Chapter 1 will describe JS, its relationship to other conditions involving the primary cilium, and why Hedgehog signaling is a potential mechanism underlying JS. Chapter 2 will describe how we selected a cellular model system to study Hedgehog signaling in JS. Chapter 3 will focus on our study looking at mutants of 9 JS-associated gene mutants and their ciliary characteristics and response to Hh signaling. Chapter 4 will discuss assay validation and modification. Chapter 5 will include future directions and how this work contributes to our understanding of JS.

Joubert syndrome and genetic causes

Joubert syndrome is a primarily recessive neurodevelopmental condition defined by a distinctive brain imaging finding called the Molar Tooth Sign (MTS, Figure 1.1).[1] Abnormal mid-brain/hindbrain development, including cerebellar vermis aplasia/hypoplasia, thick superior cerebellar peduncles, and a deep interpeduncular fossa result in appearance of the molar tooth sign.[2–5] All individuals with JS have developmental delays and low muscle tone/ataxia. Variable features include abnormal eye movements, breathing abnormalities, coloboma, polydactyly, encephalocele, and progressive features including retinal dystrophy, kidney, and liver involvement. Some of these variable features can be monitored in patients, but the debilitating progressive phenotypes and learning disabilities can result in lifelong difficulties for individuals with JS and their families.

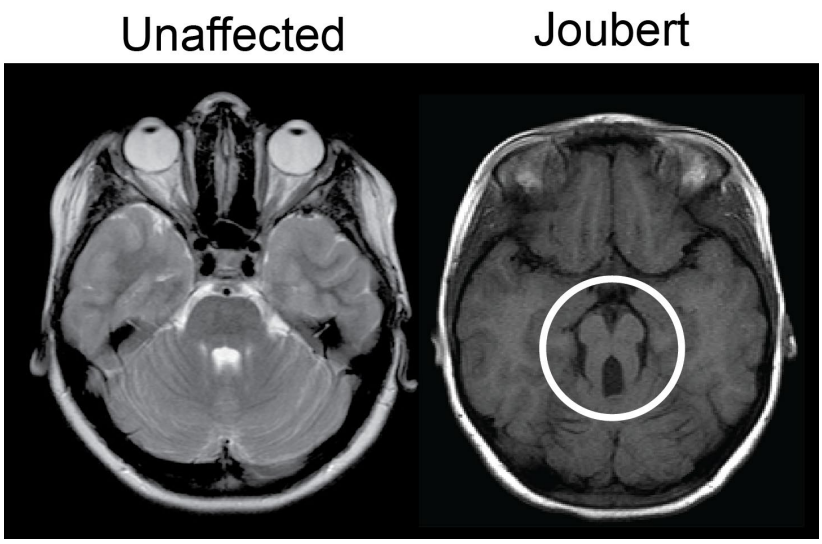

Figure 1.1. The molar tooth sign. Axial magnetic resonance imaging of an unaffected individual (left) and an individual with Joubert syndrome (right), showing the molar tooth sign, circled in white.

Joubert syndrome was first described in 1969 by Marie Joubert and colleagues.[6] In 2004, *AHI1* was published as the first JS-associated gene.[7] Currently, over 40 JS-associated genes have been identified, accounting for the genetic diagnosis of ~70-90% of individuals with JS depending on the cohort (Figure 1.2).[8–11] Five of these genes, *AHI1*, *CC2D2A*, *CEP290*, *CPLANE1*, and *TMEM67*, account for a large proportion of genetic diagnoses in the University of Washington JS cohort.[11] Most JS genetic diagnoses are biallelic variants carried in one of the JS-associated genes. However, in 2021, the first dominant form of JS was identified in the Suppressor of fused homolog (*SUFU*) gene, which causes mild JS.[12] With a proportion of diagnoses still unsolved, the list of JS-associated genes will continue to expand and include other inheritance modes. Our ability to identify genetic causes of JS has improved, while our understanding of the biology of JS at the cellular and organismal level lags.

The primary cilium and ciliopathies

All JS-associated protein products localize in and around the primary cilium (Figure 1.2). The primary cilium is an immotile, nearly ubiquitous microtubule-based organelle that acts as a cellular antenna, transducing light, mechanical, and chemical signals into cells and mediating multiple signaling pathways, including Hedgehog (Hh) signaling.[11,13–16] The primary cilium has several major sub-domains: the basal body (BB)

is a modified centriole that anchors the cilium to the cytoskeleton. The transition zone (TZ) is immediately distal to the basal body, linking the cilium to the plasma membrane and regulating protein traffic in and out of the cilium.[17–21] Membrane receptors decorate the cilium proper (CP). The ciliary tip (TIP) is a specialized compartment involved in ciliary length control, ciliary vesicle release, and the transition from incoming to outgoing ciliary protein transport.[22–25]

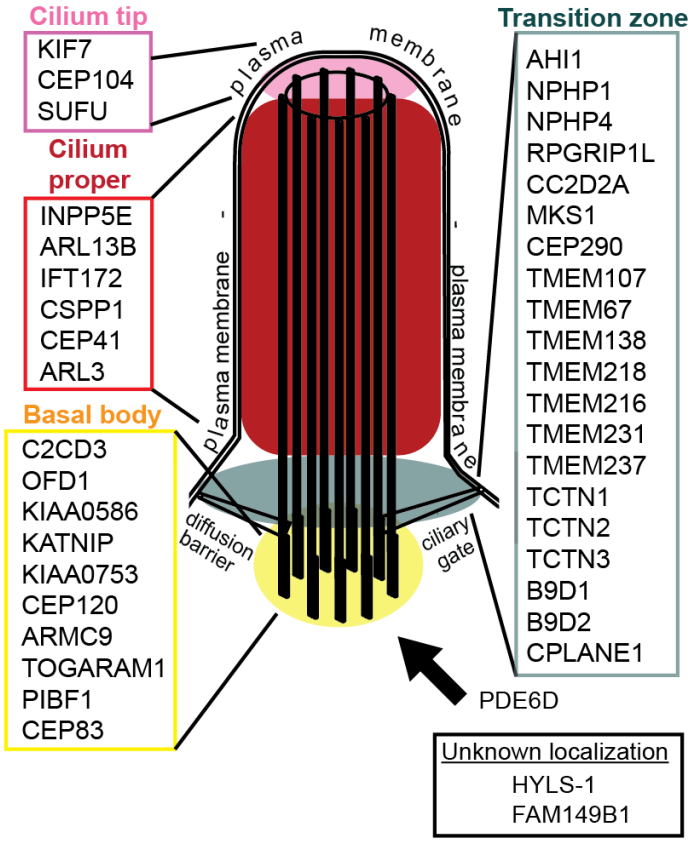

Figure 1.2. The primary cilium and JS-associated genes. A schematic of the primary cilium with ciliary sub-compartments labeled. Most proteins localize to the transition zone (teal), while the remaining proteins localize to the basal body (yellow), cilium proper (red), and cilium tip (pink).

Most vertebrate cell types have a single primary cilium protruding from the cellular surface, sharing a membrane with the cell. Primary cilia lack ribosomes and proteins diffuse into cilia or use the intraflagellar transport (IFT) system as a shuttle system for proteins. IFT trains carry cargo towards the ciliary tip (IFT-B) and back to the base of cilia (IFT-A). Proper function of IFT is required for cilium assembly and transport of ciliary localizing proteins. Loss of function in IFT and other cilia-associating proteins

can affect ciliary length, but the mechanism for cilium length control remains unclear. Work in IFT mutants, *wim* and *fxo*, identified abnormal neural tube development in murine embryos, a characteristic feature of abnormal Hh signaling.[15] This was early evidence that primary cilia play a role in Hh signaling.

Phosphoinositide (PI) composition distinguishes the ciliary membrane from the cellular membrane and controls the localization and activity of cilia-specific proteins. INPP5E, a JS-associated protein, is a phosphatase that regulates ciliary PI composition, hydrolyzing PI(4,5)P_2 and PI(3,4,5)P_3.[26] PI(4)P localizes to the ciliary axoneme, while PI(4,5)P_2 localizes to the transition zone and proximal ciliary axoneme.[27,28] INPP5E loss of function models result in higher PI(4,5)P_2 within cilia and retention of negative regulators in the Hedgehog signaling pathway.[27,28] INPP5E localizes to primary cilia in non-dividing cells, and relocalizes to the centrosome and kinetochore during mitosis.[29]

JS belongs to a group of genetic conditions arising from defects in ciliary function, called ciliopathies. Some JS phenotypes overlap with other ciliopathies, i.e. Nephronophthisis (NPH, kidney involvement), Meckel syndrome (MKS, cystic kidneys, polydactyly, occipital encephalocele, and liver fibrosis), and Bardet-Biedl syndrome (intellectual disability, retinal dystrophy, and polydactyly).[30] Along with phenotypic overlap, JS shares genetic overlap with ciliopathies, including MKS (17 genes) and NPH (2 genes). While there is phenotypic overlap between ciliopathies, JS is the only ciliopathy with the specific MTS brain malformation.

With more than 40 JS-associated genes, a shared cellular etiology has not been identified across genetic causes of JS. Data from models (animal and cellular) and patient-derived cells for JS-associated genes exhibit variable defects in cilium number, cilium morphology, multiple signaling pathways, cytoskeleton structure, autophagy, and DNA damage response, but the relevance of these defects across genetic causes of JS and disease process has not been determined.[31–38] Previous studies have identified Hh signaling abnormalities, but Hh pathway dysfunction has not been systematically evaluated across multiple genetic causes of JS in human cells or across pathway signaling steps, which is the focus of my thesis project.

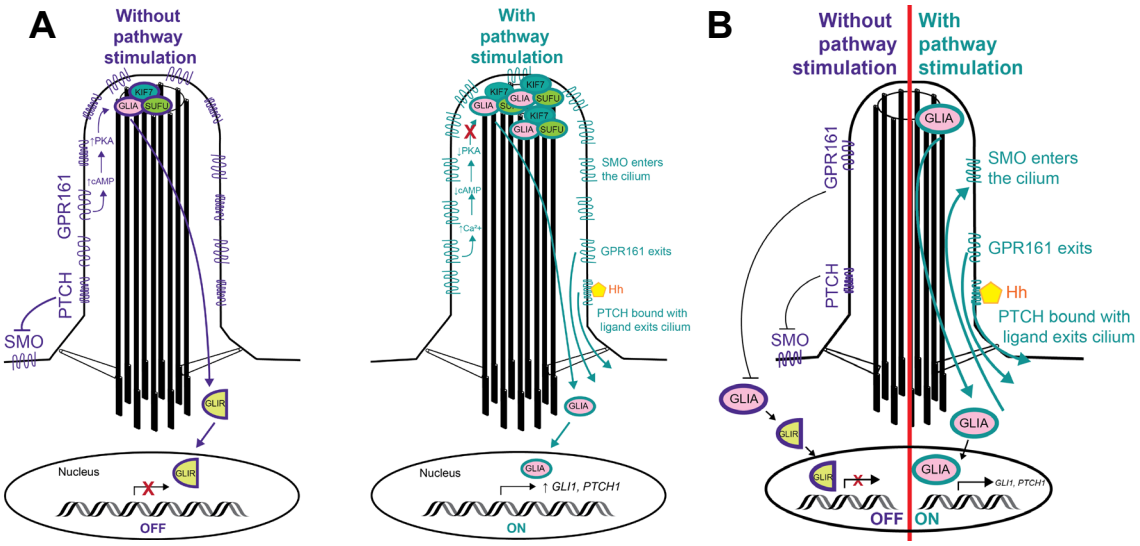

Figure 1.3. Hedgehog signaling in the primary cilium. (A) Schematic of Hh signaling showing a detailed pathway response with and without stimulation. Localization of key pathway proteins (SMO, PTCH, GPR161, GLI2/3, SUFU, KIF7) and downstream target gene induction (*GLI1, PTHC1).* (B) Simplified schematic of Hh signaling with and without pathway stimulation. Here, we are highlighting key pathway steps that are commonly measured in the literature.

Hedgehog signaling and JS-associated gene models

In vertebrates, the primary cilium plays an obligate role in canonical Hh signaling through the coordinated movement of receptors and effectors into and out of the organelle (reviewed in [39]). In the absence of Hedgehog (Hh) ligand, the pathway receptor Patched (PTCH) localizes to the primary cilium, impeding Smoothened (SMO) localization by limiting accessible cholesterol at the ciliary membrane (Figure 1.3).[40] Without stimulation, GPR161, an orphan G protein-coupled receptor and negative regulator of the pathway, helps maintain transcription factors GLI2/3 in their proteolytically cleaved repressor forms. GLI2 acts as an activator of the pathway, while GLI3 is a repressor of the pathway, with the function of both transcription factors being necessary for proper signaling and development processes.[41,42] TULP3 shuttles GPR161 into the cilium by binding to the IFT-A complex and bridging the IFT complex with the cellular membrane, enabling proteins like GPR161 to localize to the cilium.[43] The presence of GPR161 in cilia increases ciliary cAMP, maintaining PKA-mediated proteolytic cleavage of GLI3.[44] GLI2/3 complex at the ciliary tip with SUFU and KIF7, two JS-associated proteins. SUFU acts to stabilize GLI2/3 full length activators[45] and

KIF7 binds to the plus ends of microtubules, helping to maintain the ciliary tip environment.[24]

Protein localization	
SMO localization	23
GPR161 localization	8
GLI2 localization	6
GLI3 localization	6
SUFU localization	3
PTCH localization	3
TULP3 localization	2
Protein expression	
GLI3 WB	16
GLI2 WB	7
GLI1 WB	3
SUFU WB	2
TULP3 WB	1
GPR161 WB	1
Gene expression	
GLI1 mRNA	26
PTCH1 mRNA	22
PTCH1 in situ	13
GLI2 mRNA	9
GLI1 in situ	9
SHH mRNA	8
SHH in situ	8
GLI3 mRNA	7
SUFU mRNA	4
SMO mRNA	4
GLI3 in situ	2
TULP3 mRNA	1
GLI2 in situ	1
Organism phenotypes	
Neural tube organization	22
Polydactyly	20
Exencephaly	8

Table 1.1. Hedgehog-related characteristics reported in the literature. We reviewed models of JS-associated genes and recorded Hh-related characteristics. Broadly, they are grouped by protein localization, protein expression, gene expression, and organism phenotypes, with specific assays listed within each category. The numbers represent how many JS-associated genes have published evidence pertaining to the listed Hh characteristic. It includes reports of normal and abnormal characteristics. WB = western blot. Experiments to collect mRNA expression included qPCR, RNA-seq, and GLI luciferase assays.

Prior to receptor binding, HH protein goes through a process of autoproteolytic cleavage, where the C-terminal region of the protein dissociates from the N-terminal region (HH-N) and is degraded, which leads to the addition of cholesterol to the N-terminal.[46] HH-N protein is further modified via skinny hedgehog (SKI), an acetyltransferase that attaches a palmitic acid group.[47] The modified ligand can then be

secreted by the transmembrane protein Dispatched (DISP) and SCUBE2 proteins or as multimers.[48–50]

With pathway stimulation, cholesterol modified and palmitoylated HH ligand binds PTCH,[51] leaving the cilium along with GPR161. SHH binding promotes an increase in ciliary Ca2+, which decreases ciliary cAMP and PKA activity, reducing proteolytic cleavage of GLI2/3.[52,53] The KIF7, SUFU, and GLI2/3 complex increase localization to the ciliary tip, and uncleaved GLI2/3 activator forms translocate to the nucleus and upregulate transcriptional targets, including *GLI1* and *PTCH1.*[24]

To determine what steps in the pathway we wanted to measure in our experiments, we performed a literature review of Hedgehog signaling characteristics in models of JS-associated genes (Table 1.1 and Table 1.2). Our literature search included 43 JS-associated genes and candidate genes. We identified the common cellular indicators of Hh signaling as protein localization (SMO, GLI2/3, GPR161), GLI processing (GLI2/3), and pathway target gene expression (*GLI1, PTCH, SHH*) or *in situ* hybridization (*PTCH1*, *GLI1*). At the organism level, neural tube development and polydactyly were commonly used as indicators of abnormal Hh signaling. At least half of the JS-associated genes had reported experimental results for SMO localization, GLI3 western blots, *GLI1* and *PTCH1* mRNA output, and neural tube organization (Table 1.1). The predominant species used to determine response to Hh signaling were murine model systems (used in experiments for 22 JS-associated genes) followed by human and patient-derived cells (used in experiments for 20 JS-associated genes combined) (Appendix A, Table 1.2). Below, I will describe patterns in the literature for these characteristics of Hh.

Human gene	Localization				Western blot		mRNA			in situ		Neural tube	Polydactyly
	SMO	GLI2	GLI3	GPR161	GLI2	GLI3	GLI1	PTCH	SHH	PTCH	GLI1		
AHI1 [84]	NL						AB	NL					
ARL13B - KO/null [76,85,86,86–91]	AB NL	NL	AB	AB		NL	AB NL	AB	AB			AB	AB
ARL13B – KD [87,88,92]	AB NL	NL	AB				AB	AB NL					
ARL3 [61,93]	AB		AB			AB							
ARMC9 [64]	NL	AB	AB										
B9D1 [62,94]	AB					AB	AB	AB				AB	AB
B9D2 [94]													AB
C2CD3 [74,95,96]					AB	AB		AB	AB	AB	AB	AB	AB
CC2D2A [17,62,97]	AB											AB	AB
CEP104 [80,98]	AB			AB			AB						
CEP290 [55,99–101]	AB NL	AB		AB		AB	AB NL	AB	NL				
CPLANE1 [102]							AB	AB					
CSPP1 [78,98]	AB						AB						
FAM149B1 [103]							AB	AB					AB
HYLS1 [104]			AB	AB			AB	AB					
IFT172 [15,16,77,105–108]	AB					AB	AB			AB	AB	AB	AB
INPP5E- *KO/null* [27,28,59,60]	AB NL	AB	AB	AB	NL	NL	AB	AB				AB	AB
KIAA0586 [109–113]					AB	AB	AB	AB		AB	AB	AB	AB
KIAA0753 [114]							AB	AB					
KIF7- KO/null [63,115–121]	NL	AB	AB		AB	AB	AB NL	AB			AB	AB	AB
KIF7- KD [24,93,102,118,122–126]	NL	AB NL	AB NL		AB	AB	NL	AB NL		AB		AB	AB
MKS1 [108,127–129]	AB	AB		AB						AB	AB	AB	AB
OFD1 [79]						AB	AB	AB	NL				
RPGRIP1L [58,75,130]	AB					AB	AB	AB		AB		AB	AB
SUFU- KO/null [54,121,131–140]	AB	AB	AB	AB	AB	AB NL	AB NL	AB	AB	AB	AB	AB	AB
SUFU- KD [57,121,134,136,137,141–143]	NL				AB NL	AB NL	AB NL	AB NL	NL	AB		AB	AB
TCTN1 [17]	AB					AB				AB	AB		AB
TCTN2 [17,144–146]	AB					AB	AB	AB				AB	AB
TCTN3 [147,148]	AB				AB	AB	AB	AB				AB	AB
TMEM67- KO/null [17,149]	NL								AB			AB	
TMEM67- *KD* [81]							NL	NL		NL	AB		
TMEM107 [150,151]							AB			AB	AB	AB	AB
TMEM216 [37]													AB
TMEM231 [62]	AB						AB					AB	AB
TOGARAM1 [152]	AB												

Table 1.2. Commonly reported Hedgehog signaling characteristics in models of JS-associated genes. A summary table of commonly reported Hh pathway characteristics, including cellular and organism characteristics. In a subset of genes, *ARL13B, INPP5E, KIF7, SUFU,* and *TMEM67,* we separated reported knockout/null from knockdown/hypomorph model systems to determine whether the severity of the mutations/variants affected the assay output. AB = reported abnormal, NL = reported normal.

Pathway protein localization in JS models

Hh ligand binding to PTCH promotes its ciliary exit and SMO ciliary entrance. SMO entry increases ciliary β-arrestin, promoting GPR161 ciliary exit and GLI2/3 accumulation at the ciliary tip.[54] Smoothened agonist (SAG) and recombinant SHH (SHH-N) are commonly used to stimulate the Hh pathway in vitro. JS-associated gene animal/cell models and a limited number of patient cell lines[55–58] suggest localization of Hh pathway proteins are disrupted. For example, in *INPP5E* knockouts, abnormal protein localization in SMO, GLI2, GLI3, and GPR161 is presented, but there is evidence of normal SMO localization in one of the studies (Table 1.2).[27,28,59,60] This is one of three genes where protein localization is available for the four proteins we were interested in and none of the studies reported data for SMO, GPR161, GLI2 and GLI3 in the same system (Table 1.2). Methods for measuring protein localization varied and included counting signal positive vs negative cilia, measuring fluorescence intensity, and sub-categorizing fluorescence signal patterns.

Protein localization data was primarily generated from cilium tip, cilium proper, and transition zone mutants (Table 1.2). GPR161 localization data from tip and cilium proper mutants commonly reported higher baseline and stimulated levels of ciliary GPR161. Transition zone mutants had variable results, and there were no models for basal body genes. GPR161 data shows a trend towards blunted Hedgehog signaling across genes with available data. In the positive regulator of the pathway, SMO, there were examples of differing data in *ARL3* (CP)*, ARMC9* (BB)*, KIF7* (TIP)*, and CC2D2A* (TZ) mutants. In *Arl3* IMCD3 knockdown cells, baseline Smo fluorescence is normal, and stimulated fluorescence intensity is low, similar to *Cc2d2a* IMCD3 knockdowns.[61,62] In contrast, *ARMC9* NIH/3T3 knockout cells, *Kif7* KO MEFs, and *Kif7* knockdown MEFs, have normal Smo at baseline and with stimulation.[24,63,64] While these results are conflicting, these studies provide a premise for our investigation into Hh pathway protein localization being disrupted across genetic causes of JS. Differences in cell type could contribute to the differences, which provides basis for using the same system to look across mutants.

GLI2/3 processing

In a downstream step of the pathway signaling cascade, GLI transcription factors are processed dependent on their phosphorylation status.[44,65,66] In the absence of

pathway stimulation, GLI2/3 transcription factors are proteolytically cleaved into repressor forms.[44,67] These transcription factors are specialized, with full length GLI2 being the predominant activator, and cleaved GLI3 being the predominant repressor.[68–70] Western blots were used to detect GLI2/3 full length (FL) and repressor (R) isoforms and measure differences in expression with and without pathway stimulation. GLI2 data collection was inconsistent with some papers reporting GLI2 FL and R isoform, while others only reported a single band. Most often, protein lysate was collected from embryonic tissues (murine and chick) with fewer experiments using cell lysates. While using tissue lysates has the advantage of having higher protein levels, it makes it difficult to determine which cells in each tissue are stimulated versus unstimulated, limiting our understanding of the human disease state.

There were fewer instances of conflicting data for GLI2/3 processing, but this category had fewer data available (Table 1.2). While there were fewer instances of conflicting data within this category, there was conflicting data across the experiments within genes. If an upstream step in the signaling cascade is abnormal, we would expect that downstream steps would be affected. In models of *INPP5E* that were discussed in the prior section, evidence for abnormal pathway protein localization was presented in the literature, but one study provided evidence for normal GLI2 and GLI3 processing.[60] In this study, protein was extracted from whole embryo, which may dilute protein and could be masking any subtle changes that may be occurring.

Gene expression

The predominant downstream readouts of the Hh pathway are *GLI1* and *PTCH1*, with *SHH* being reported in several models.[71–73] Expression experiments were reported at the cellular level, most often using qPCR, and in embryonic tissues, using *in situ* hybridization. Evidence in animal models and human cell lines suggests that several JS genes act upstream of GLI2/3 processing, and therefore *GLI1* and *PTCH1* induction.[55,74–79] In our literature review, we noted differences in expression across mutants and models, for example, between *CEP104* (Tip) and *Cep290* (TZ) (Table 1.2). In knockdown *CEP104* hTERT RPE-1 cells, baseline and SAG stimulated *GLI1* expression were lower than controls.[80] In contrast, *CEP290* patient fibroblasts at baseline were comparable to unaffected cells, while SAG stimulated cells had a higher

GLI1 induction compared to unaffected cells.[55] Some of the variation between qPCR experiments could arise from differing reference gene expression between baseline and stimulated cells. If assay validation was not performed for each cell/tissue type, even commonly used reference genes could mask or enhance differences in target gene expression.

Performance of *in situ* hybridization consistently showed abnormal *GLI1*/*PTCH1* expression in embryonic tissues. The only exception was a *Tmem67* knockdown model that did not differ in *Ptch1* expression between mutants and controls.[81] Overall, target gene expression was one of the most measured cellular phenotypes. It was consistently perturbed, but experiments were performed in different model systems and using different assays, making it difficult to understand the relevance to human disease.

Organism features of Hedgehog signaling

At the organism level, neural tube development and polydactyly were common markers of abnormal Hh signaling. HH is a morphogen that helps determine cell fate in the neural tube[82] and proper digit formation,[83] attributing these phenotypes to abnormal Hh signaling. Like other assays, data from cilium tip, cilium proper, and transition zone mutants were commonly reported, while basal body mutants had fewer data reported. These broader phenotypes at the organism level provide evidence that Hh signaling at the cellular level is likely perturbed in models of JS-associated genes.

Proposed study

Previous studies in animal/cell models and a limited number of patient-derived cell lines have identified Hh signaling abnormalities, but Hh pathway dysfunction has not been systematically evaluated across multiple genetic causes of JS in human cells using the same assays to measure changes in pathway signaling. We want to determine response to Hh signaling across a subset of JS genes, in the same model system, using the following assays: 1) Protein localization of GPR161 and SMO, 2) GLI3 processing, and 3) Target gene induction. Within these assays, our goal is to measure baseline, stimulated, and ratios when possible. These experiments will lay the groundwork for future research to determine the developmental basis of the JS-associated brain and organ defects. Once we have a better mechanistic understanding of JS, we can utilize patient-derived cells to explore the human disease state of pathway

response, with the ultimate goal of identifying therapeutic target genes to improve the quality of life of individuals with JS.

References

1. Maria, B. L. *et al.* 'Joubert syndrome' revisited: key ocular motor signs with magnetic resonance imaging correlation. *J. Child Neurol.* **12**, 423–430 (1997).
2. Parisi, M. A. *et al.* Cerebral and cerebellar motor activation abnormalities in a subject with Joubert syndrome: functional magnetic resonance imaging (MRI) study. *J. Child Neurol.* **19**, 214–218 (2004).
3. Juric-Sekhar, G., Adkins, J., Doherty, D. & Hevner, R. F. Joubert syndrome: brain and spinal cord malformations in genotyped cases and implications for neurodevelopmental functions of primary cilia. *Acta Neuropathol. (Berl.)* **123**, 695–709 (2012).
4. Poretti, A., Huisman, T. a. G. M., Scheer, I. & Boltshauser, E. Joubert syndrome and related disorders: spectrum of neuroimaging findings in 75 patients. *AJNR Am. J. Neuroradiol.* **32**, 1459–1463 (2011).
5. Bachmann-Gagescu, R. *et al.* Healthcare recommendations for Joubert syndrome. *Am. J. Med. Genet. A.* **182**, 229–249 (2020).
6. Joubert, M., Eisenring, J. J., Robb, J. P. & Andermann, F. Familial agenesis of the cerebellar vermis. A syndrome of episodic hyperpnea, abnormal eye movements, ataxia, and retardation. *Neurology* **19**, 813–825 (1969).
7. Ferland, R. J. *et al.* Abnormal cerebellar development and axonal decussation due to mutations in AHI1 in Joubert syndrome. *Nat. Genet.* **36**, 1008–1013 (2004).
8. Srour, M. *et al.* Joubert Syndrome in French Canadians and Identification of Mutations in CEP104. *Am. J. Hum. Genet.* **97**, 744–753 (2015).
9. Knopp, C. *et al.* Syndromic ciliopathies: From single gene to multi gene analysis by SNP arrays and next generation sequencing. *Mol. Cell. Probes* **29**, 299–307 (2015).
10. Kroes, H. Y. *et al.* Joubert syndrome: genotyping a Northern European patient cohort. *Eur. J. Hum. Genet. EJHG* **24**, 214–220 (2016).
11. Bachmann-Gagescu, R. *et al.* Joubert syndrome: a model for untangling recessive disorders with extreme genetic heterogeneity. *J. Med. Genet.* **52**, 514–522 (2015).
12. Serpieri, V. *et al.* SUFU haploinsufficiency causes a recognisable neurodevelopmental phenotype at the mild end of the Joubert syndrome spectrum. *J. Med. Genet.* jmedgenet-2021-108114 (2021) doi:10.1136/jmedgenet-2021-108114.
13. Goetz, S. C. & Anderson, K. V. The primary cilium: a signalling centre during vertebrate development. *Nat. Rev. Genet.* **11**, 331–344 (2010).
14. Berbari, N. F., O'Connor, A. K., Haycraft, C. J. & Yoder, B. K. The primary cilium as a complex signaling center. *Curr. Biol. CB* **19**, R526-535 (2009).
15. Huangfu, D. *et al.* Hedgehog signalling in the mouse requires intraflagellar transport proteins. *Nature* **426**, 83–87 (2003).
16. Huangfu, D. & Anderson, K. V. Cilia and Hedgehog responsiveness in the mouse. *Proc. Natl. Acad. Sci. U. S. A.* **102**, 11325–11330 (2005).
17. Garcia-Gonzalo, F. R. *et al.* A transition zone complex regulates mammalian ciliogenesis and ciliary membrane composition. *Nat. Genet.* **43**, 776–784 (2011).
18. Szymanska, K. & Johnson, C. A. The transition zone: an essential functional compartment of cilia. *Cilia* **1**, 10 (2012).

19. Craige, B. *et al.* CEP290 tethers flagellar transition zone microtubules to the membrane and regulates flagellar protein content. *J. Cell Biol.* **190**, 927–940 (2010).
20. Garcia-Gonzalo, F. R. & Reiter, J. F. Open Sesame: How Transition Fibers and the Transition Zone Control Ciliary Composition. *Cold Spring Harb. Perspect. Biol.* **9**, a028134 (2017).
21. Omran, H. NPHP proteins: gatekeepers of the ciliary compartment. *J. Cell Biol.* **190**, 715–717 (2010).
22. Garcia, G., Raleigh, D. R. & Reiter, J. F. How the Ciliary Membrane Is Organized Inside-Out to Communicate Outside-In. *Curr. Biol. CB* **28**, R421–R434 (2018).
23. Satish Tammana, T. V., Tammana, D., Diener, D. R. & Rosenbaum, J. Centrosomal protein CEP104 (Chlamydomonas FAP256) moves to the ciliary tip during ciliary assembly. *J. Cell Sci.* **126**, 5018–5029 (2013).
24. He, M. *et al.* The kinesin-4 protein Kif7 regulates mammalian Hedgehog signalling by organizing the cilium tip compartment. *Nat. Cell Biol.* **16**, 663–672 (2014).
25. Buisson, J. *et al.* Intraflagellar transport proteins cycle between the flagellum and its base. *J. Cell Sci.* **126**, 327–338 (2013).
26. Kisseleva, M. V., Wilson, M. P. & Majerus, P. W. The isolation and characterization of a cDNA encoding phospholipid-specific inositol polyphosphate 5-phosphatase. *J. Biol. Chem.* **275**, 20110–20116 (2000).
27. Chávez, M. *et al.* Modulation of Ciliary Phosphoinositide Content Regulates Trafficking and Sonic Hedgehog Signaling Output. *Dev. Cell* **34**, 338–350 (2015).
28. Garcia-Gonzalo, F. R. *et al.* Phosphoinositides Regulate Ciliary Protein Trafficking to Modulate Hedgehog Signaling. *Dev. Cell* **34**, 400–409 (2015).
29. Sierra Potchanant, E. A. *et al.* INPP5E Preserves Genomic Stability through Regulation of Mitosis. *Mol. Cell. Biol.* **37**, e00500-16 (2017).
30. Waters, A. M. & Beales, P. L. Ciliopathies: an expanding disease spectrum. *Pediatr. Nephrol. Berl. Ger.* **26**, 1039–1056 (2011).
31. Lancaster, M. A. *et al.* Defective Wnt-dependent cerebellar midline fusion in a mouse model of Joubert syndrome. *Nat. Med.* **17**, 726–731 (2011).
32. Chaki, M. *et al.* Exome capture reveals ZNF423 and CEP164 mutations, linking renal ciliopathies to DNA damage response signaling. *Cell* **150**, 533–548 (2012).
33. Slaats, G. G. *et al.* DNA replication stress underlies renal phenotypes in CEP290-associated Joubert syndrome. *J. Clin. Invest.* **125**, 3657–3666 (2015).
34. Halbritter, J. *et al.* Defects in the IFT-B component IFT172 cause Jeune and Mainzer-Saldino syndromes in humans. *Am. J. Hum. Genet.* **93**, 915–925 (2013).
35. Plotnikova, O. V. *et al.* INPP5E interacts with AURKA, linking phosphoinositide signaling to primary cilium stability. *J. Cell Sci.* **128**, 364–372 (2015).
36. Slaats, G. G. *et al.* MKS1 regulates ciliary INPP5E levels in Joubert syndrome. *J. Med. Genet.* **53**, 62–72 (2016).
37. Valente, E. M. *et al.* Mutations in TMEM216 perturb ciliogenesis and cause Joubert, Meckel and related syndromes. *Nat. Genet.* **42**, 619–625 (2010).
38. Lee, J. E. *et al.* CEP41 is mutated in Joubert syndrome and is required for tubulin glutamylation at the cilium. *Nat. Genet.* **44**, 193–199 (2012).
39. Briscoe, J. & Thérond, P. P. The mechanisms of Hedgehog signalling and its roles in development and disease. *Nat. Rev. Mol. Cell Biol.* **14**, 416–429 (2013).

40. Kinnebrew, M. *et al.* Cholesterol accessibility at the ciliary membrane controls hedgehog signaling. *eLife* **8**, e50051 (2019).
41. Motoyama, J. *et al.* Essential function of Gli2 and Gli3 in the formation of lung, trachea and oesophagus. *Nat. Genet.* **20**, 54–57 (1998).
42. Haycraft, C. J. *et al.* Gli2 and Gli3 localize to cilia and require the intraflagellar transport protein polaris for processing and function. *PLoS Genet.* **1**, e53 (2005).
43. Mukhopadhyay, S. *et al.* TULP3 bridges the IFT-A complex and membrane phosphoinositides to promote trafficking of G protein-coupled receptors into primary cilia. *Genes Dev.* **24**, 2180–2193 (2010).
44. Wang, B., Fallon, J. F. & Beachy, P. A. Hedgehog-Regulated Processing of Gli3 Produces an Anterior/Posterior Repressor Gradient in the Developing Vertebrate Limb. *Cell* **100**, 423–434 (2000).
45. Wang, C., Pan, Y. & Wang, B. Suppressor of fused and Spop regulate the stability, processing and function of Gli2 and Gli3 full-length activators but not their repressors. *Dev. Camb. Engl.* **137**, 2001–2009 (2010).
46. Porter, J. A., Young, K. E. & Beachy, P. A. Cholesterol modification of hedgehog signaling proteins in animal development. *Science* **274**, 255–259 (1996).
47. Chamoun, Z. *et al.* Skinny hedgehog, an acyltransferase required for palmitoylation and activity of the hedgehog signal. *Science* **293**, 2080–2084 (2001).
48. Creanga, A. *et al.* Scube/You activity mediates release of dually lipid-modified Hedgehog signal in soluble form. *Genes Dev.* **26**, 1312–1325 (2012).
49. Tukachinsky, H., Kuzmickas, R. P., Jao, C. Y., Liu, J. & Salic, A. Dispatched and scube mediate the efficient secretion of the cholesterol-modified hedgehog ligand. *Cell Rep.* **2**, 308–320 (2012).
50. Zeng, X. *et al.* A freely diffusible form of Sonic hedgehog mediates long-range signalling. *Nature* **411**, 716–720 (2001).
51. Lewis, P. M. *et al.* Cholesterol modification of sonic hedgehog is required for long-range signaling activity and effective modulation of signaling by Ptc1. *Cell* **105**, 599–612 (2001).
52. Belgacem, Y. H. & Borodinsky, L. N. Sonic hedgehog signaling is decoded by calcium spike activity in the developing spinal cord. *Proc. Natl. Acad. Sci. U. S. A.* **108**, 4482–4487 (2011).
53. Mukhopadhyay, S. *et al.* The Ciliary G-Protein-Coupled Receptor Gpr161 Negatively Regulates the Sonic Hedgehog Pathway via cAMP Signaling. *Cell* **152**, 210–223 (2013).
54. Pal, K. *et al.* Smoothened determines β-arrestin–mediated removal of the G protein–coupled receptor Gpr161 from the primary cilium. *J. Cell Biol.* **212**, 861–875 (2016).
55. Shimada, H. *et al.* In Vitro Modeling Using Ciliopathy-Patient-Derived Cells Reveals Distinct Cilia Dysfunctions Caused by CEP290 Mutations. *Cell Rep.* **20**, 384–396 (2017).
56. Luo, M. *et al.* Disrupted intraflagellar transport due to IFT74 variants causes Joubert syndrome. *Genet. Med. Off. J. Am. Coll. Med. Genet.* **23**, 1041–1049 (2021).

57. Schröder, S. *et al.* Heterozygous truncating variants in SUFU cause congenital ocular motor apraxia. *Genet. Med. Off. J. Am. Coll. Med. Genet.* **23**, 341–351 (2021).
58. Wang, L. *et al.* Ciliary gene RPGRIP1L is required for hypothalamic arcuate neuron development. *JCI Insight* **4**, 123337 (2019).
59. Dyson, J. M. *et al.* INPP5E regulates phosphoinositide-dependent cilia transition zone function. *J. Cell Biol.* **216**, 247–263 (2017).
60. Constable, S., Long, A. B., Floyd, K. A., Schurmans, S. & Caspary, T. The ciliary phosphatidylinositol phosphatase Inpp5e plays positive and negative regulatory roles in Shh signaling. *Dev. Camb. Engl.* **147**, dev183301 (2020).
61. Lai, C. K. *et al.* Functional characterization of putative cilia genes by high-content analysis. *Mol. Biol. Cell* **22**, 1104–1119 (2011).
62. Chih, B. *et al.* A ciliopathy complex at the transition zone protects the cilia as a privileged membrane domain. *Nat. Cell Biol.* **14**, 61–72 (2011).
63. Liu, Y. C. *et al.* The PPFIA1-PP2A protein complex promotes trafficking of Kif7 to the ciliary tip and Hedgehog signaling. *Sci. Signal.* **7**, ra117 (2014).
64. Breslow, D. K. *et al.* A CRISPR-based screen for Hedgehog signaling provides insights into ciliary function and ciliopathies. *Nat. Genet.* **50**, 460–471 (2018).
65. Kim, J., Kato, M. & Beachy, P. A. Gli2 trafficking links Hedgehog-dependent activation of Smoothened in the primary cilium to transcriptional activation in the nucleus. *Proc. Natl. Acad. Sci. U. S. A.* **106**, 21666–21671 (2009).
66. Niewiadomski, P. *et al.* Gli protein activity is controlled by multisite phosphorylation in vertebrate Hedgehog signaling. *Cell Rep.* **6**, 168–181 (2014).
67. Li, J., Wang, C., Pan, Y., Bai, Z. & Wang, B. Increased proteolytic processing of full-length Gli2 transcription factor reduces the hedgehog pathway activity in vivo. *Dev. Dyn. Off. Publ. Am. Assoc. Anat.* **240**, 766–774 (2011).
68. Matise, M. P., Epstein, D. J., Park, H. L., Platt, K. A. & Joyner, A. L. Gli2 is required for induction of floor plate and adjacent cells, but not most ventral neurons in the mouse central nervous system. *Dev. Camb. Engl.* **125**, 2759–2770 (1998).
69. Litingtung, Y. & Chiang, C. Specification of ventral neuron types is mediated by an antagonistic interaction between Shh and Gli3. *Nat. Neurosci.* **3**, 979–985 (2000).
70. Wen, X. *et al.* Kinetics of Hedgehog-Dependent Full-Length Gli3 Accumulation in Primary Cilia and Subsequent Degradation. *Mol. Cell. Biol.* **30**, 1910–1922 (2010).
71. Niswander, L., Jeffrey, S., Martin, G. R. & Tickle, C. A positive feedback loop coordinates growth and patterning in the vertebrate limb. *Nature* **371**, 609–612 (1994).
72. Dai, P. *et al.* Sonic Hedgehog-induced activation of the Gli1 promoter is mediated by GLI3. *J. Biol. Chem.* **274**, 8143–8152 (1999).
73. Chen, Y. & Struhl, G. Dual roles for patched in sequestering and transducing Hedgehog. *Cell* **87**, 553–563 (1996).
74. Hoover, A. N. *et al.* C2cd3 is required for cilia formation and Hedgehog signaling in mouse. *Dev. Camb. Engl.* **135**, 4049–4058 (2008).
75. Vierkotten, J., Dildrop, R., Peters, T., Wang, B. & Rüther, U. Ftm is a novel basal body protein of cilia involved in Shh signalling. *Dev. Camb. Engl.* **134**, 2569–2577 (2007).

76. Larkins, C. E., Aviles, G. D. G., East, M. P., Kahn, R. A. & Caspary, T. Arl13b regulates ciliogenesis and the dynamic localization of Shh signaling proteins. *Mol. Biol. Cell* **22**, 4694–4703 (2011).
77. Gorivodsky, M. *et al.* Intraflagellar transport protein 172 is essential for primary cilia formation and plays a vital role in patterning the mammalian brain. *Dev. Biol.* **325**, 24–32 (2009).
78. Shaheen, R. *et al.* Mutations in CSPP1, encoding a core centrosomal protein, cause a range of ciliopathy phenotypes in humans. *Am. J. Hum. Genet.* **94**, 73–79 (2014).
79. D'Angelo, A. *et al.* Ofd1 controls dorso-ventral patterning and axoneme elongation during embryonic brain development. *PloS One* **7**, e52937 (2012).
80. Yamazoe, T., Nagai, T., Umeda, S., Sugaya, Y. & Mizuno, K. Roles of TOG and jelly-roll domains of centrosomal protein CEP104 in its functions in cilium elongation and Hedgehog signaling. *J. Biol. Chem.* **295**, 14723–14736 (2020).
81. Lee, S.-H. *et al.* Functional validation of novel MKS3/TMEM67 mutations in COACH syndrome. *Sci. Rep.* **7**, 10222 (2017).
82. Brooks, E. R., Islam, M. T., Anderson, K. V. & Zallen, J. A. Sonic hedgehog signaling directs patterned cell remodeling during cranial neural tube closure. *eLife* **9**, e60234 (2020).
83. Bouldin, C. M., Gritli-Linde, A., Ahn, S. & Harfe, B. D. Shh pathway activation is present and required within the vertebrate limb bud apical ectodermal ridge for normal autopod patterning. *Proc. Natl. Acad. Sci. U. S. A.* **107**, 5489–5494 (2010).
84. Muñoz-Estrada, J. & Ferland, R. J. Ahi1 promotes Arl13b ciliary recruitment, regulates Arl13b stability and is required for normal cell migration. *J. Cell Sci.* **132**, jcs230680 (2019).
85. Su, C.-Y., Bay, S. N., Mariani, L. E., Hillman, M. J. & Caspary, T. Temporal deletion of Arl13b reveals that a mispatterned neural tube corrects cell fate over time. *Dev. Camb. Engl.* **139**, 4062–4071 (2012).
86. Nozaki, S. *et al.* Regulation of ciliary retrograde protein trafficking by the Joubert syndrome proteins ARL13B and INPP5E. *J. Cell Sci.* **130**, 563–576 (2017).
87. Mariani, L. E. *et al.* Arl13b regulates Shh signaling from both inside and outside the cilium. *Mol. Biol. Cell* mbc.E16-03-0189 (2016) doi:10.1091/mbc.E16-03-0189.
88. Gigante, E. D., Taylor, M. R., Ivanova, A. A., Kahn, R. A. & Caspary, T. ARL13B regulates Sonic hedgehog signaling from outside primary cilia. *eLife* **9**, e50434 (2020).
89. Caspary, T., Larkins, C. E. & Anderson, K. V. The graded response to Sonic Hedgehog depends on cilia architecture. *Dev. Cell* **12**, 767–778 (2007).
90. Li, Y. *et al.* Deletion of ADP Ribosylation Factor-Like GTPase 13B Leads to Kidney Cysts. *J. Am. Soc. Nephrol. JASN* **27**, 3628–3638 (2016).
91. Ferent, J. *et al.* The Ciliary Protein Arl13b Functions Outside of the Primary Cilium in Shh-Mediated Axon Guidance. *Cell Rep.* **29**, 3356-3366.e3 (2019).
92. Bay, S. N., Long, A. B. & Caspary, T. Disruption of the ciliary GTPase Arl13b suppresses Sonic hedgehog overactivation and inhibits medulloblastoma formation. *Proc. Natl. Acad. Sci. U. S. A.* **115**, 1570–1575 (2018).
93. Schwarz, N. *et al.* Arl3 and RP2 regulate the trafficking of ciliary tip kinesins. *Hum. Mol. Genet.* **26**, 2480–2492 (2017).

94. Dowdle, W. E. *et al.* Disruption of a ciliary B9 protein complex causes Meckel syndrome. *Am. J. Hum. Genet.* **89**, 94–110 (2011).
95. Chang, C.-F. *et al.* The cellular and molecular etiology of the craniofacial defects in the avian ciliopathic mutant talpid2. *Dev. Camb. Engl.* **141**, 3003–3012 (2014).
96. Brooks, E. C. *et al.* Mutation in the Ciliary Protein C2CD3 Reveals Organ-Specific Mechanisms of Hedgehog Signal Transduction in Avian Embryos. *J. Dev. Biol.* **9**, 12 (2021).
97. Veleri, S. *et al.* Ciliopathy-associated gene Cc2d2a promotes assembly of subdistal appendages on the mother centriole during cilia biogenesis. *Nat. Commun.* **5**, 4207 (2014).
98. Frikstad, K.-A. M. *et al.* A CEP104-CSPP1 Complex Is Required for Formation of Primary Cilia Competent in Hedgehog Signaling. *Cell Rep.* **28**, 1907-1922.e6 (2019).
99. Kilander, M. B. C. *et al.* A rare human CEP290 variant disrupts the molecular integrity of the primary cilium and impairs Sonic Hedgehog machinery. *Sci. Rep.* **8**, 17335 (2018).
100. Hynes, A. M. *et al.* Murine Joubert syndrome reveals Hedgehog signaling defects as a potential therapeutic target for nephronophthisis. *Proc. Natl. Acad. Sci. U. S. A.* **111**, 9893–9898 (2014).
101. Srivastava, S. *et al.* A human patient-derived cellular model of Joubert syndrome reveals ciliary defects which can be rescued with targeted therapies. *Hum. Mol. Genet.* **26**, 4657–4667 (2017).
102. Asadollahi, R. *et al.* Clinical and experimental evidence suggest a link between KIF7 and C5orf42-related ciliopathies through Sonic Hedgehog signaling. *Eur. J. Hum. Genet. EJHG* **26**, 197–209 (2018).
103. Shaheen, R. *et al.* Bi-allelic Mutations in FAM149B1 Cause Abnormal Primary Cilium and a Range of Ciliopathy Phenotypes in Humans. *Am. J. Hum. Genet.* **104**, 731–737 (2019).
104. Chen, C. *et al.* Ciliopathy protein HYLS1 coordinates the biogenesis and signaling of primary cilia by activating the ciliary lipid kinase PIPKIγ. *Sci. Adv.* **7**, eabe3401 (2021).
105. Ocbina, P. J. R. & Anderson, K. V. Intraflagellar transport, cilia, and mammalian Hedgehog signaling: analysis in mouse embryonic fibroblasts. *Dev. Dyn. Off. Publ. Am. Assoc. Anat.* **237**, 2030–2038 (2008).
106. Ocbina, P. J. R., Tuson, M. & Anderson, K. V. Primary cilia are not required for normal canonical Wnt signaling in the mouse embryo. *PloS One* **4**, e6839 (2009).
107. Friedland-Little, J. M. *et al.* A novel murine allele of Intraflagellar Transport Protein 172 causes a syndrome including VACTERL-like features with hydrocephalus. *Hum. Mol. Genet.* **20**, 3725–3737 (2011).
108. Goetz, S. C., Bangs, F., Barrington, C. L., Katsanis, N. & Anderson, K. V. The Meckel syndrome- associated protein MKS1 functionally interacts with components of the BBSome and IFT complexes to mediate ciliary trafficking and hedgehog signaling. *PloS One* **12**, e0173399 (2017).
109. Bashford, A. L. & Subramanian, V. Mice with a conditional deletion of Talpid3 (KIAA0586) - a model for Joubert syndrome. *J. Pathol.* **248**, 396–408 (2019).

110. Alby, C. *et al.* Mutations in KIAA0586 Cause Lethal Ciliopathies Ranging from a Hydrolethalus Phenotype to Short-Rib Polydactyly Syndrome. *Am. J. Hum. Genet.* **97**, 311–318 (2015).
111. Davey, M. G. *et al.* The chicken talpid3 gene encodes a novel protein essential for Hedgehog signaling. *Genes Dev.* **20**, 1365–1377 (2006).
112. Davey, M. G., McTeir, L., Barrie, A. M., Freem, L. J. & Stephen, L. A. Loss of cilia causes embryonic lung hypoplasia, liver fibrosis, and cholestasis in the talpid3 ciliopathy mutant. *Organogenesis* **10**, 177–185 (2014).
113. Bangs, F. *et al.* Generation of mice with functional inactivation of talpid3, a gene first identified in chicken. *Dev. Camb. Engl.* **138**, 3261–3272 (2011).
114. Inskeep, K. A. *et al.* Genetic and phenotypic heterogeneity in KIAA0753-related ciliopathies. *Am. J. Med. Genet. A.* **188**, 104–115 (2022).
115. Hsu, S.-H. C. *et al.* Kif7 promotes hedgehog signaling in growth plate chondrocytes by restricting the inhibitory function of Sufu. *Dev. Camb. Engl.* **138**, 3791–3801 (2011).
116. Endoh-Yamagami, S. *et al.* The mammalian Cos2 homolog Kif7 plays an essential role in modulating Hh signal transduction during development. *Curr. Biol. CB* **19**, 1320–1326 (2009).
117. Cheung, H. O.-L. *et al.* The kinesin protein Kif7 is a critical regulator of Gli transcription factors in mammalian hedgehog signaling. *Sci. Signal.* **2**, ra29 (2009).
118. Li, Z. J. *et al.* Kif7 regulates Gli2 through Sufu-dependent and -independent functions during skin development and tumorigenesis. *Dev. Camb. Engl.* **139**, 4152–4161 (2012).
119. Law, K. K. L. *et al.* Antagonistic and cooperative actions of Kif7 and Sufu define graded intracellular Gli activities in Hedgehog signaling. *PloS One* **7**, e50193 (2012).
120. Putoux, A. *et al.* Altered GLI3 and FGF8 signaling underlies acrocallosal syndrome phenotypes in Kif7 depleted mice. *Hum. Mol. Genet.* **28**, 877–887 (2019).
121. Zhulyn, O. & Hui, C.-C. Sufu and Kif7 in limb patterning and development. *Dev. Dyn. Off. Publ. Am. Assoc. Anat.* **244**, 468–478 (2015).
122. Yue, Y., Engelke, M. F., Blasius, T. L. & Verhey, K. J. Hedgehog-induced ciliary trafficking of kinesin-4 motor KIF7 requires intraflagellar transport but not KIF7's microtubule binding. *Mol. Biol. Cell* **33**, br1 (2022).
123. Liem, K. F., He, M., Ocbina, P. J. R. & Anderson, K. V. Mouse Kif7/Costal2 is a cilia-associated protein that regulates Sonic hedgehog signaling. *Proc. Natl. Acad. Sci. U. S. A.* **106**, 13377–13382 (2009).
124. Putoux, A. *et al.* KIF7 mutations cause fetal hydrolethalus and acrocallosal syndromes. *Nat. Genet.* **43**, 601–606 (2011).
125. Terhune, E. A. *et al.* Mutations in KIF7 implicated in idiopathic scoliosis in humans and axial curvatures in zebrafish. *Hum. Mutat.* **42**, 392–407 (2021).
126. Tay, S. Y., Ingham, P. W. & Roy, S. A homologue of the Drosophila kinesin-like protein Costal2 regulates Hedgehog signal transduction in the vertebrate embryo. *Dev. Camb. Engl.* **132**, 625–634 (2005).
127. Cui, C. *et al.* Disruption of Mks1 localization to the mother centriole causes cilia defects and developmental malformations in Meckel-Gruber syndrome. *Dis. Model. Mech.* **4**, 43–56 (2011).

128. Weatherbee, S. D., Niswander, L. A. & Anderson, K. V. A mouse model for Meckel syndrome reveals Mks1 is required for ciliogenesis and Hedgehog signaling. *Hum. Mol. Genet.* **18**, 4565–4575 (2009).
129. Burnicka-Turek, O. *et al.* Cilia gene mutations cause atrioventricular septal defects by multiple mechanisms. *Hum. Mol. Genet.* **25**, 3011–3028 (2016).
130. Chen, J. *et al.* The ciliopathy gene Rpgrip1l is essential for hair follicle development. *J. Invest. Dermatol.* **135**, 701–709 (2015).
131. Chen, M.-H. *et al.* Cilium-independent regulation of Gli protein function by Sufu in Hedgehog signaling is evolutionarily conserved. *Genes Dev.* **23**, 1910–1928 (2009).
132. Yabut, O. R., Fernandez, G., Huynh, T., Yoon, K. & Pleasure, S. J. Suppressor of Fused Is Critical for Maintenance of Neuronal Progenitor Identity during Corticogenesis. *Cell Rep.* **12**, 2021–2034 (2015).
133. Lin, C. *et al.* Differential regulation of Gli proteins by Sufu in the lung affects PDGF signaling and myofibroblast development. *Dev. Biol.* **392**, 324–333 (2014).
134. Hoelzl, M. A. *et al.* Differential requirement of SUFU in tissue development discovered in a hypomorphic mouse model. *Dev. Biol.* **429**, 132–146 (2017).
135. Yin, W.-C. *et al.* Dual Regulatory Functions of SUFU and Targetome of GLI2 in SHH Subgroup Medulloblastoma. *Dev. Cell* **48**, 167-183.e5 (2019).
136. Li, J. *et al.* Suppressor of Fused Is Required for Determining Digit Number and Identity via Gli3/Fgfs/Gremlin. *PloS One* **10**, e0128006 (2015).
137. Makino, S. *et al.* T396I mutation of mouse Sufu reduces the stability and activity of Gli3 repressor. *PloS One* **10**, e0119455 (2015).
138. Svärd, J. *et al.* Genetic elimination of Suppressor of fused reveals an essential repressor function in the mammalian Hedgehog signaling pathway. *Dev. Cell* **10**, 187–197 (2006).
139. Noguchi, H., Castillo, J. G., Nakashima, K. & Pleasure, S. J. Suppressor of fused controls perinatal expansion and quiescence of future dentate adult neural stem cells. *eLife* **8**, e42918 (2019).
140. Hoelzl, M. A. *et al.* Suppressor of Fused Plays an Important Role in Regulating Mesodermal Differentiation of Murine Embryonic Stem Cells In Vivo. *Stem Cells Dev.* **24**, 2547–2560 (2015).
141. Kim, J. J. *et al.* Suppressor of fused controls mid-hindbrain patterning and cerebellar morphogenesis via GLI3 repressor. *J. Neurosci. Off. J. Soc. Neurosci.* **31**, 1825–1836 (2011).
142. De Mori, R. *et al.* Hypomorphic Recessive Variants in SUFU Impair the Sonic Hedgehog Pathway and Cause Joubert Syndrome with Cranio-facial and Skeletal Defects. *Am. J. Hum. Genet.* **101**, 552–563 (2017).
143. Svärd, J., Rozell, B., Toftgård, R. & Teglund, S. Tumor suppressor gene co-operativity in compound Patched1 and suppressor of fused heterozygous mutant mice. *Mol. Carcinog.* **48**, 408–419 (2009).
144. Weng, R. R. *et al.* Super-Resolution Imaging Reveals TCTN2 Depletion-Induced IFT88 Lumen Leakage and Ciliary Weakening. *Biophys. J.* **115**, 263–275 (2018).
145. Sang, L. *et al.* Mapping the NPHP-JBTS-MKS protein network reveals ciliopathy disease genes and pathways. *Cell* **145**, 513–528 (2011).

146. Shaheen, R. *et al.* A TCTN2 mutation defines a novel Meckel Gruber syndrome locus. *Hum. Mutat.* **32**, 573–578 (2011).
147. Wang, C., Li, J., Meng, Q. & Wang, B. Three Tctn proteins are functionally conserved in the regulation of neural tube patterning and Gli3 processing but not ciliogenesis and Hedgehog signaling in the mouse. *Dev. Biol.* **430**, 156–165 (2017).
148. Thomas, S. *et al.* TCTN3 mutations cause Mohr-Majewski syndrome. *Am. J. Hum. Genet.* **91**, 372–378 (2012).
149. Abdelhamed, Z. A. *et al.* Variable expressivity of ciliopathy neurological phenotypes that encompass Meckel-Gruber syndrome and Joubert syndrome is caused by complex de-regulated ciliogenesis, Shh and Wnt signalling defects. *Hum. Mol. Genet.* **22**, 1358–1372 (2013).
150. Shaheen, R. *et al.* Identification of a novel MKS locus defined by TMEM107 mutation. *Hum. Mol. Genet.* **24**, 5211–5218 (2015).
151. Christopher, K. J., Wang, B., Kong, Y. & Weatherbee, S. D. Forward genetics uncovers Transmembrane protein 107 as a novel factor required for ciliogenesis and Sonic hedgehog signaling. *Dev. Biol.* **368**, 382–392 (2012).
152. Latour, B. L. *et al.* Dysfunction of the ciliary ARMC9/TOGARAM1 protein module causes Joubert syndrome. *J. Clin. Invest.* **130**, 4423–4439 (2020).

Chapter 2: Systematic analysis of cilia characteristics and Hedgehog signaling in five immortal cell lines

Authors: Arianna Gómez[1], Julie Craft Van De Weghe[1], Malaney Finn[1], and Dan Doherty[1]
[1]University of Washington, Department of Pediatrics

Conceptualization, investigation, data analysis, and writing (drafting and review/editing) performed by AG. Investigation, validation, and review/editing of chapter performed by MF. Conceptualization and review/editing of chapter performed by JCV and DD.

Abstract

Dysfunction of the primary cilium, a microtubule-based signaling organelle, leads to genetic conditions called ciliopathies. Hedgehog (Hh) signaling is mediated by the primary cilium in vertebrates and is therefore implicated in ciliopathies; however, it is not clear which immortal cell lines are the most appropriate for modeling pathway response in human disease; therefore we systematically evaluated Hh in five commercially available, immortal mammalian cell lines: ARPE-19, HEK293T, hTERT RPE-1, NIH/3T3, and SH-SY5Y. All of the cell lines ciliated adequately for our subsequent experiments, except for SH-SY5Y which were excluded from further analysis. hTERT RPE-1 and NIH/3T3 cells relocalized Hh pathway components Smoothened (SMO) and GPR161 and upregulated Hh target genes in response to pathway stimulation. In contrast, pathway stimulation did not induce target gene expression in ARPE-19 and HEK293T cells, despite SMO and GPR161 relocalization. These data indicate that human hTERT RPE-1 cells and murine NIH/3T3 cells, but not ARPE-19 and HEK293T cells, are suitable for modeling the role of Hh signaling in ciliopathies.

Background

Primary cilia are microtubule-based organelles that transduce light, mechanical, and chemical signals into cells.[1] Protruding from the surface of most cell types, primary cilia mediate multiple signaling pathways, including Hedgehog (Hh), that play important roles in development and tissue homeostasis. Cilium dysfunction results in conditions called ciliopathies, and while abnormal Hh signaling has been described in models of ciliopathy-associated genes, details of the disease mechanism have not been clearly elucidated.[2] Immortal cell lines are frequently used to study primary cilium biology and the mechanisms underlying ciliopathies;[3–6] however, the strengths and weaknesses of commonly used human cell lines have not been systematically compared. The goal of this study was to identify immortal cell lines suitable for studying Hh signaling in human health and disease.

In vertebrates, the primary cilium modulates the canonical Hh signaling pathway through the coordinated translocation of Hh pathway proteins in and out of the cilium (reviewed in [7]). In the absence of Hh ligand, ciliary localization of the Patched (PTCH) receptor indirectly represses ciliary localization of Smoothened (SMO), maintaining the

pathway in an inactive state. This repression is reinforced by ciliary GPR161, an orphan constitutively active G-coupled protein receptor and negative regulator of the pathway, which maintains high ciliary cyclic AMP (cAMP) levels which in turn increases protein kinase A (PKA) activity. Increased PKA activity lead to proteolytic cleavage of GLI transcription factors into their repressor forms, maintaining expression of target genes low.[8] During pathway stimulation, Hh ligand binds PTCH, promoting its export from the cilium, which results in SMO entry and GPR161 exit. In concert, GLI2/3, KIF7, and Suppressor of Fused (SUFU) localization to the ciliary tip increases, and is associated with reduced GLI2/3 cleavage.[9,10] Uncleaved GLI2/3 activator forms translocate to the nucleus and induce transcriptional targets including *GLI1* and *PTCH1.*[11,12] In this work, we focus on canonical Hh signaling because it has been implicated in the mechanisms underlying ciliopathies across multiple model systems. We compare two steps in the Hh pathway in immortal cell lines: initial ciliary localization of Hh pathway components and downstream Hh target gene expression.

Results

Cell line selection

We identified candidate models for human Hh signaling by evaluating the following characteristics in commercially available cell lines: human-derived, evidence of ciliation, immortal, required imaging characteristics (adherent, monolayer growth), evidence of Hh pathway response, and genetic tractability. ARPE-19, HEK293T, hTERT RPE-1, NIH/3T3, and SH-SY5Y cells met most criteria (Table 2.1). We included murine NIH/3T3 cells as a non-human control since these cells are frequently used to model Hh pathway function.[6,20–22]

	ARPE-19	HEK293T	hTERT RPE-1	SH-SY5Y	NIH/3T3
Cell origin	Retinal pigment epithelial cells	Embryonic kidney cells	Retinal pigment epithelial cells	Bone marrow derived Neuroblastoma cells	Murine embryonic fibroblast cells
Human-derived	Y	Y	Y	Y	N
Ciliated	Y	Y	Y	Y	Y
Immortal	Y	Y	Y	Y	Y
Adherent	Y	S	Y	Y	Y
Monolayer growth	Y	N	Y	N	Y
Hh pathway response	Y	Y	Y	Y	Y
Gross chromosomal abnormalities	N	Y	N	N	N
Genetic tractability	Y	Y	Y	NR	Y

Table 2.1. Desired cell line characteristics for modeling Hh signaling. We searched the literature for evidence of the desired characteristics listed. ATCC often provided information about the following categories: human-derived, immortal, gross chromosomal abnormalities. When considering any known response to Hedgehog signaling, this included assays that measured response differently from the assays discussed in this paper (i.e. GLI3 processing, GLI luciferase assays). Y= Yes, N= No, S = semi-adherent, NR= Not reported.

Proportion of cells with cilia

While all the cell lines have been reported to ciliate, the time course of ciliation for different cell lines is scattered across studies.[23,24] Therefore, we aimed to define the optimal serum starvation conditions for Hh signaling experiments by determining the proportion of ciliated cells across time points after serum starvation: 0, 8, 16, 24, 48, 72, and 96 hours. Serum starvation removes growth factors available to cells, causing cells to drop out of the cell cycle and promoting ciliogenesis. For Hh imaging assays, we wanted cells to be in a monolayer, but we were unable to measure the 96-hour time point for HEK293T cells because they became overgrown when grown for >72 hours under standard conditions.

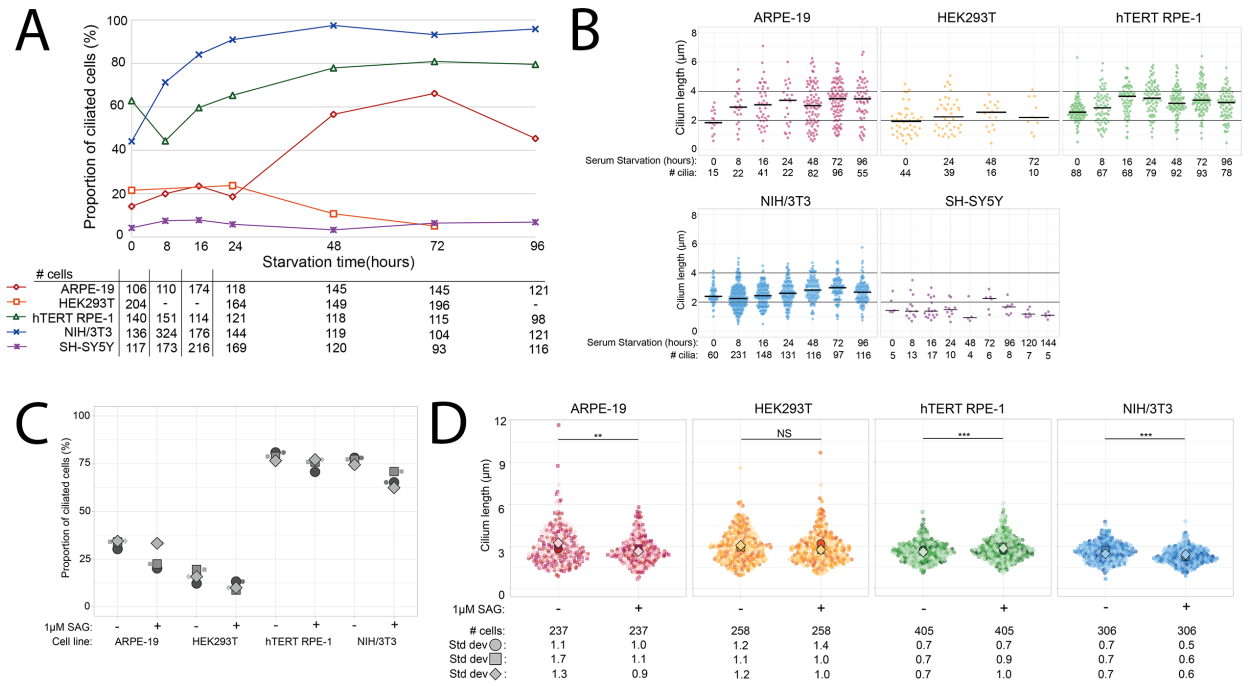

Figure 2.1. Ciliation time course and cilia length for immortal cell lines. A) Proportion of ciliated cells at 0, 8, 16, 24, 48, 72, and 96 hours post serum starvation. The numbers of cells counted at each time point are listed below each column of the graphs. B) Cilium length across time points. Black bars across graphs delineate 2 and 4µm. Black bars in each column represent median length. C) Proportion of ciliated cells without and with stimulation. Each symbol represents the proportion of ciliated cells in one batch. D) Cilium length without stimulation and with stimulation. Large symbols = median cilium length within a batch. Small symbols = cilium length of one cilium. One coverslip was imaged for each cell line and time point. The total number of cells counted across three batches are listed below each column of the graphs.

Baseline ciliation varied between cell types, ranging from ~5% in SH-SY5Y to ~62% in hTERT RPE-1 (Figure 2.1). Serum starvation was associated with >15% higher ciliation rates over baseline in ARPE-19, hTERT RPE-1, and NIH/3T3 cell lines. Peak ciliation in these cell lines typically occurred 48 hours post-starvation and ranged from 56% in ARPE-19 to 97% in NIH/3T3. In contrast, HEK293T and SH-SY5Y ciliation rates were the same with and without serum starvation.

SH-SY5Y cells ciliated at low proportions through 96 hours of starvation, prompting us to evaluate 120- and 144-hour time points to determine whether ciliation was delayed compared to other cell lines. Even with prolonged starvation, <8% of SH-SY5Y cells had cilia at each time point (Supplementary Figure 2.1).

We and others have previously documented proportions of ciliated HEK239T cells >20%.[25] To determine whether the low proportions of cells with cilia was a characteristic of the specific isolate of HEK293T cells, we repeated the time course experiment using three different isolates of HEK293T cells in our collection (Supplementary Figure 2.2A). Baseline ciliation rates were similar to our initial experiment (~20%) and increased to 32-39% by 24 hours. At 48 and 72 hours, the proportion of cells with cilia was lower than at 24 hours. We compared images of areas monolayer and multilayer growth, finding that more densely grown areas had more cilia (Supplementary Figure 2.2B,C). For the Hh experiments described below, we continued with monolayer cultures to allow for accurate quantitative immunofluorescence measurements.

Cilium length

We measured cilium length across all timepoints (Figure 2.1B). Cilium length was shorter at 0 hours for ARPE-19, HEK293T, hTERT RPE-1, and NIH/3T3 cells, stabilizing between 8-24 hours, while cilium length was similar across timepoints in SH-SY5Y cells. Maximum median length for each cell line was 3.5μm for ARPE-19 (SD ±1.2μm), 2.5μm for HEK293T (SD ±0.9μm), 3.6μm for hTERT RPE-1 (SD ±1.0μm), 3.0 μm for NIH/3T3 (SD ±0.8μm), and 2.3μm for SH-SY5Y cells (SD ±0.6μm). Based on the low ciliation rate and exceptionally short cilia, we did not continue evaluating SH-SY5Y cells for Hh pathway response.

Hedgehog pathway response

We next measured canonical Hh pathway activity in the cell lines using two Hh pathway assays commonly reported in the literature: 1) upstream localization of Hh pathway effectors SMO and GPR161 into and out of the cilium, respectively,[8,26] and 2) downstream target gene (*GLI1* and *PTCH1)* induction.[11]

Hh pathway protein localization

We measured the ciliary localization of SMO and GPR161 in unstimulated and Smoothened agonist (SAG) stimulated cells using our established quantitative immunofluorescence (qIF) protocol that determines relative protein localization between different cell lines and conditions.[15]

Proportion of cells with cilia and cilium length in response to Hh stimulation

Proportion of ciliated cells and cilium length were moderately affected by pathway stimulation (Figure 2.1C, D). Proportion of ciliated cell was lower in stimulated cells compared to unstimulated cells across cell lines in a majority of batches. Cilium length was significantly decreased in ARPE-19 and NIH/3T3 cells, significantly increased in hTERT RPE-1 cells, and was not significantly different in HEK293T cells.

SMO localization

Normalized mean ciliary SMO signal was significantly higher in stimulated cells compared to unstimulated cells across all cell lines, with fluorescence intensity reported in arbitrary units (au): 1.5 – 2.6 au in ARPE-19 (SD ±0.7 – 1.1), 1.2 – 2.7 au in HEK293T (SD ±0.9 – 1.6), 2.1 – 2.9 au in hTERT RPE-1 (SD ±0.7 – 0.9), and 7.0 – 10.3 au in NIH/3T3 cells (SD ±0.5) (Figure 2.2A). In ARPE-19 and HEK293T cells, SMO ciliary fluorescence intensity was weaker and background signal was higher compared to hTERT RPE-1 and NIH/3T3 cells (Supplementary Figure 2.2A).

GPR161 localization

We detected cilium-specific GPR161 signal in HEK293T and hTERT RPE-1 cells, a faint cilium-specific signal in ARPE-19 cells, and no cilium-specific signal in NIH/3T3 cells (Figure 2.2B), so we could not measure GPR161 response in NIH/3T3 cells. Across three batches, normalized mean GPR161 intensity was lower with SAG stimulation: 0.57- 0.73 au in ARPE-19 (SD ±0.5 – 0.6), 0.64 - 0.76 au in HEK293T (SD ±0.7 – 0.8),

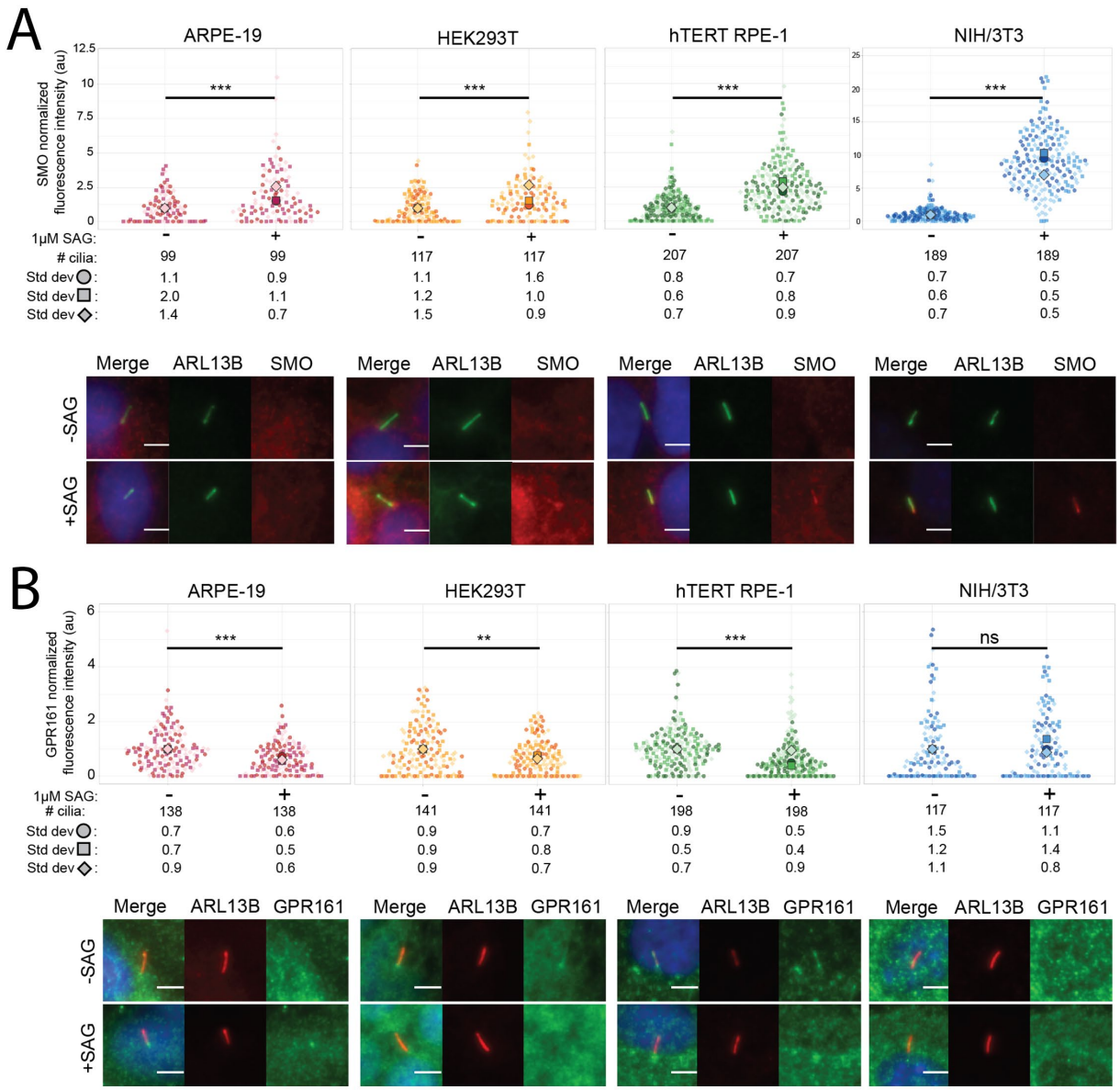

Figure 2.2. SMO and GPR161 localization in response to Hh pathway stimulation. Normalized fluorescence intensity (au) of A) SMO and B) GPR161 with and without pathway stimulation. Large symbol = median normalized fluorescence intensity for individual coverslip data. Small symbol = normalized fluorescence intensity of one cilium. Measurement from three separate batches are indicated by a unique symbol shape and color. Total number of cilia measured listed in the second row below the graph. Representative images are shown below graphs for unstimulated (-SAG) and stimulated (+SAG) cells. Two-tailed Student's *t*-test was performed. *P*-values represented significant differences if they ranged from 0.01 to 0.05 (*), 0.001 to 0.01 (**), and <0.001 (***).

and 0.40 – 0.95 au in hTERT RPE-1 (SD ±0.4 – 0.9) (Figure 2.2B). For one of the three

hTERT RPE-1 passages (Batch 3), the GPR161 signal was the same with and without stimulation. We suspect that this was due to an undetermined technical issue since hTERT RPE-1 cells responded when we repeated the experiment on an additional passage (Supplementary Figure 2.2C).

Hh target gene expression

GLI1 and *PTCH1* are direct transcriptional outputs of the canonical Hh pathway and are commonly used to measure pathway activity.[11] To measure *GLI1* and *PTCH1* expression, we optimized our quantitative PCR assays using the $2^{-\Delta\Delta CT}$ method.[27]

To accurately measure transcriptional responses to pathway stimulation using the $2^{-\Delta\Delta CT}$ quantitative PCR method, we identified suitable reference genes whose expression levels were similar to *GLI1* and *PTCH1* (>20 cycles, <30 cycles) and did not change with pathway stimulation in each cell line. We searched the literature for commonly used reference genes, identifying ten candidates for human cell lines and nine candidates for the mouse cell line (Methods table 2.1). We chose the genes with the most similar expression levels in stimulated and unstimulated cells, with the amplification cycles closest to *GLI1* and *PTCH1*: *PUM1* for ARPE-19 cells, *TBP* and *PMBS* for HEK293T cells, *TBP* for hTERT RPE-1 cells, and *Sdha* for NIH/3T3 cells (Supplementary Figure 2.4). We also used murine specific *Gli1* and *Ptch1* primer sets for NIH/3T3 cells. Although we tested *TBP* and *PMBS* for HEK293T, and used *PMBS* in our experiment, neither was ideal: *TBP* expression was variable in stimulated cells, and *PMBS* expression varied with stimulation in one out of the three batches (Supplementary Figure 2.4).

In hTERT RPE-1 cells, *GLI1* expression was 2.8 to 3.8-fold higher and *PTCH1* expression was 1.7 to 1.9-fold higher with stimulation (Figure 2.3). In contrast, stimulation was not associated with marked expression differences in ARPE-19 cells (*GLI1* 0.9 to 1.4-fold, *PTCH1* 1.0 to 1.1-fold) or HEK293T cells (*GLI1* 0.5 to 1.7-fold, *PTCH1* 0.3 to 0.7 fold), consistent with the lack of relocalization of SMO and GPR161 with SAG stimulation. Strikingly, *Gli1* expression was 1993 to 3034-fold higher with stimulation in NIH/3T3 cells. Similarly, *Ptch1* expression was also markedly higher (46 to 70-fold).

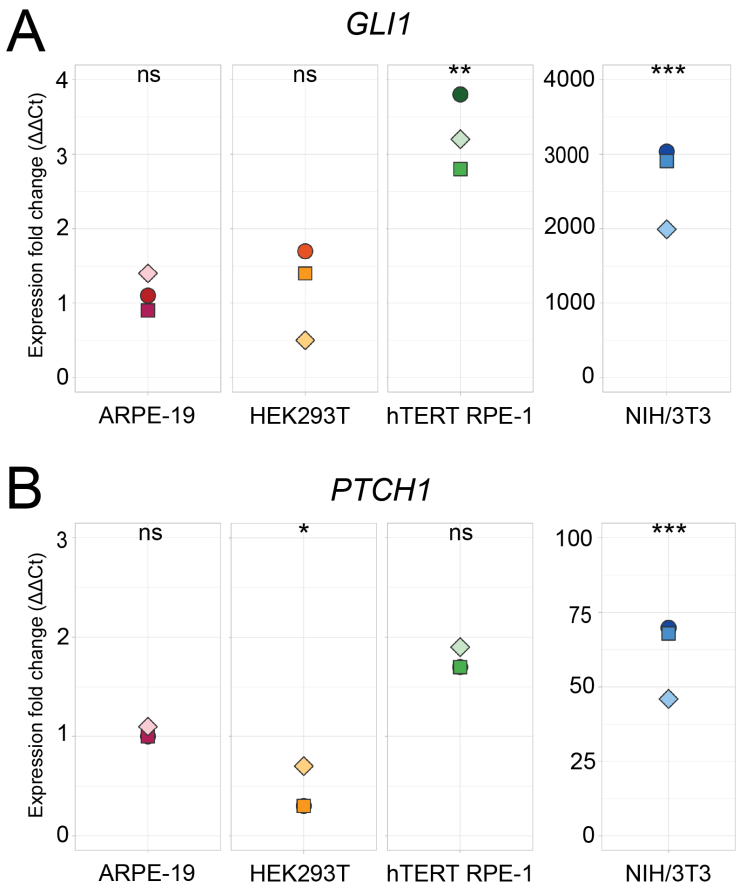

Figure 2.3. *GLI1* and *PTCH1* expression in response to Hh pathway stimulation. A) *GLI1* and B) *PTCH1* target gene induction. Each data point represents the expression fold change of stimulated cells from the same batch. Expression fold change was normalized to unstimulated values, which were set to 1. Two-tailed Student's *t*-test was performed. *P*-values represented significant differences if they ranged from 0.01 to 0.05 (*), 0.001 to 0.01 (**), and <0.001 (***).

Discussion

This systematic evaluation of cilium characteristics and Hh signaling in five commercially available, immortal, mammalian cell lines revealed that hTERT RPE-1 and NIH/3T3 cells are suitable for modeling Hh signaling (Table 2.2). By using the same assays in different cell types, we determined differences in response to Hh stimulation. Based on our experiments, SH-SY5Y cells were not suitable because of their low ciliation rate and very short cilia. ARPE-19 and HEK239T cells localized the Hh pathway proteins SMO and GPR161 in response to stimulation; however, they did not upregulate the Hh target genes *GLI1* and *PTCH1.* Only hTERT RPE-1 and NIH/3T3 cells ciliated well and showed robust responses to stimulation in both sets of assays. Our

experiments also demonstrate that Hh pathway stimulation moderately impacts ciliation rates and cilium length across all of the cell lines, but not in a consistent manner across batches. We observed a range of responses to stimulation, from minimally responsive (ARPE-19 and HEK293T), to modestly responsive (hTERT RPE-1) to robustly responsive (NIH/3T3) (Table 2.2). It is not clear whether this represents species-specific or cell line-specific differences, but it does indicate that results should be validated across model systems before they can be considered generalizable.

	Max proportion of cells with cilia	**Cilium length (mean)**	**SMO and GPR161 response to stimulation**	***GLI1*/*PTCH1* induction**
ARPE-19	65% (72 hr)	3.0μm	SMO: ↑2.50-fold GPR161: ↓0.25-fold	*GLI1*: ND *PTCH1*: ND
HEK293T	22% (24 hr)[1]	2.0μm	SMO: ↑2.50-fold GPR161: ↓0.25-fold	*GLI1*: ND *PTCH1*: ND
hTERT RPE-1	80% (72 hr)	3.1μm	SMO: ↑2.50-fold GPR161: ↓0.50-fold	*GLI1*: ↑3-fold *PTCH1*: ↑2-fold
NIH/3T3	97% (48 hr)	2.9μm	SMO: ↑9.50-fold GPR161: ND	*GLI1*: ↑3000-fold *PTCH1*: ↑60-fold
SH-SY5Y	8% (16 hr)	1.3μm		

Table 2.2. Overview of results. We summarized the outcome of our ciliary characterization and Hedgehog assays. hTERT RPE-1 cells were the most response human-derived cell line and NIH/3T3 cells were the most responsive cell line overall. We did not measure SH-SY5Y response to Hedgehog signaling because of low proportion of ciliated cells and short cilia.
[1]In follow-up experiments, proportion of ciliated cells was increased by allowing cells to grow at a higher density.

It is also clear from our experiments that each Hh assay requires optimization for each cell line. Prior to assessing Hh response, we had to determine acceptable seeding, growth conditions, and fixation. In HEK293T cells, we had to balance the upside of higher ciliation rates in confluent cultures with the downside of overlapping cells complicating qIF measurements; therefore, low ciliation rates in HEK293T cells may have contributed to the low Hh target gene induction.

For our qIF experiments, we had to identify antibodies that worked across cell

lines and were specific to the protein of interest. The limited response to SAG stimulation in ARPE-19 and HEK293T cells could be due to difference in expression of Hh negative regulators in these cell lines that differ from hTERT RPE-1 and NIH/3T3 cells, for example SUFU expression which complexes with GLI2/3 and stabilizes the activator forms of the proteins.[28] Alternatively, these cells might respond to native Hh ligand or other agonists, but not SAG. There is prior evidence that hTERT RPE-1 and NIH/3T3 cells relocalize SMO and GPR161 and upregulate pathway target genes in response to Hh stimulation.[22,29,30] ARPE-19 cells have been used to determine Hh response to cyclopamine, a down-regulator of the pathway.[31] We could not detect Gpr161 in NIH/3T3 cells by immunofluorescence, despite the 94% amino acid identity between the human and mouse for the antigen used to generate the antibody. This may be due to differences between the human and mouse proteins at the key epitopes recognized by the polyclonal antibody. Alternatively, Gpr161 expression has been demonstrated in other studies using different stimulation time points.[32] Future work could explore ligand dose-response, and optimal timing for SMO and GPR161 localization in response to Hh stimulation.

qPCR also needs to be tailored to each line. We optimized primer sets, template concentrations, and amplification parameters. Importantly, expression of the commonly used reference gene, *GAPDH,* differed between unstimulated and stimulated HEK293T cells. *GAPDH* expression responds to serum starvation,[33,34] adding to the importance of screening reference genes for each cell line. During *GLI1* primer optimization, we identified high CT values in our cell lines (>30 CT), which introduces variability.[35] To bring the CT values into a better range, we increased template concentration and added a touchdown step in ARPE-19 and HEK293T, lowering the CT values by 3-4 cycles.[17] Unstimulated NIH/3T3 samples also had a CT >30, but the touchdown step did not decrease CT values in this cell line, suggesting the *GLI1* expression is below the level of detection in this cell line and increases substantially with stimulation.

While we confirmed that hTERT RPE-1 and NIH/3T3 cells are appropriate cell lines to model Hh signaling, we have not demonstrated that they recapitulate all aspects of Hh signaling across cell types *in vivo*; therefore, Hh experiments in these cell lines should be validated in additional models, ideally *in vivo*. In addition, we have not fully

excluded ARPE-19 and HEK293T cells as potential models, since we did not evaluate all aspects of Hh signaling such as dose-response to ligand, time course, and other important characteristics. If there were compelling reasons to use these cell lines for Hh-related experiments, further characterization might reveal intact Hh responses at different timepoints or different agonist concentrations.

hTERT RPE-1 and NIH/3T3 cells respond consistently to Hh pathway stimulation across two standard assays and are genetically tractable. Many of these characteristics have been discussed casually at meetings, but this work provides a resource for the cilium community. These cell lines provide models originating from two organisms and could be used individually or in parallel to study Hh response. hTERT RPE-1 cells are a good model system for exploring these mechanistic details at the cellular level, therefore, we decided to use them for our experiments generating a library of loss of function JS-associated gene mutants, which will be discussed in Chapter 3.

Methods

Cell culture

Cell lines were obtained from the American Type Cell Collection (ATCC, www.atcc.org) and grown in cell specific medium. ARPE-19 (ATCC, CRL-2302) and hTERT RPE-1 (ATCC, CRL- 4000) cells were cultured in DMEM/F12 with 10% fetal bovine serum (FBS) and 1% penicillin-streptomycin. HEK293T (ATCC, CRL-3216) cells were cultured in DMEM with 10% FBS and 1% penicillin-streptomycin. NIH/3T3 (ATCC, CRL-1658) cells were cultured in DMEM with 10% bovine calf serum and 1% penicillin-streptomycin. SH-SY5Y (ATCC, CRL-2266) cells were cultured in 1:1 Eagle's Minimum Essential Medium:F12 with 10% FBS and 1% penicillin-streptomycin. 0.05% trypsin was used for all cell dissociation.

Time course assay

For each set of experiments, cells were seeded on pairs of coverslips coated with 0.3mg/mL poly-D-lysine and allowed to grow for 2-3 days, until they reached 60-80% confluency. We define batches as cells that were grown, treated, and collected at the same time. After reaching the desired confluency, we serum starved the first pair of coverslips that would be starved for the longest time point (96- or 72-hours). Serum starvation included removing the complete growth medium, rinsing with PBS, and adding serum free medium. This step was repeated for each time point, with all coverslips from the same cell line and batch collected at the end of the time course (0-hour serum starvation). We placed the plates holding the coverslips on ice for 10 minutes, then fixed coverslips using 4% paraformaldehyde for 5 minutes followed by permeabilization using cold methanol for 3 minutes and stored in PBS at 4°C until ready to stain. We only stained one coverslip from the pair, leaving the replicate available as a backup.

For HEK293T cells, we incubated the 0.3 mg/mL poly-D-lysine coated coverslips with 0.05% gelatin for 15-20 minutes prior to seeding cells to promote adhesion since this cell line is semi-adherent. Otherwise, we followed the same seeding and fixation method described above.

All plots were generated using Plots of Data and Super Plots of Data.[13,14]

Hedgehog pathway protein

Cells in the same batch were seeded on pairs of coverslips and allowed to expand until they reached 60-80% confluency, as above. Cells were serum starved for a total of 48 hours. After the initial 24 hours of serum starvation, we replaced the media on half of the coverslips with serum free medium + 1μM Smoothened Agonist (SAG) (Millipore, 566661). We placed the plates holding the coverslips on ice for 10 minutes, then fixed coverslips using 4% paraformaldehyde for 5 minutes followed by permeabilization using cold methanol for 3 minutes and stored in PBS at 4°C until ready to stain. We only stained one coverslip from the pair, leaving the replicate available as a backup.

Quantitative immunofluorescence

We blocked coverslips in 2% bovine albumin serum (BSA) in phosphate buffered solution (PBS) for 20 minutes at room temperature. Time course assay coverslips were incubated with mouse anti-acetylated α-tubulin (1:2000, Sigma Aldrich, T6793) and rabbit anti-ARL13B (1:800, Proteintech, 17711-1-AP) antibodies diluted in blocking buffer. Hedgehog pathway protein localization coverslips were incubated with either 1) mouse anti-SMO (1:50, Santa Cruz Biotechnology, sc-166685) and rabbit anti-ARL13B (1:800, Proteintech, 17711-1-AP) antibodies or 2) mouse anti-ARL13B (1:200, NeuroMab, 75-287) and rabbit anti-GPR161 (1:200, Proteintech, 13398-1-AP) antibodies diluted in blocking buffer. Coverslips were incubated with primary antibodies for 1 hour at room temperature or at 4°C overnight, then washed in PBS for 5 minutes, three times. Coverslips were incubated with the following secondary antibodies at 1:400 dilution for 1 hour at room temperature: Goat anti-Rabbit IgG, Alexa Fluor 488 (Thermo Fisher Scientific #A11008) and Donkey anti-Mouse IgG, Alexa Fluor 568 (Thermo Fisher Scientific, #A10037). After incubation, we washed coverslips in PBS for 5 minutes, three times. Coverslips were mounted on slides using a Fluoromount with DAPI (Invitrogen, #00-4959-52), then sealed with nail polish after sitting for at least 1 hour.

We quantified ciliary protein localization using a validated protocol previously established in the laboratory.[15] We imaged coverslips using the same microscopy settings to acquire z-stack images for >20 cells with cilia for each condition and batch using

identical microscope settings. We converted z-stack images to sum-projections and randomized these images using the FIJI[16] script, Filename_randomizer (https://imagej.nih.gov/ij/macros/Filename_Randomizer.txt) to minimize bias between cell lines and conditions. Prior to data collection, we checked a subset of images to ensure that the cilium marker (ARL13B) and protein of interest (SMO or GPR161) signals were adequate for measurement. Blinded to the condition, we drew a cilium mask in the cilium marker channel (ARL13B) using summed Z-stack images in ImageJ. We used this mask to measure the signal intensity for the protein of interest and measured the signal intensity of an adjacent region to subtract background signal. Normalized fluorescence intensity was calculated using the following formula:

$$\frac{(Un)stimulated\ (Cilium\ average\ fluorescence\ intensity - Background\ average\ fluorescence\ intensity)}{\bar{x}\ Unstimulated\ (Cilium\ average\ fluorescence\ intensity - Background\ average\ fluorescence\ intensity)}$$

Finally, we unblinded the data and visually inspected the images to ensure that our qualitative assessment of ciliary signal was consistent with the quantitative data. We also used the same data set to determine proportion of cells with cilia and cilium length in baseline and stimulated cells.

GLI1 and *PTCH1* qPCR

Cells were grown in pairs of T-75 cell culture flasks until 60-80% confluent, then starved for a total of 48 hours. After the initial 24 hours, half the flasks had their media replaced with serum free medium + 1μM SAG. We dissociated the cells and extracted RNA using the Aurum Total RNA mini kit (Biorad, 7326820). We measured RNA concentration using a spectrophotometer and only included RNA that had an A260/280 >1.8. cDNA was generated using the BioRad iScript cDNA Synthesis kit. We set up qPCR reactions using the PowerUp SYBR Green Master Mix (Thermo Fisher Scientific, #A25741). For cell lines that required the touchdown qPCR protocol, we followed the protocol outlined in Zhang et al.[17] Briefly, the touchdown qPCR protocol went as follows: 50C (2 min), 95C (2 min), 4x [95C (20 sec), 65C (10 sec, decrease 3C/cycle, 72C (1 min)], 40x [95C (15 sec), 55C (15 sec), 72C (1 min)], ending with a melt temperature curve. qPCR data acquisition was performed on the Bio-Rad CFX96 Touch Real-Time PCR Detection System.

Human *GLI1* primers
Forward 5'-GATGACCCCACCACCAATCAGTAG-3'
Reverse 5'-AGACAGTCCTTCTGTCCCCACA-3'
Human *PTCH1 primers*
Forward 5'-GAGCACTTCAAGGGGTACGA-3'
Reverse 5'-GGAAAGCACCTTTTGAGTGG-3'
Mouse *Gli1* primers
Forward 5'-CCGACGGAGGTCTCTTTGTC-3'
Reverse 5'-GCGTCTCAGGGAAGGATGAG-3'
Human *Ptch1 primers*
Forward 5'-GAGCAGATTTCCAAGGGGAAG -3'
Reverse 5'-CCACAACCAAAAACTTGCCG -3'

Reference gene identification

To ensure robust data acquisition, we identified an ideal reference gene for each cell line. We identified 10 human candidate reference genes and 9 mouse candidate reference genes (Methods Table 2.1) to evaluate expression stability between baseline and stimulated cDNA. To select a reference gene, we evaluated the cycle threshold (CT) of three starting primer concentrations, and cDNA dilution curve efficiency.[18]

In our initial screen, we were looking for 1) small ΔCT between unstimulated and stimulated within each cell line, indicating unchanged expression level between experimental conditions, and 2) a CT between 20-30 cycles so that expression levels were similar to *GLI1* and *PTCH* expression. We optimized primer concentration by diluting forward and reverse primers sets to three concentrations, 3μM, 5μM, and 7μM. Next, we determined primer efficiency by performing a cDNA dilution series. We followed widely accepted primer efficiency standards, which includes an efficiency of 80-120% and $R^2 \geq 0.99$.

During assay validation, we determined that *GLI1* in ARPE-19, HEK293T, and NIH/3T3 cells amplified at >29 cycles, close to the limit of reliable detection; therefore, we performed a modified qPCR assay in these cell lines, which included a touchdown step prior to the 40-cycle amplification. This lowered the detection level by 3 cycles in ARPE-19 and HEK293T cells. In NIH/3T3 cells, we did not see a difference in unstimulated cycle values and only saw a difference of 1 cycle in stimulated cells.

Gene symbol	Gene name	Forward and Reverse Primer
ACTB	Actin Beta	5'-GAGCACAGAGCCTCGCCTTT-3' 5'-TCATCATCCATGGTGAGCTGG-3'
GAPDH	Glyceraldehyde 3-phosphate dehydrogenase	5'-AGGTGAAGGTCGGAGTCAAC-3' 5'-TTCACACCCATGACGAACAT-3'
IPO8	Importin 8	5'-TGCAGTCCGGCCTACTGTTC-3' 5'-TGTAGGACTGGTTGAGCTCGTTC-3'
PUM1	Pumillio RNA Binding Family Member	5'-AAGGACAGCAGCAGGTTCTC-3' 5'-CCTTGTCCAAATGCAAGGGC-3'
RPLP0	Ribosomal Protein Lateral Stalk Subunit P0	5'-CGTCCTCGTGGAAGTGACAT-3' 5'-TAGTTGGACTTCCAGGTCGC-3'
SDHA	Succinate dehydrogenase complex flavoprotein subunit A	5'-GCATTTGGCCTTTCTGAGGC-3' 5'-TTGATTCCTCCCTGTGCTGC-3'
TBP	TATA Binding Protein	5'-GTGACCCAGCATCACTGTTTC-3' 5'-AGAGCATCTCCAGCACACTC-3'
UBC	Ubiquitin C	5'-CCGGGATTTGGGTCGCAG-3' 5'-TCACGAAGATCTGCATTGTCAAG-3'
YWHAZ	Tryosine 3-Monooygenase.Tryptophan 5-Monooygenase Activation Protein Zeta	5'-GACACAGAACATCCAGTCATGG-3' 5'-TCATATCGCTCAGCCTGCTC-3'
18S[19]	18S rRNA	5'-AGAAACGGCTACCACATCCA-3' 5'-CACCAGACTTGCCCTCCA-3'
Actb	Actin Beta	5'-TAGGCACCAGGGTGTGATG-3' 5'-TCTCCATGTCGTCCCAGTTG-3'
Gapdh	Glyceraldehyde 3-phosphate dehydrogenase	5'-AATGTGTCCGTCGTGGATCT-3' 5'-ATACGGCTACAGCAACAGGG-3'
Ipo8	Importin 8	5'-ACAAGCTCTGCTGACTGTGC-3' 5'-CAGTGTCCTTCGGTGCTCTG-3'
Pum1	Pumillio RNA Binding Family Member	5'-GAAAGGTAAGGGGGAGCGAG-3' 5'-CTCATTCCACCAACACGGGC-3'
Rplp0	Ribosomal Protein Lateral Stalk Subunit P0	5'-TCCTCGTTGGAGTGACATCG-3' 5'-AGTTGGACTTCCAGGTCGC-3'
Sdha	Succinate dehydrogenase complex flavoprotein subunit A	5'-ACTGTTATTGCTACTGGGGGC-3' 5'-CCCTAGTGACCATGGCTGTG-3'
Tbp	TATA Binding Protein	5'-GGTATCTGCTGGCGGTTTGG-3' 5'-GAAATAGTGATGCTGGGCACTG-3'
Ubc	Ubiquitin C	5'-CCCACACAAAGCCCCTCAAT-3' 5'-AAGATCTGCATCGTCTCTCTCACG-3'
Ywhaz	Tryosine 3-Monooygenase.Tryptophan 5-Monooygenase Activation Protein Zeta	5'-GGTATCTGCTGGCGGTTTGG-3' 5'-GAAATAGTGATGCTGGGCACTG-3'

Methods table 2.1. Candidate qPCR reference gene names and primer sequences. We included 10 candidate reference genes for human-derived cell lines and 9 candidate gene reference genes for the NIH/3T3 murine-derived cell line.

Statistical analysis

An unpaired two-tailed Student's *t*-test was performed for comparison between unstimulated and stimulated cells with a hypothesized mean difference of 0. α level was set at 0.05. $P < 0.05$ was significant. Symbols for significance represent *p*-values from 0.01 to 0.05 (*), 0.001 to 0.01 (**), and <0.001 (***).

Supplementary Figures

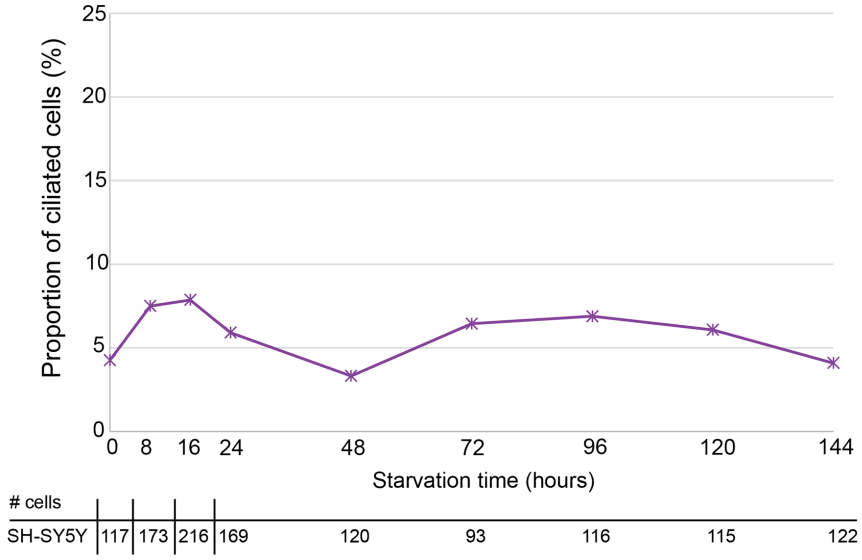

Supplementary Figure 2.1. Extended SH-SY5Y ciliation time course. Proportion of ciliated cells for SH-SY5Y cells from 0-144 hours. One coverslip was imaged for each timepoint, with number of cells counted at each time point listed below each column in the graph.

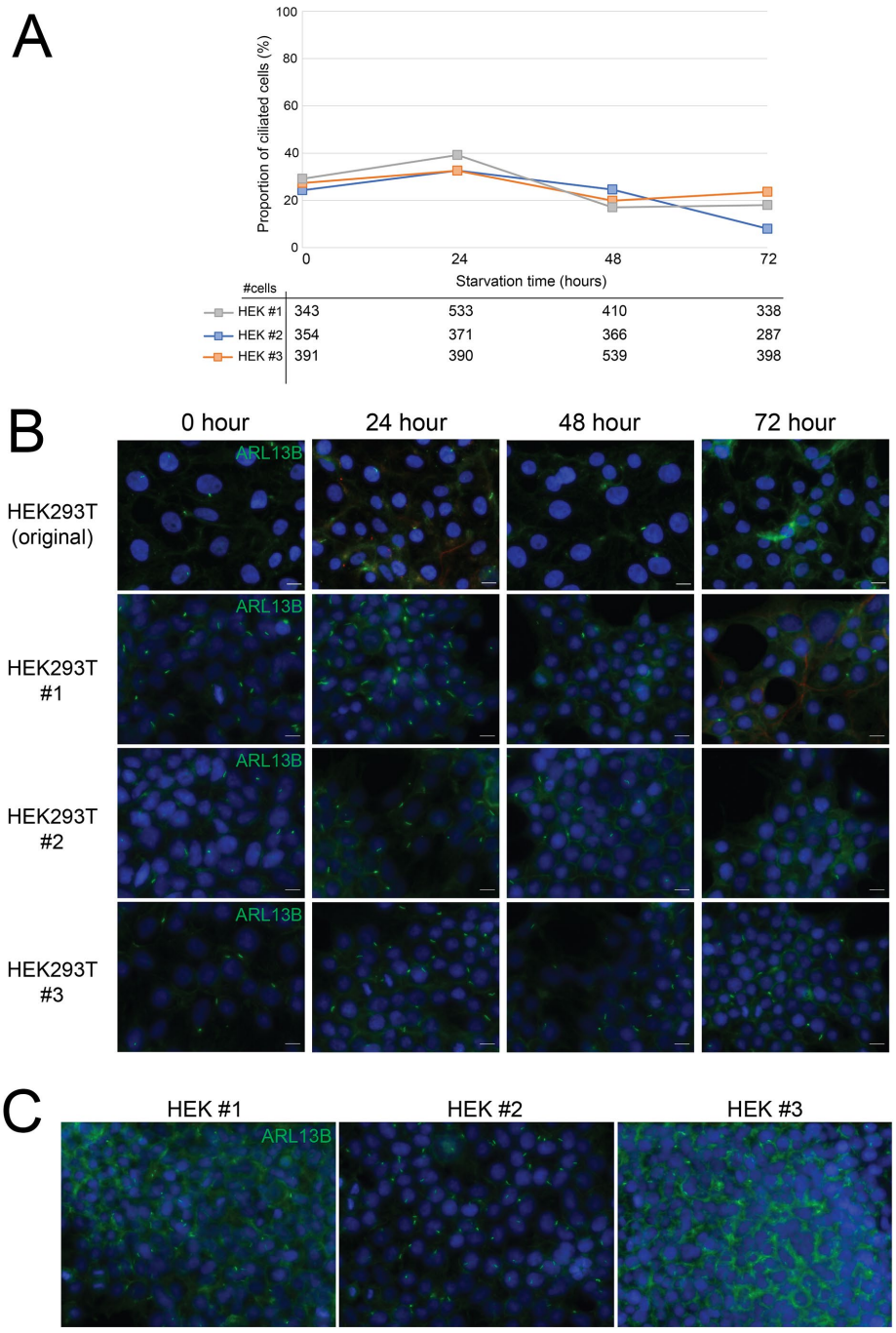

Supplementary Figure 2.2. HEK293T ciliation data. A) Proportion of ciliated HEK293T cells at 0, 24, 48, and 72 hours post serum starvation from additional thaws. B) Representative images of monolayer areas of HEK293T cell growth from Figure 1 (top row) and repeat experiments with additional thaws of HEK293T cells. Cilia were stained with anti-ARL13B antibody. C) Representative images displaying ciliation in areas with multi-layer growth from additional thaws of HEK293T cells. Cilia were stained with anti-ARL13B antibody. Scale bars are 10μm.

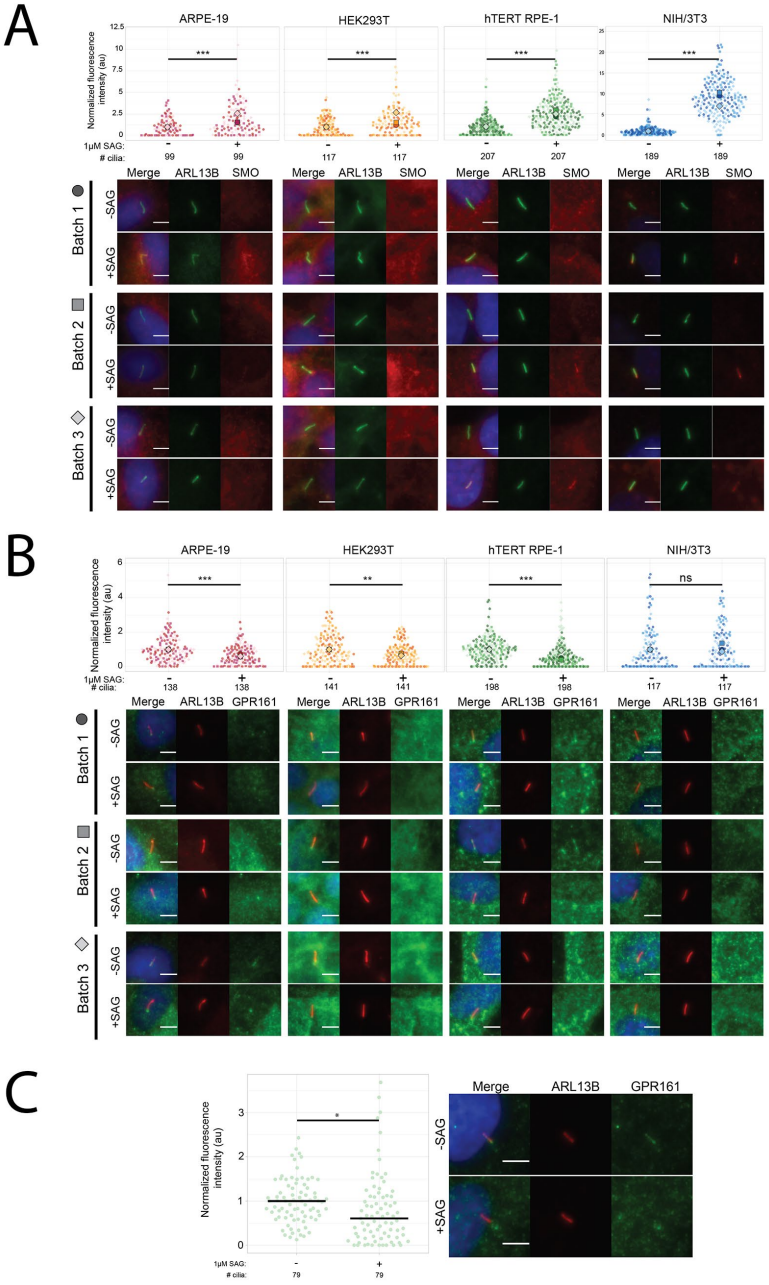

Supplementary Figure 2.3. GPR161 and SMO localization. Representative images from each batch showing variation in A) SMO and B) GPR161 localization. C) Normalized fluorescence intensity (arbitrary units, au) of GPR161 with and without stimulation in an additional passage of hTERT RPE-1 cells. Black bars = median normalized fluorescence intensity. Small symbol = normalized fluorescence intensity of one cilium. Numbers of cilia measured are listed below each column in the graph. Representative cilia are shown next to the graphs for unstimulated (-SAG) and stimulated (+SAG) cells. Scale bars are 5μm. T-test of equal variances was performed. p-values: * 0.01 to 0.05, ** 0.001 to 0.01, and *** <0.001.

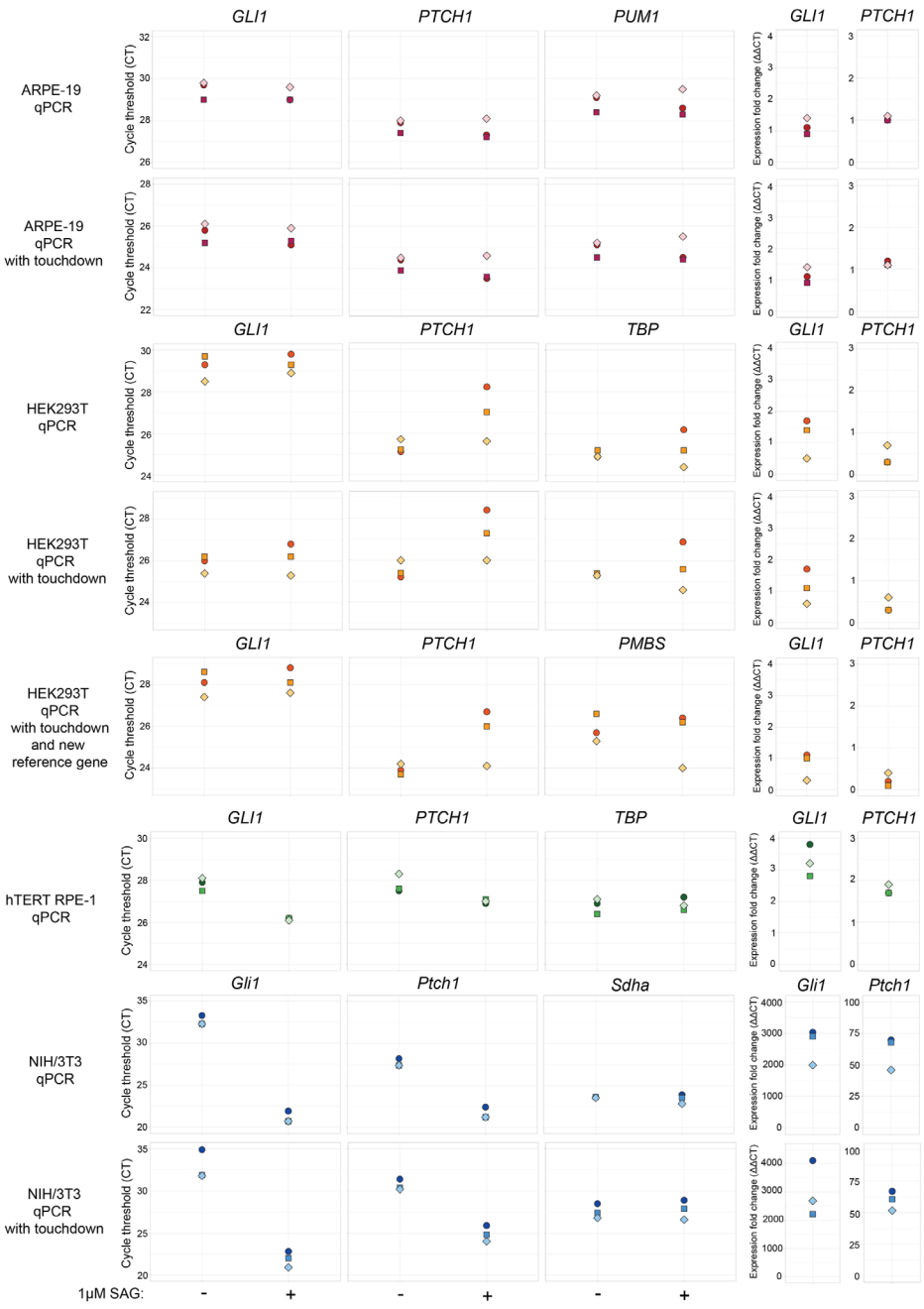

Supplementary Figure 2.4. Variable *GLI1*, *PTCH1*, and reference gene expression in response to Hh pathway stimulation. *GLI1, PTCH1,* and reference gene CT (cycle threshold) for ARPE-19, HEK293T, hTERT RPE-1, and NIH/3T3 cell lines with and without stimulation. For cell lines with high CT values (>29), we used a touchdown qPCR method. For each condition (with or without stimulation), we collected mRNA from three batches for each cell line. Normalized *GLI1* and *PTCH1* expression for each qPCR condition is on the far right. Each symbol in the left panels represents the average CT from three technical replicates for each batch. Each symbol in the right panels represents the expression fold change for each batch.

References

1. Berbari, N. F., O'Connor, A. K., Haycraft, C. J. & Yoder, B. K. The primary cilium as a complex signaling center. *Curr. Biol. CB* **19**, R526-535 (2009).
2. Goetz, S. C. & Anderson, K. V. The primary cilium: a signalling centre during vertebrate development. *Nat. Rev. Genet.* **11**, 331–344 (2010).
3. Pietrobono, S. *et al.* MAPK15 Controls Hedgehog Signaling in Medulloblastoma Cells by Regulating Primary Ciliogenesis. *Cancers* **13**, 4903 (2021).
4. Yoon, J. W. *et al.* Noncanonical regulation of the Hedgehog mediator GLI1 by c-MYC in Burkitt lymphoma. *Mol. Cancer Res. MCR* **11**, 604–615 (2013).
5. Hulleman, J. D. *et al.* A novel H395R mutation in MKKS/BBS6 causes retinitis pigmentosa and polydactyly without other findings of Bardet-Biedl or McKusick-Kaufman syndrome. *Mol. Vis.* **22**, 73–81 (2016).
6. Breslow, D. K. *et al.* A CRISPR-based screen for Hedgehog signaling provides insights into ciliary function and ciliopathies. *Nat. Genet.* **50**, 460–471 (2018).
7. Briscoe, J. & Thérond, P. P. The mechanisms of Hedgehog signalling and its roles in development and disease. *Nat. Rev. Mol. Cell Biol.* **14**, 416–429 (2013).
8. Mukhopadhyay, S. *et al.* The Ciliary G-Protein-Coupled Receptor Gpr161 Negatively Regulates the Sonic Hedgehog Pathway via cAMP Signaling. *Cell* **152**, 210–223 (2013).
9. He, M. *et al.* The kinesin-4 protein Kif7 regulates mammalian Hedgehog signalling by organizing the cilium tip compartment. *Nat. Cell Biol.* **16**, 663–672 (2014).
10. Wen, X. *et al.* Kinetics of Hedgehog-Dependent Full-Length Gli3 Accumulation in Primary Cilia and Subsequent Degradation. *Mol. Cell. Biol.* **30**, 1910–1922 (2010).
11. Platt, K. A., Michaud, J. & Joyner, A. L. Expression of the mouse Gli and Ptc genes is adjacent to embryonic sources of hedgehog signals suggesting a conservation of pathways between flies and mice. *Mech. Dev.* **62**, 121–135 (1997).
12. Haycraft, C. J. *et al.* Gli2 and Gli3 localize to cilia and require the intraflagellar transport protein polaris for processing and function. *PLoS Genet.* **1**, e53 (2005).
13. Postma, M. & Goedhart, J. PlotsOfData—A web app for visualizing data together with their summaries. *PLOS Biol.* **17**, e3000202 (2019).
14. Goedhart, J. SuperPlotsOfData—a web app for the transparent display and quantitative comparison of continuous data from different conditions. *Mol. Biol. Cell* **32**, 470–474 (2021).
15. Slaats, G. G. *et al.* MKS1 regulates ciliary INPP5E levels in Joubert syndrome. *J. Med. Genet.* **53**, 62–72 (2016).
16. Schindelin, J. *et al.* Fiji: an open-source platform for biological-image analysis. *Nat. Methods* **9**, 676–682 (2012).
17. Zhang, Q. *et al.* TqPCR: A Touchdown qPCR Assay with Significantly Improved Detection Sensitivity and Amplification Efficiency of SYBR Green qPCR. *PLOS ONE* **10**, e0132666 (2015).
18. Bustin, S. A. *et al.* The MIQE guidelines: minimum information for publication of quantitative real-time PCR experiments. *Clin. Chem.* **55**, 611–622 (2009).
19. Jacob, F. *et al.* Careful selection of reference genes is required for reliable performance of RT-qPCR in human normal and cancer cell lines. *PloS One* **8**, e59180 (2013).

20. Guo, S. *et al.* Resveratrol Activated Sonic Hedgehog Signaling to Enhance Viability of NIH3T3 Cells in Vitro via Regulation of Sirt1. *Cell. Physiol. Biochem. Int. J. Exp. Cell. Physiol. Biochem. Pharmacol.* **50**, 1346–1360 (2018).
21. Kilander, M. B. C. *et al.* A rare human CEP290 variant disrupts the molecular integrity of the primary cilium and impairs Sonic Hedgehog machinery. *Sci. Rep.* **8**, 17335 (2018).
22. Rohatgi, R., Milenkovic, L. & Scott, M. P. Patched1 Regulates Hedgehog Signaling at the Primary Cilium. *Science* **317**, 372–376 (2007).
23. Westlake, C. J. *et al.* Primary cilia membrane assembly is initiated by Rab11 and transport protein particle II (TRAPPII) complex-dependent trafficking of Rabin8 to the centrosome. *Proc. Natl. Acad. Sci. U. S. A.* **108**, 2759–2764 (2011).
24. Kim, S. *et al.* Nde1-mediated inhibition of ciliogenesis affects cell cycle re-entry. *Nat. Cell Biol.* **13**, 351–360 (2011).
25. Takahashi, K., Nagai, T., Chiba, S., Nakayama, K. & Mizuno, K. Glucose deprivation induces primary cilium formation through mTORC1 inactivation. *J. Cell Sci.* **131**, (2018).
26. Corbit, K. C. *et al.* Vertebrate Smoothened functions at the primary cilium. *Nature* **437**, 1018–1021 (2005).
27. Livak, K. J. & Schmittgen, T. D. Analysis of relative gene expression data using real-time quantitative PCR and the 2(-Delta Delta C(T)) Method. *Methods San Diego Calif* **25**, 402–408 (2001).
28. Wang, C., Pan, Y. & Wang, B. Suppressor of fused and Spop regulate the stability, processing and function of Gli2 and Gli3 full-length activators but not their repressors. *Dev. Camb. Engl.* **137**, 2001–2009 (2010).
29. Frasca, A. *et al.* MECP2 mutations affect ciliogenesis: a novel perspective for Rett syndrome and related disorders. *EMBO Mol. Med.* **12**, e10270 (2020).
30. Hey, C. A. B. *et al.* BBS Proteins Affect Ciliogenesis and Are Essential for Hedgehog Signaling, but Not for Formation of iPSC-Derived RPE-65 Expressing RPE-Like Cells. *Int. J. Mol. Sci.* **22**, 1345 (2021).
31. Duan, F. *et al.* Effects of inhibition of hedgehog signaling on cell growth and migration of uveal melanoma cells. *Cancer Biol. Ther.* **15**, 544–559 (2014).
32. Hong, S.-R. *et al.* Spatiotemporal manipulation of ciliary glutamylation reveals its roles in intraciliary trafficking and Hedgehog signaling. *Nat. Commun.* **9**, 1732 (2018).
33. Schmittgen, T. D. & Zakrajsek, B. A. Effect of experimental treatment on housekeeping gene expression: validation by real-time, quantitative RT-PCR. *J. Biochem. Biophys. Methods* **46**, 69–81 (2000).
34. Krzystek-Korpacka, M. *et al.* Serum availability affects expression of common house-keeping genes in colon adenocarcinoma cell lines: implications for quantitative real-time PCR studies. *Cytotechnology* **68**, 2503–2517 (2016).
35. Taylor, S. C. *et al.* The Ultimate qPCR Experiment: Producing Publication Quality, Reproducible Data the First Time. *Trends Biotechnol.* **37**, 761–774 (2019).

Chapter 3: Hedgehog signaling with Joubert syndrome gene dysfunction

Authors: Arianna Gómez[1], Julie Craft Van De Weghe[1], Dan Doherty[1]
[1]Department of Pediatrics, University of Washington

Conceptualization, investigation, data analysis, and writing (drafting and review/editing) of chapter performed by AG. Conceptualization and review/editing of chapter performed by JCV and DD.

Introduction

Joubert syndrome (JS) is a largely recessive, neurodevelopmental condition characterized by a distinctive hindbrain malformation visualized as the molar tooth sign (MTS) on axial brain imaging.[1,2] All individuals with JS have the MTS, developmental delays, and hypotonia/ataxia, while subsets of individuals have variable features including abnormal eye movements, dysregulated breathing, retinal dystrophy, cystic kidney disease, liver fibrosis, and/or polydactyly.[3] Since the identification of the first JS-associated gene in 2004, more than 40 genes have been associated with the condition. All proteins localize in and around the primary cilium, an organelle that transduces light, mechanical, and chemical signals in cells. Thus, JS belongs to a group of conditions that all result from dysfunction of the primary cilium, called ciliopathies. While JS shares some features with other ciliopathies, the MTS is unique to JS and is required for the diagnosis.

One crucial developmental pathway mediated by primary cilia is Hedgehog signaling (Hh).[4] In vertebrates, canonical Hh signaling occurs through the coordinated movement of receptors and effectors into and out of the primary cilium (reviewed in [5]). In the absence of Hh ligand, the pathway receptor Patched (PTCH) localizes to the primary cilium, impeding Smoothened (SMO) localization by limiting accessible cholesterol at the ciliary membrane.[6] In parallel, ciliary GPR161, an orphan G protein-coupled receptor negatively regulates the pathway by generating ciliary cyclic AMP (cAMP). Increased cAMP levels facilitate PKA-mediated proteolytic cleavage of the GLI3 transcription factors into repressor forms.[7] GLI2/3 complexes with two JS-associated proteins (SUFU and KIF7) at the ciliary tip, functionally linking GLI2/3 to JS.

With pathway stimulation, Hh ligand binds PTCH, and both PTCH and GPR161 leave the cilium. Hh binding promotes an increase in ciliary $Ca2^{+}$, which decreases ciliary cAMP and PKA activity, reducing proteolytic cleavage of GLI2/3, shifting the balance to activator forms.[8,9] In concert, KIF7, SUFU, and GLI2/3 increase their localization to the ciliary tip, and uncleaved GLI2/3 activator forms translocate to the nucleus and upregulates transcriptional targets including *GLI1* and *PTCH1.*[10–13]

Perturbed Hh signaling has been described in models of >50% JS-associated genes.[14–18] Localization of Hh pathway proteins (e.g. SMO, GPR161, GLI2/3), GLI

transcription factor processing, and target gene expression have been measured in various model systems, cell types, and organisms. Developmental defects in the dorsal-ventral axis of the neural tube are often associated with abnormal Hh signaling in animal models, and distal limb patterning defects occur in a subset of individuals with JS.[19–23] While substantial evidence suggests that perturbed Hh signaling contributes to the mechanism(s) underlying JS, the evidence is scattered across organisms, cell types, and assays, making it difficult to determine whether aberrant Hh signaling is an obligate feature of JS, and if so, which aspects of Hh signaling are defective.

Based on the downstream manifestation of the MTS, we hypothesized that Hh signaling is aberrant across genetic causes of JS at the same step of the Hh pathway. During development, Hh signaling helps control axon guidance, and disrupted axon guidance attributes in part to the formation of the MTS.[24–26] To test our hypothesis, we decided to evaluate Hh signaling response using the same set of assays (localization of SMO and target gene expression) in a single model system (hTERT RPE-1, hTERT RPE-1 immortalized retinal pigment epithelial cells). In contrast to previously published in-depth examinations of one or two genes, our experiments provide a broad view of Hh response across 9 genetic causes of JS.

Results

Genome engineering and cell line validation

As described in Chapter 2, we selected hTERT RPE-1 cells for modeling JS based on their desirable ciliary characteristics and response to Hh signaling. These cells robustly ciliate, are genetically tractable, and respond to Hh pathway stimulation by relocalizing Hh pathway proteins and upregulating Hh target genes. To generate our library of mutants, we targeted a subset of JS-associated genes: 1) previously implicated in the Hh pathway, 2) commonly mutated in JS, 3) encoding proteins that localize to each of the major ciliary sub compartments (ciliary tip, cilium proper, transition zone, and basal body). We also included a non-JS ciliopathy gene, *BBS1*, to help determine whether any observed Hh signaling defects are JS-specific or a more common feature across ciliopathies.

We attempted to generate mutants for 13 JS genes using Sanger sequencing to identify genomic changes at targeted sites. We identified ≥3 mutants with unique events

for 9 of the 13 genes. We evaluated each line for the impact of the mutations on the protein by immunofluorescence staining and/or western blots when a working antibody was available, and on the transcript by qPCR if an antibody was not available. We also evaluated for off-target CRISPR-Cas9 events by Sanger sequencing the top two predicted cut sites in coding regions (Table 3.1).

Gene name	# of candidate lines with unique mutations	Off target Sanger sequencing	IF	WB	qPCR
ARL13B	7	Yes	Yes	Yes	No
ARMC9	3	Yes	No	No	Yes
CC2D2A	5	Yes	Yes	Yes	No
CPLANE1	7	Yes	No	No	Yes
CSPP1	5	Yes	Yes	Yes	No
INPP5E	3	Yes	Yes	Yes	No
KIF7	7	Yes	Yes	Yes	No
TMEM67	3	Yes	Yes	Yes	No
TOGARAM1	7	Yes	No	No	Yes
BBS1	3	Yes	No	No	Yes

Table 3.1. Validation experiments of candidate JS mutant cell lines. Assays used to validate hTERT RPE-1 mutant cell lines. Yes = assay was performed on mutant candidates, No = assay was not performed on mutant candidates. IF = immunofluorescence, WB = western blot

When ≥3 candidate mutant lines were generated for a gene (*ARL13B, CC2D2A, CPLANE1, CSPP1, KIF7, TMEM67, and TOGARAM1*), we used the validation data to select the best mutant lines for our experiments. In this case, we selected the mutants without detectable signal of immunofluorescence for the targeted protein and the lowest protein expression by western. We also prioritized cell lines that ciliated well and had normal cellular morphology, i.e. normal cell shape. We kept all candidate mutant cell lines which provides an opportunity to take a deeper dive into specific genes that had >3 mutants in the future. When only 3 mutant lines were generated within a gene (*ARMC9*,

INPP5E, BBS1, TMEM67) we ensured that protein localization or expression was disrupted, and cellular morphology was normal. In genes where only qPCR was used as validation (*ARMC9, BBS1, CPLANE1,* and *TOGARAM1*), we selected cell lines that had the lowest expression of the targeted gene from the candidates, presumably due to nonsense-mediated decay of transcripts with premature stop codons.

We included two groups of controls in our experiments: 1) the heterogenous hTERT RPE-1 parent populations that were used to generate the single-cell expanded mutants (WT), and 2) single-cell expanded controls (SC) that went through the same sorting and transfection process as the mutant lines except for leaving out the gRNA or including a non-targeting gRNA. Using the library of JS-gene mutants, we evaluated ciliary characteristics (proportion of cells with cilia and cilium length) and Hh pathway outputs (SMO localization and target gene induction) with and without pathway stimulation.

Proportion of cells with cilia

Differences in proportion of ciliated cells have been described in JS-associated models, and this characteristic should influence Hh signaling assays performed on cell populations; therefore, we determined ciliation rates for all of the lines with and without Hh pathway stimulation with Smoothened Agonist (SAG) (Figure 3.1A).[27,28] We used an anti-ARL13B antibody to mark cilia, except in *ARL13B* mutant lines, for which we used anti-detyrosinated tubulin antibody. Differences in ciliation with SAG stimulation was variable in control cell lines, some having higher, lower, or similar proportions of cells with cilia with and without stimulation. The proportion of cells with cilia in control lines was 58-88% (SD ±9.4%) for cilia measured with anti-ARL13B antibody and 36-92% (SD ±17.5%) for cilia measured with anti-detyrosinated tubulin antibody. Our preliminary immunofluorescence staining with anti-detyrosinated tubulin and anti-ARL13B suggested all cilia would be stained in controls, but the proportion of cells with cilia was different between the two stains in these experiments. To determine whether detyrosinated tubulin stains all cilia or only a fraction, we will go back and count the number of cilia in each channel (detyrosinated tubulin and ARL13B).

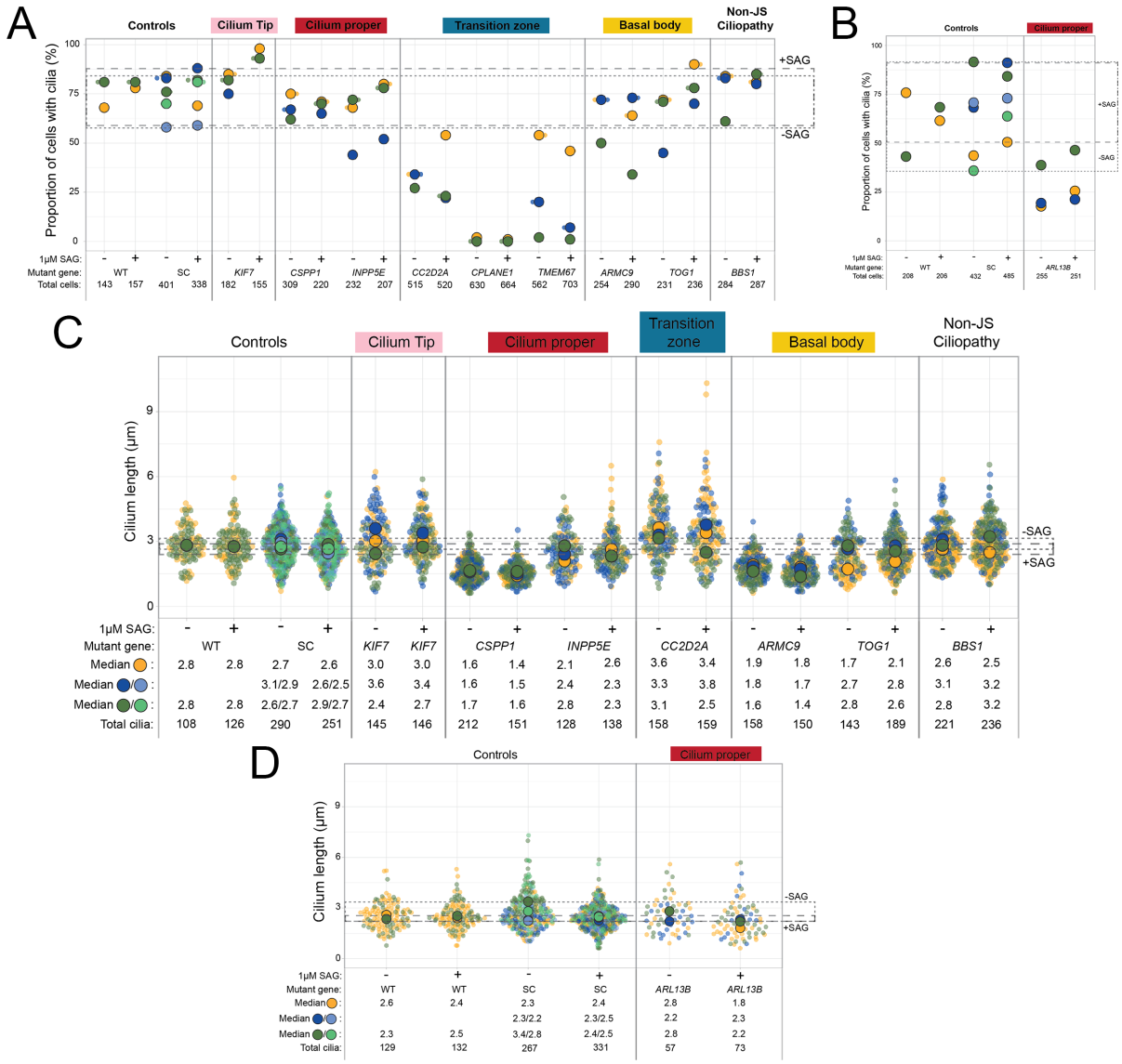

Figure 3.1. Proportion of ciliated cells and cilium length. (A and B) Proportion of ciliated cells in unstimulated and stimulated controls and JS mutants. The data set was generated using SMO localization experiments. Cilia were stained with (A) anti-ARL13B or (B) anti-detyrosinated tubulin. (C and D) Cilium length of unstimulated and stimulated control and JS mutants. Data set was generated using SMO localization experiments. Cilia were stained with (C) anti-ARL13B or (D) anti-detyrosinated tubulin. Upper and lower limits of control data are outlined by small dashes (unstimulated) or large dashes (stimulated). Circle color corresponds to experimental batch. In controls, shades of green and blue correspond to the same experimental batch. Large dots represent the median of each cell line, while small dots represent individual data points. Median length and total cilia measured are listed below each column.

In control lines, the proportion of ciliated cells increased in 4 lines, decreased in 1, and were similar between the two conditions in 2 cell lines. In *ARL13B, INPP5E, KIF7,* and *TOG1* mutants, cells had higher proportions of ciliated cells with pathway stimulation compared to unstimulated cells. In *ARMC9, CC2D2A, CSPP1,* and *TMEM67* mutants, a majority of mutants had lower proportions of ciliated cells with stimulation compared to unstimulated cells. Two *BBS1* mutants had lower ciliation in stimulated cells compared to stimulated cells, while once mutant had higher ciliation rates in stimulated cells.

Next, we compared proportions of ciliated cells between mutants and controls. In the mutant cell lines for the one cilium tip gene, *KIF7*, proportion of ciliated cells was similar to controls at baseline and increased above the level of control with stimulation. Mutants for cilium proper genes, *CSPP1* and *INPP5E,* had similar proportions of ciliated cells compared to controls with and without stimulation, except for one *INPP5E* mutant that had a lower proportion of cells with cilia. To determine whether this outlier is a result of technical error or is a unique characteristic of this cell line, we can repeat the experiment using the three *INPP5E* cell lines. *ARL13B* mutants had a lower proportion of cells with cilia, ranging from 17-46% (SD ±11.7%). In transition zone mutants, the proportion of ciliated cells was lower than control: *CC2D2A* mutants ciliated between 22-54% (SD ±11.7%), *CPLANE1* mutants ciliated between 0-2% (SD ±0.77%), and *TMEM67* mutants ciliated between 1-54% (SD ±23.1%). The low proportion of ciliated cells in all *CPLANE1* and 2 of 3 *TMEM67* mutants would generate small data sets, therefore, we did not measure SMO localization in these lines. Proportion of cells with cilia in basal body mutants were similar to controls. *BBS1* mutant cell lines ciliated within the normal range (61-85%, SD ±9.1%).

Cilium length

We next determined whether disrupted JS-gene function affected cilium length with and without Hh stimulation (Figure 3.1C, D). Cilium lengths did not differ in controls with the different cilium markers: 2.5-3.1μm (SD ±0.85μm) with anti-ARL13B antibody and 2.2- 3.4μm (SD ±0.84μm) with anti-detyrosinated tubulin antibody. Hh pathway stimulation did not uniformly affect ciliary length in the mutant lines. *CSPP1* (1.4 – 1.7μm, SD ±0.5μm) and *ARMC9* (1.4 – 1.9μm, SD ±0.6μm) cilia were shorter than

controls. *INPP5E* (2.1 – 2.8μm, SD ±0.9μm), *TOG1* (1.7 – 2.8μm, SD ±0.9μm), and *ARL13B* (1.8 – 2.8μm, SD ±1.1μm) mutants had similar lengths to controls but fell on the shorter end of control ciliary length. In *KIF7* (2.4 – 3.6μm, SD ±1.1μm) and *CC2D2A* mutants (2.5 – 2.8μm, SD ±1.4μm) mutants, ciliary lengths varied from falling within control range to being longer than controls. *BBS1* mutants had ciliary lengths similar to controls (2.5 – 3.2μm, SD ±0.9μm).

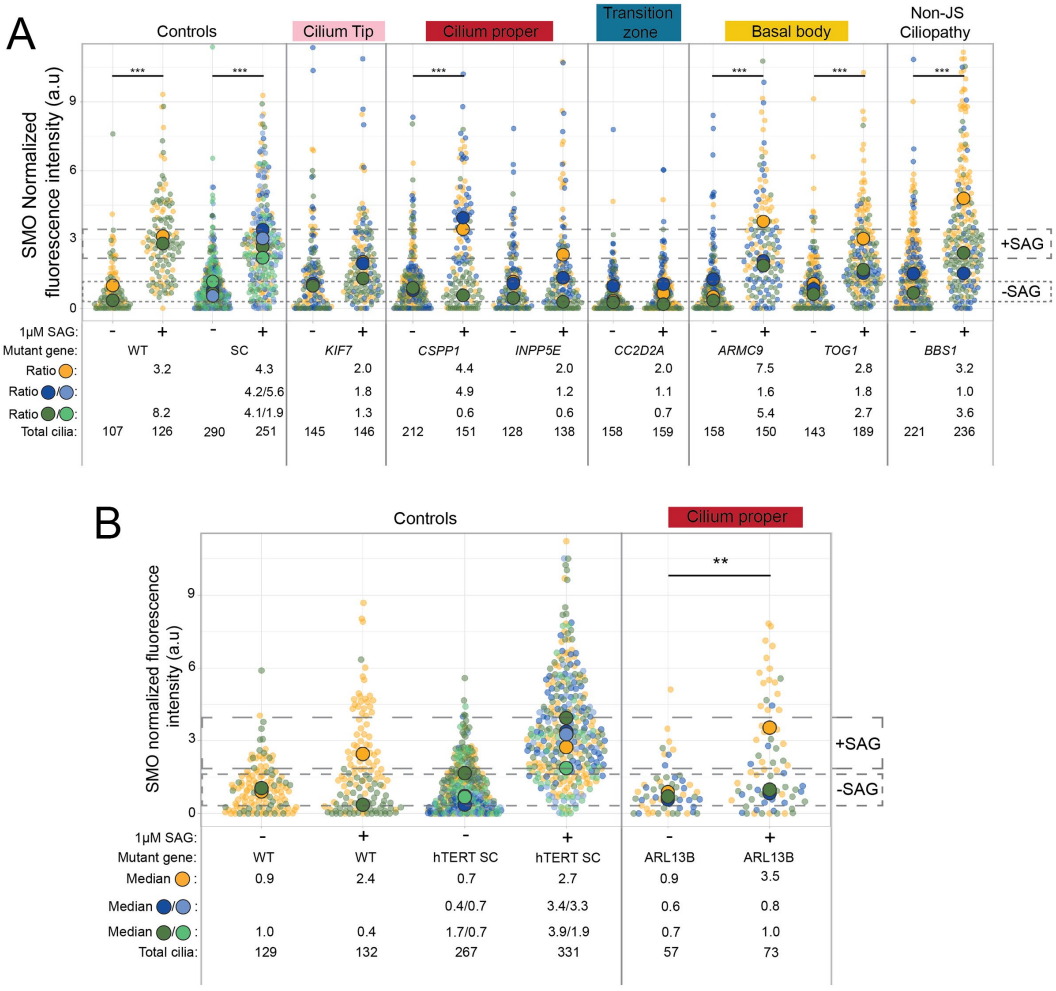

Figure 3.2. SMO localization with and without Hh pathway stimulation. Normalized fluorescence intensity of cells stained with SMO and (A) anti-ARL13B or (B) anti-detyrosinated tubulin. Upper and lower limits of control data are outlined by small dashes (unstimulated) and large dashes (stimulated). Circle color corresponds to experimental batch. The ratio and total number of cilia measured are listed below each column. Large dots represent the median value of each cell line, while small dots represent individual data points. Ratios were calculated by dividing median normalized fluorescence intensity of stimulated cells over median normalized fluorescence intensity of baseline cells in each batch.

SMO localization

Hh pathway proteins change their localization in response to pathway stimulation. SMO is the predominant pathway activator that is mostly excluded from cilia at without stimulated and localizes to cilia with pathway stimulation. At baseline, median normalized SMO fluorescence intensity was similar in controls (0.3 – 1.2 arbitrary units (au)) and mutants (0.3 – 1.5 au) (Supplementary Figure 3.1A). *KIF7* and *BBS1* mutants had significantly different SMO localization at baseline compared to controls. With stimulation, median normalized fluorescence intensity in controls was substantially higher (2.2 – 3.4 au, SD ±3.14 au) (Figure 3.2A). SMO localized to cilia with stimulation in mutant lines for 2 of the 7 JS genes (*CSPP1* and *ARMC9)*, and only 5 of 18 mutant lines had stimulated ciliary SMO levels at or above the range seen in controls (Supplementary Figure 3.1B). With stimulation, *KIF7, ARL13B, INPP5E, CC2D2A, and TOG1* had significantly different SMO normalized fluorescence intensity compared to single cell controls. In *BBS1* mutant lines, SMO localization was variable in response to SAG.

For each cell line, we calculated the ratio of SMO fluorescence intensity with and without stimulation, as an indicator of the dynamic range of the pathway response. In control lines, SAG treatment was associated with 1.9 to 8.2-fold higher ciliary SMO. Again, the different mutants showed different responses; some had responses outside the range of controls: *KIF7* (1.3 – 2.0-fold)*, INPP5E* (0.6 – 2.0-fold)*,* and *CC2D2A* (0.7 – 2.0-fold), while others responded within the range of controls: *CSPP1* (0.6 – 4.9-fold), *ARMC9* (1.6 – 7.5-fold), and *TOGARAM1* (1.8 – 2.8-fold). *BBS1* mutants responded similarly to controls with 1.0 – 3.6-fold induction.

In the separate experiment for *ARL13B* mutants using the anti-detyrosinated tubulin antibody as a ciliary marker, baseline median normalized fluorescence intensity for *ARL13B* mutants (0.6 – 0.9 au, SD±1.0 au) overlapped with controls (0.4 – 1.7 au, SD ±1.4 au). Similarly, with pathway stimulation SMO fluorescence intensity overlapped between *ARL13B* mutants (0.8 – 3.5 au, SD ±2.6 au) and controls (1.9 – 3.9 au, SD ±2.3 au). One control line in the *ARL13B* data set did not respond to pathway stimulation. Based on the normal SMO response for this line in other experiments, we suspect that an unknown technical error occurred such as not adding SAG. We again

calculated the stimulated/unstimulated ratios for control and *ARL13B* mutant cells. Here, control ratios ranged from 2.4 – 9.1-fold, excluding the non-responsive control. In *ARL13B* mutants, ratios ranged from 1.4 – 4.0-fold.

Hh pathway target gene induction

Figure 3.3. *PTCH1* and *GLI1* expression with and without stimulation. Expression of (A) *PTCH1* and (B) *GLI1* in unstimulated and stimulated cells. Upper and lower limits of control data are outlined by small dashes (unstimulated) and large dashes (stimulated). Circle color corresponds to experimental batch. In controls, shares of green and blue correspond to the same experimental batch.

In multiple systems, Hh pathway activation leads to upregulation of target genes, including *GLI1* and *PTCH1*.[12,13,29] Here, we measured expression levels in unstimulated and stimulated cells using RNA-seq, which we will use for future experimental questions

and hypothesis generation, but currently used to determine expression of the most well studied Hh pathway target genes, *PTCH1* and *GLI1*.

Without stimulation, *KIF7, CC2D2A, TMEM67,* and *ARMC9* mutants had significantly higher *PTCH1* expression compared to single cell controls, while *ARL13B, CSPP1, INPP5E, CPLANE1,* and *TOG1* mutants had *PTCH1* expression levels similar to controls (Figure 3.3). Within each gene, we compared expression of stimulated and unstimulated cells (Supplementary Figure 3.2). *KIF7* was the only mutant line that had a significant increase in expression between unstimulated and stimulated cells, while other lines exhibited a blunted response. *BBS1* did not significantly upregulate PTCH1. In WT and SC control lines, there was an overlap in the range of expression between unstimulated and stimulated cells. This made it difficult to distinguish whether the blunted response in mutants was biologically relevant.

We also measured expression of pathway target gene *GLI1*. At baseline, *KIF7* and *TOG1* mutants had significantly higher *PTCH1* expression compared to controls, while all other mutants had similar *PTCH1* expression compared to controls. With stimulation, *INPP5E, ARMC9,* and *TOGARAM1* mutants similar *PTCH1* expression levels to controls. In contrast, *KIF7, ARL13B, CSPP1, CC2D2A, CPLANE1, and TMEM67* had significantly lower *PTCH1* expressions compared to controls. When we compared unstimulated and stimulated expression within each gene, *KIF7, CSPP1, INPP5E, CC2D2A, ARMC9,* and *TOG1* significantly upregulated *GLI1* expression, while *ARL13B, CPLANE1,* and *TMEM67* did not significantly upregulate *GLI1* expression.

Correlation across assays

We would predict that mutants with low numbers of cilia would have dampened Hh response, since primary cilia mediate the signaling pathway.[4,27–30] In mutants with the lowest proportions of ciliated cells, *CPLANE1* and *TMEM67*, the ratio of *GLI1* expression was blunted across mutants (Figure 3.3). In cell lines with proportions of ciliated cells lower than controls, *ARL13B* and *CC2D2A*, we also observed a blunted response in SMO localization and *GLI1* expression, with blunted *GLI1* expression having a similar response as mutant lines with little or no cilia. Finally, in cell lines with proportions of ciliated cells that were similar to controls, *CSPP1, ARMC9,* and *TOGARAM1,* the SMO localization and *GLI1* expression ratios more comparable to

controls, except in *INPP5E*, which had a more significantly blunted response. Unlike proportion of ciliated cells, cilium length did not appear to greatly affect response to Hh signaling.

Next, we looked at correlation between our two Hedgehog assays, as we predict early aberrant steps in the signaling cascade would affect downstream signaling transduction. We used the ratios to make these comparisons. There were instances where ratios of normalized SMO fluorescence were perturbed, while *GLI1* expression ratios were not. This includes *KIF7* blue batch, *CSPP1* green batch, *INPP5E* green batch, and *CC2D2A* green batch. Since several of these occurrences were from replicates in the green batch, we will have to determine whether this was caused by a batch effect.

We also observed outliers in our experiments. In *ARL13B* mutants, the yellow replicate (Figure 3.2A) relocalized SMO similar to controls, while *PTCH1* and *GLI1* expression in that replicate was blunted compared to controls. In SMO experiments, the *CSPP1* green replicate had blunted SMO localization, therefore, we expected a lack of *PTCH1* and *GLI1* upregulation compared to the other replicates. Instead, we see similar upregulation compared to the other two *CSPP1* mutants. In *ARMC9, TOG1,* and *BBS1* mutants, the yellow replicate in stimulated cells has a higher SMO normalized fluorescence intensity than the other replicates. We will need to perform technical replicates with these mutants to determine whether there were technical errors in the experiment or if these results are replicable.

Discussion

We hypothesized that JS-associated gene dysfunction would result in disruption of Hh signaling at the same step across genetic causes of JS and that this represents a unifying mechanism underlying the condition. Proportion of cells with cilia and cilium length varied across JS gene mutants, making defects in these cellular characteristics unlikely to be involved in a unifying mechanism. We then looked at response to Hh pathway stimulation using assays of SMO localization and target gene induction. Many mutants showed evidence of decreased Hh signaling, including *ARL13B, CSPP1, INPP5E, CC2D2A, CPLANE1, and TMEM67*, while data from other samples was variable, including *KIF7, ARMC9,* and *TOGARAM1* (Table 3.1). That said, the data from

these two assays did not clearly identify a shared perturbation across genetic causes of JS, but the data do not entirely exclude a Hh signaling defect as a unifying mechanism underlying the condition.

Interpreting our results in the context of published studies using other models and other assays is complex, because some results are concordant and others are discordant (Table 3.2).

		SMO baseline	SMO stimulated	SMO ratio	*PTCH1* baseline	*PTCH1* stimulated	*PTCH1* ratio	*GLI1* baseline	*GLI1* stimulated	*GLI1* ratio
Ciliary tip	KIF7	– – –	↓↓↓	– ↓↓	– ↑↑	↑↑↑	↑ – –	– – ↑	↑ – ↑	– – ↓
Cilium proper	ARL13B	– – –	– ↓↓	– ↓↓	↑↑ –	– – ↓	↓ ↓ –	– – –	↓↓↓	↓↓↓
	CSPP1	– – –	– ↑↓	– – ↓	– – –	↓ – –	↓ ↓ –	– – –	↓↓↓	– – –
	INPP5E	– – –	– ↓↓	– ↓↓	– – ↑	↓ – –	– – –	– ↑ –	↓ – ↓	– ↓ –
Transition zone	CC2D2A	– – –	↓↓↓	– ↓↓	↑↑ –	– – –	↓ ↓↓	– ↑ –	↓↓↓	↓↓ –
	CPLANE1	N/A	N/A	N/A	↑ – ↑	↑ – –	↓ – –	↑ – –	↓↓↓	↓↓↓
	TMEM67	N/A	N/A	N/A	↑↑↑	– – –	↓ – ↓	– – –	↓↓↓	↓↓↓
Basal body	ARMC9	– ↑ –	↑↓↓	↑↓ –	↑↑↑	↑ – –	– ↓↓	– – ↑	– – ↓	– – ↓
	TOG1	– – –	– ↓↓	– ↓ –	↑↑↑	– – ↑	– – –	↑↑↑	↑ – ↑	– ↓ –
Non JS- ciliopathy	BBS1	↑↑ –	↑↓ –	– ↓ –	– – –	↓ – –	– – –	– – ↑	– ↓↓	↓↓↓

↑ Higher than range of controls
– Within range of controls
↓ Lower than range of controls
N/A Not assessed

Table 3.1. Summary of SMO localization and target gene induction. Arrows indicate whether a replicate had a value higher or lower than controls. *CPLANE1* and *TMEM67* mutants had a low proportion of cilia, so we wer unable to accurately determine SMO localization. The order of arrows corresponds to batch 1, batch 2, and batch 3 for each experiment.

Ciliary tip

The ciliary tip localizes key Hh pathway proteins (SMO, KIF7, GLI2/3). KIF7 plays a role in Hh signaling, specifically regulating GLI transcription factors by maintaining them in their repressor form at baseline, and increasing localization of the activator forms to the ciliary tip with pathway stimulation.[10,34–36] *KIF7* knockout and knockdown mouse embryonic fibroblasts have reported normal SMO localization,[10,34] low or normal *GLI1,* and normal or high *PTCH1* expression levels.[21,34,35,37,38] This is one example of mixed results across studies in the literature. The published SMO localization was performed in mouse embryonic fibroblasts (MEF), while the *GLI1* expression experiments were performed in MEFs, keratinocytes, and patient-derived cells. The varying results and model systems make it difficult to interpret what is relevant to the human condition. The advantage of our experimental design was performing the

experiments in parallel, in the same system, and using the same assays. This limits variation based on different model systems.

Human gene	Protein localization				Gene expression		
	SMO	GLI2	GLI3	GPR161	GLI1	PTCH	SHH
KIF7- KO/null [23,26–32]	NL	AB	AB		AB NL	AB	
KIF7- KD [10,21,29,33–38]	NL	AB NL	AB NL		NL	AB NL	
ARL13B - KO/null [24,39,40,40–45]	AB NL	NL	AB	AB	AB NL	AB	AB
ARL13B – KD [24,42,46]	AB NL	NL	AB		AB	AB NL	
CSPP1 [47,48]	AB				AB		
INPP5E- KO/null [49–52]	AB NL	AB	AB	AB	AB	AB	
CC2D2A [53–55]	AB						
CPLANE1 [38]					AB	AB	
TMEM67- KO/null [54,56]	NL						AB
TMEM67- KD [57]					NL	NL	
ARMC9 [58]	NL	AB	AB				
TOGARAM1 [19]	AB						

NL = normal, AB = abnormal, KO = knockout, KD = knockdown

Table 3.2. Summary of protein localization and gene expression from the literature. We considered a result abnormal if results were statistically different from controls or if the authors stated there was a difference between controls and the model. Blank cells indicate no published data was available at the time this table was generated. We separated *KIF7, ARL13B, INPP5E, and TMEM67* by knockout/null and knockdown models to get a general sense whether severity of mutations affected experimental outcome.

In our experiments, *KIF7* SMO localization was blunted in response to pathway stimulation, while *PTCH1* and *GLI1* expression were higher at baseline and with stimulation in our experiments. These cell lines responded differently to than others, by

having higher baseline and stimulated *GLI1* expression compared to controls. We would expect a cell line with blunted SMO localization to have lower *GLI1* expression, but we will need to take a deeper dive into other *KIF7* mutants we generated to better understand whether these results are biologically significant.

Cilium proper

Cilium proper proteins *ARL13B* and *INPP5E* help maintain the unique composition of the ciliary membrane, and dysfunction of these proteins has been shown to disrupt Hh signaling.[39–41] Prior studies have shown that dysfunction of the cilium proper genes *CSPP1* and *INPP5E* consistently result in blunted SMO localization and target gene expression in response to pathway stimulation. In contrast, *ARL13B* loss of function is associated with normal or high SMO localization with and without stimulation, but counterintuitively, normal or low target gene induction with stimulation.[27,27,42,42–46] In our data set, we see a similar pattern in *CSPP1* mutants, where the SMO ratio is normal in two replicates and low in one, while target gene induction is lower across mutants compared to controls. *GLI1* induction data aligned with the literature, with cilium proper mutants having a blunted response to pathway stimulation.

Transition zone

The transition zone regulates active protein trafficking into and out of the cilium. The transition zone mutants *CPLANE1* and *TMEM67* had low proportions of ciliated cells, which did not allow us to perform SMO localization experiments. As introduced above, there was some correlation between lack of cilia and blunted response to pathway stimulation, but we will need to further investigate whether increasing cellular density or extending serum starvation affects ciliation and response to pathway stimulation.

In our experiments, SMO localization was blunted with pathway stimulation in *CC2D2A* mutants, and *GLI1* expression was blunted with stimulation in *CC2D2A, CPLANE1,* and *TMEM67* mutants. Published data in *Cc2d2a* mouse embryonic fibroblasts and murine inner medullary collecting duct cells displayed lower SMO localization, similar to mutants in our library.[47,48] We did not find any evidence of Hh pathway protein mislocalization in the literature in *CPLANE1* models. In one study that presented *CPLANE1* patient-derived cells, proportion of ciliated cells were lower than

controls (20-40% in patient-derived cells vs 60% in unaffected cells) and cilium length was comparable to unaffected cells, but no data on SMO localization were presented.[49] *CPLANE1* mutants in our library did not ciliate well, suggesting that the mutations we introduced might be affecting ciliation, and potentially introducing hypomorphic variants rather than loss of function variants would allow for increased ciliation and measurement of SMO localization.

Basal body

Ciliary basal bodies are modified centrioles, with the mother centriole providing a template for the microtubule-based ciliary axoneme.[50] *ARMC9* and *TOGARAM1* were recently identified as JS-associated genes, and data on Hh signaling are limited for these genes. In the literature, SMO localization is normal at baseline and normal or low in stimulated cells.[19,33] In our experiments, SMO localization ranged from low to normal, and *GLI1* expression ranged from normal to high in stimulated cells.

The differing results across studies suggest that Hh signaling may be perturbed differently depending on the genetic background. Differences across different models for a gene demonstrate that Hh signaling is dependent on cell type, tissue context, genetic background, and organism. We will continue to utilize our library of mutants to further understand Hh response across genetic causes of JS.

Looking across nine JS-genetic mutant cell lines, we did not identify a shared characteristic of abnormal Hh signaling, but this does not rule out the possibility that the pathway is perturbed. Our approach provided an opportunity to look broadly across genetic causes of JS, but there were limitations to our project design. This included the use of one cell type, only looking at two steps in the pathway, and only using one time point for pathway stimulation. Expanding the library to include other cell types would provide some data on differences in cell specific response to pathway stimulation. Despite our efforts to uniformly generate multiple knockout mutants for each gene, some of these biological replicates did not perform similarly in the assays. Since we did not perform technical replicates for each cell line, we do not know whether this variability represents experimental mistakes (e.g. sample mix up, pipetting errors) versus different biological effects of the different mutations. We attempted to limit these biological differences by using the same gRNA within a gene to generate

insertion/deletion mutants that are predicted to result in non-functional truncated proteins, and we showed the absence of protein when antibodies were available; however, we cannot exclude the possibility of alternative splicing, translational readthrough, or other phenomena resulting in functional protein for some mutant lines.

We looked at two steps in the Hh pathway, SMO localization and target gene induction of *GLI1* and *PTCH1* and did not identify a shared perturbation across mutants. However, we can use our library of mutants and the RNA-seq data set to look at other steps in the pathway and search for other genes that are upregulated or downregulated in response to Hh stimulation. SMO is one pathway protein that relocalizes with pathway stimulation, but we could look at other components, including GPR161, PTCH, KIF7, SUFU, and GLI2/3 to determine whether dysfunction of JS-associated genes disrupts localization of Hh pathway proteins. Expanding our qIF data would provide a wider view of positive and negative regulators of the pathway. At the gene expression level, we can use our RNAseq data to screen for changes in expression of pathway components and move into cellular experiments to validate those findings. We could also be missing changes in target gene expression of genes that have not been previously associated with Hh signaling.

There are future possibilities to look at other steps in the pathway, such as GLI3 protein processing and GLI2 protein using western blots. We attempted GLI3 processing western blots (discussed in Chapter 4) but did not see a consistent response to stimulation, so we need to evaluate different time points and stimulation conditions. Interestingly, most published GLI processing data in JS-mutants have been performed in tissues rather than cell lines, so it may be that some cultured cells have less robust GLI processing responses to pathway stimulation than cells in their native environment.

While it should be possible to identify a unifying cellular defect underlying JS (should one exist), it would be very difficult to fully exclude a unifying mechanism, since it would require showing that all aspects of Hh signaling are unperturbed in the relevant cell type. Ideally, to rule out Hh signaling as a mechanism underlying JS, we would want to look at multiple mutants across JS genes, in several types of cell lines, across different timepoints of pathway stimulation, and using multiple assays/outputs. The

addition of other non-JS ciliopathy controls will also help determine whether perturbed Hh signaling is seen broadly across ciliopathies.

Our experiments evaluated Hh signaling across genetic causes of JS using two assays in a single immortal cell line. We observed a blunted response to pathway stimulation in cilium proper and transition zone mutants, but no shared defect across all types of mutants. Additional experiments would be needed to more fully exclude a specific, shared Hh signaling defect as a unifying cause of JS. This work is an important step forward in understanding the role of Hh signaling in JS, and lays the foundation for taking a broader look at potential JS-related mechanisms across genetic causes using libraries of engineered cells like the ones generated for this work.

Methods

Cell culture

hTERT RPE-1 cells (ATCC: CRL4000) were maintained in DMEM-F12 medium (Thermo Fisher Scientific, #11320082) supplemented with 10% Fetal Bovine Serum and 1% Penicillin/Streptomycin (Gibco, #15140-122) in a humidified incubator at 37°C and 5% CO_2. 0.05% Trypsin was used for cell dissociation.

Genetic editing of hTERT RPE-1 cells

Single gene mutations were accomplished using the Integrated DNA Technologies (IDT) Alt-R CRISPR-Cas9 System of hTERT RPE-1 cells with gene-specific gRNA's. Transfection was performed using the Lipofectamine CRISPRMAX Transfection reagent (Thermo Fisher Scientific #CMAX00008) following the IDT protocol "Alt-R CRISPR-Cas9 System: Cationic lipid delivery of CRISPR ribonucleoprotein complexes into mammalian cells." About 24 hours after transfection, we performed Fluorescence-activated cell sorting using a BD Aria III cytometer. Cells were sorted into 96-well plates, single cell expanded, and sequenced to determine editing events. gRNA's and sequencing primers are listed below:

Gene	gRNA	Forward primer (5' --> 3')	Reverse primer (5' --> 3')
ARL13B	ATGGTGGGACTTGATAATGC	TCCCTACCTCCCTTTCCATCTT	TAAGACAGAGCCTATTCGCCAC
ARMC9	CTTGTCGCTGCATTTGACAA	TGGGAGATCTGTGGTGTTGA	TGACAGCACAGCCACATATG
BBS1	GGATGCGCACTACGACCCAA	TTTCCCACCCGTGTAAAGAG	CCCATCCCCATGTAAATCTG
CPLANE1	ATGTAGTAACAAGAGTCCCG	AAAGGCTACCAGGGGTCAAT	TCACCCACGTTCAGGTGATA
CC2D2A	TAGAGCGGGAACTAATCAAG	TTCAACTTTGATCCCGAACC	CATACCACCCACAGTTGCAG
CSPP1	TCTGAACCAAAGACGACTAG	GCTTGTTTATCCATTCCCCTGT	ACTAGGGAGAAGCAGTTTTGAT
INPP5E	GGAAATCCCCAAGTCCCGCG	AGGACCTGGAAGCCCGGAAT	AAGGGAACAGTCGTCGCAG
KIF7	CTACCTGGAAGTGTACAAGG	GCCTTCTCCATCCTAGAGCA	AAGCACTCCACTCCAAACAG
TMEM67	GTACTTTGATATCTCCGCCC	TTCCTCCCTCGCTTCTTACA	CTCTGCCTTGGCTTCCTCTA
TOG1	CGAGTTGGGGGCATTATGAG	CGCCCTTTCCAGTCCTCT	CCGAGAGAAGTTGCAAGCAG

Methods table 3.1. gRNA sequences and PCR sequencing primers to determine editing events.

Cell-based assays Hedgehog assays

hTERT RPE-1 mutants and controls were grown in three batches, with replicates listed below:

Experimental name	Cell line name	Wild type amino acid length	Mutant predicted amino acid length	Cell culture batch
ARL13B_1	ARL13B_4.29	428 AA	42AA	1
ARL13B_2	ARL13B_4.26		48AA/47AA	2
ARL13B_3	ARL13B_4.35		49AA	3
ARMC9_1	ARMC9_4.09	817 AA	122AA	1
ARMC9_2	ARMC9_4.02		122AA	2
ARMC9_3	ARMC9_4.06		122AA/108AA	3
BBS1_1	BBS1_3.01	593 AA	97/40AA	1
BBS1_2	BBS1_3.11		40/91 AA	2
BBS1_3	BBS1_3.17		40/94 AA	3
CPLANE1_1	C5ORF42_5.08	3197 AA	309AA/309AA	1
CPLANE1_2	C5ORF42_5.10		310AA/317AA	2
CPLANE1_3	C5ORF42_3.07		316/304AA	3
CC2D2A_1	CC2D2A_3.51	1620 AA	233/245 AA	1
CC2D2A_2	CC2D2A_3.07		238/255AA	2
CC2D2A_3	CC2D2A_3.34		235/255 AA	3
CSPP1_1	CSPP1_4.31	1221 AA	228AA/198AA	1
CSPP1_2	CSPP1_4.15		228AA/230AA	2
CSPP1_3	CSPP1_3.26		227/228 AA	3
INPP5E_1	INPP5E_3.03	644 AA	149AA	1
INPP5E_2	INPP5E_3.23		149/147 AA	2
INPP5E_3	INPP5E_3.29		609/609AA	3
KIF7_1	KIF_6.42	1343 AA	181/161 AA	1
KIF7_2	KIF_6.23		164 AA	2
KIF7_3	KIF_6.19		164/181 AA	3
TMEM67_1	TMEM67_3.47	995 AA	60AA/988AA	1
TMEM67_2	TMEM67_4.01		53AA/53AA	2
TMEM67_3	TMEM67_4.10		55AA	3
TOG1_1	TOG_3.29	1720 AA	83/81 AA	1
TOG1_2	TOG_3.32		83/79 AA	2
TOG1_3	TOG_3.07		80/46 AA	3
wt_1	hTERT parent round 3	N/A	N/A	1
wt_3	hTERT parent 2 round 6		N/A	3
hTERT SC_1	No Template control 3.03		N/A	1
hTERT SC_2.1	No RNA_3.01		N/A	2
hTERT SC_2.2	No Template control 3.01		N/A	2
hTERT SC_3.1	No RNA_3.02		N/A	3
hTERT SC_3.2	No Template control 3.06		N/A	3

Methods table 3.2. List of JS-gene mutants used in our experiments. The experimental name was a generic name given to de-identify the different mutant lines. The cell line name corresponds with the name cataloged in the Doherty freezer data sheets. The predicted amino acid length in the mutant lines is listed. If a single predicted amino acid length is listed, than the event was homozygous. In mutant lines with xxAA/xxAA listed, there were heterozygous events.

Proportion of ciliated cells, cilium length, and SMO localization data was generated using the same data set and coverslips. Cells were seeded on pairs of coverslips coated with 0.3mg/mL poly-D-lysine and allowed to grow for 2-3 days, until they reach 60-80% confluency. Cells in the same batch were seeded at the same cell density and starved for 48 hours starting at the same time. Cells were serum starved for a total of 48 hours. After the initial 24 hours of serum starvation, we replaced the media on half of the coverslips with DMEM only + 1uM Smoothened Agonist (Millipore, 566661). After 24 hours of starvation, we fixed coverslips using 4% paraformaldehyde for 5 minutes, followed by permeabilization using cold Methanol for 3 minutes and stored in PBS at 4°C until ready to stain.

Cells for RNA collection were grown at the same time as coverslips. T-75 flasks were grown in pairs, and allowed to grow for 2-3 days, until cell lines reached 60-80% confluency. Cells were starved for a total of 48 hours. Half the flasks had their media replaced after the initial 24 hours with DMEM only + 1uM SAG. We lysed cells for RNA extraction using Trizol (Thermo Fisher Scientific #15596018). Trizol was added directly to cells and collected in a 15ml conical. Lysates were stored at -80°C until ready for extraction.

Immunofluorescence and microscopy

Antibody Name	Species	Concentration	Supplier	Product number
SMO	Mouse Monoclonal	1:200	Santa Cruz Biotechnology	sc-166685
ARL13B	Mouse	1:200	NeuroMab	75-287
Anti-tubulin, detyrosinated	Rabbit polyclonal	1:200	Sigma Aldrich	AB3201

Methods table 3.3. Antibodies used for immunofluorescence staining in SMO localization experiments.

We blocked coverslips in 2% BSA in PBS for 20 minutes at room temperature. GPR161, SMO, and ARL13B antibodies were diluted as shown in the chart above. We incubated coverslips with primary antibodies at either 4°C overnight or for 1 hour at room temperature, then washed three times in PBS for 5 minutes. We incubated coverslips with the following secondary antibodies at 1:400 dilution for 1 hour at room temperature: Goat anti-Rabbit IgG, Alexa Fluor 488 (Thermo Fisher Scientific #A11008)

and Donkey anti-Mouse IgG, Alexa Fluor 568 (Thermo Fisher Scientific, #A10037). After incubation, we washed coverslips three times in PBS for 5 minutes. Coverslips were mounted on slides using a Fluoromount with DAPI (Invitrogen, #00-4959-52), then sealed with nail polish after sitting for at least 1 hour.

Quantitative immunofluorescence

We quantified ciliary protein localization using a validated protocol previously established in the laboratory[47]. We acquired z-stack images for >20 cells for each condition using identical microscope settings. We converted z-stack images to sum-projections and randomized these images using the FIJI[48] script, Filename_randomizer (https://imagej.nih.gov/ij/macros/Filename_Randomizer.txt) to minimize bias. We created cilium masks using the cilia marker (ARL13B) channel. We used this mask to measure the signal intensity for the protein of interest and measured the signal intensity of an adjacent region to subtract background signal.

All figures and graphs were generated using Plots Of Data and Super Plots Of Data.[49,50]

RNA isolation and RNA-seq

When ready to extract, frozen lysates were thawed and chloroform was added (Millipore #C2432). After sitting for 2 minutes, the sample was centrifuged for 15 minutes at 12,000x g. The aqueous phase was then collected and used for RNA cleanup (RNA Clean and Concentrator kit, Zymo research, #R1013). Following RNA cleanup, RNA concentration and purity were determined using a spectrophotometer. RIN RNA purity was determined using the Agilent 2100 Bioanalyzer (#G2939BA). Total RNA samples were submitted to Novogene for Eukaryotic RNA-seq (cDNA library). Only samples with a RIN score ≥4 with smooth baseline, A260/280 >1.8-2.2, and A260/230 ≥1.8 were used, as outlined by the company. Sample submission included RNA sample QC, mRNA library prep (poly A enrichment), Sequencing (Illumina – PE150 – 30M paired reads), data quality control, and raw data. Sequence data was generated in a single run in the same lane.

Sequencing quality was assessed using FASTQC results. Read alignment was performed using GRCh38.p12 with reference genome GENCODE human release 30 using STAR (v2.7.9a). The aligned BAM files were used for analysis and the number of

reads that overlap each gene were counted using the featureCounts function in Bioconducted Rsubread[125] package and gene definitions were used from the GENCODE human release 30 GTF files. Read counts are used to compare the expression of each gene in different samples.

Statistical methods

An unpaired two-tailed Student's *t*-test was performed for comparison between unstimulated and stimulated cells with a hypothesized mean difference of 0. α level was set at 0.05. $P < 0.05$ was significant. For RNA-seq expression data, adjusted p-values were determined using the Benjamani-Hochburg procedure. Symbols for significance represent *p*-values from 0.01 to 0.05 (*), 0.001 to 0.01 (**), and <0.001 (***).

Supplementary Figures

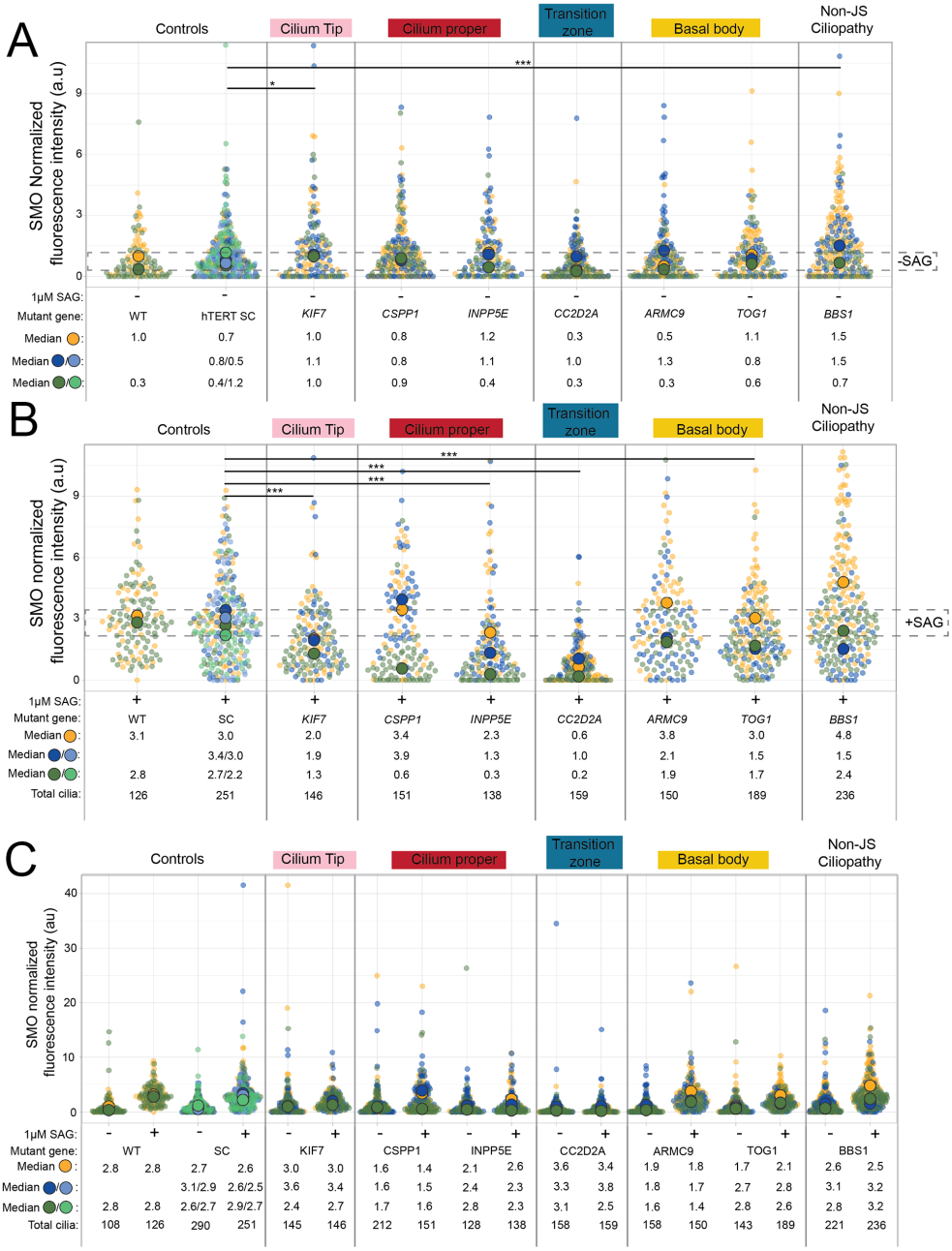

Supplementary Figure 3.1. Baseline and stimulated SMO localization with medians. Normalized fluorescence intensity of cells stained with SMO and ARL 13B at (A) baseline or (B) with stimulation. Upper and lower limits of control data are outlined in each graph. (C) SMO fluorescence graph showing the full fluorescence intensity y-axis. Circle color corresponds to experimental batch. In controls, shades of green and blue correspond to the same experimental batch. Large dots represent the median of each cell line, while small dots represent individual data points. Median normalized fluorescence intensity for each batch is listed below each column.

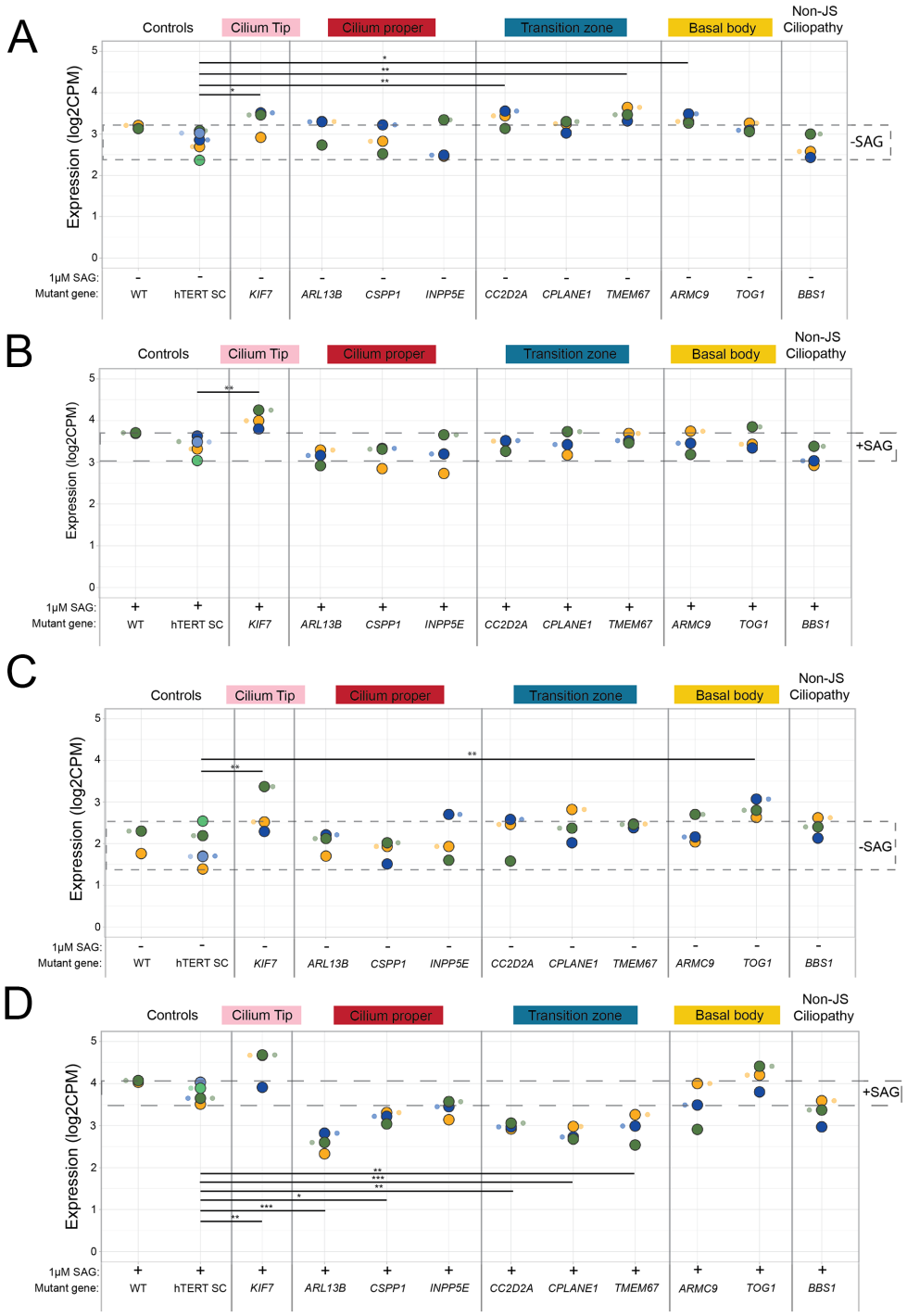

Supplementary Figure 3.2. Baseline and stimulated *PTCH1* and *GLI1* expression by RNA-seq. Data from Figure 3 separated by (A) unstimulated *PTCH1*, (B) stimulated *PTCH1*, (C) unstimulated *GLI1*, and (D) stimulated *GLI1*.

References

1. Joubert, M., Eisenring, J. J., Robb, J. P. & Andermann, F. Familial agenesis of the cerebellar vermis. A syndrome of episodic hyperpnea, abnormal eye movements, ataxia, and retardation. *Neurology* **19**, 813–825 (1969).
2. Maria, B. L. *et al.* 'Joubert syndrome' revisited: key ocular motor signs with magnetic resonance imaging correlation. *J. Child Neurol.* **12**, 423–430 (1997).
3. Dhooghe, B. *et al.* Resveratrol increases F508del-CFTR dependent salivary secretion in cystic fibrosis mice. *Biol. Open* **4**, 929–936 (2015).
4. Huangfu, D. & Anderson, K. V. Cilia and Hedgehog responsiveness in the mouse. *Proc. Natl. Acad. Sci. U. S. A.* **102**, 11325–11330 (2005).
5. Briscoe, J. & Thérond, P. P. The mechanisms of Hedgehog signalling and its roles in development and disease. *Nat. Rev. Mol. Cell Biol.* **14**, 416–429 (2013).
6. Lewis, P. M. *et al.* Cholesterol modification of sonic hedgehog is required for long-range signaling activity and effective modulation of signaling by Ptc1. *Cell* **105**, 599–612 (2001).
7. Wang, B., Fallon, J. F. & Beachy, P. A. Hedgehog-Regulated Processing of Gli3 Produces an Anterior/Posterior Repressor Gradient in the Developing Vertebrate Limb. *Cell* **100**, 423–434 (2000).
8. Belgacem, Y. H. & Borodinsky, L. N. Sonic hedgehog signaling is decoded by calcium spike activity in the developing spinal cord. *Proc. Natl. Acad. Sci. U. S. A.* **108**, 4482–4487 (2011).
9. Mukhopadhyay, S. *et al.* The Ciliary G-Protein-Coupled Receptor Gpr161 Negatively Regulates the Sonic Hedgehog Pathway via cAMP Signaling. *Cell* **152**, 210–223 (2013).
10. He, M. *et al.* The kinesin-4 protein Kif7 regulates mammalian Hedgehog signalling by organizing the cilium tip compartment. *Nat. Cell Biol.* **16**, 663–672 (2014).
11. Lee, J., Platt, K. A., Censullo, P. & Ruiz i Altaba, A. Gli1 is a target of Sonic hedgehog that induces ventral neural tube development. *Dev. Camb. Engl.* **124**, 2537–2552 (1997).
12. Dai, P. *et al.* Sonic Hedgehog-induced activation of the Gli1 promoter is mediated by GLI3. *J. Biol. Chem.* **274**, 8143–8152 (1999).
13. Chen, Y. & Struhl, G. Dual roles for patched in sequestering and transducing Hedgehog. *Cell* **87**, 553–563 (1996).
14. Lin, C. *et al.* Differential regulation of Gli proteins by Sufu in the lung affects PDGF signaling and myofibroblast development. *Dev. Biol.* **392**, 324–333 (2014).
15. Lai, C. K. *et al.* Functional characterization of putative cilia genes by high-content analysis. *Mol. Biol. Cell* **22**, 1104–1119 (2011).
16. Sang, L. *et al.* Mapping the NPHP-JBTS-MKS protein network reveals ciliopathy disease genes and pathways. *Cell* **145**, 513–528 (2011).
17. Inskeep, K. A. *et al.* Genetic and phenotypic heterogeneity in KIAA0753-related ciliopathies. *Am. J. Med. Genet. A.* **188**, 104–115 (2022).
18. Shaheen, R. *et al.* Bi-allelic Mutations in FAM149B1 Cause Abnormal Primary Cilium and a Range of Ciliopathy Phenotypes in Humans. *Am. J. Hum. Genet.* **104**, 731–737 (2019).
19. Latour, B. L. *et al.* Dysfunction of the ciliary ARMC9/TOGARAM1 protein module causes Joubert syndrome. *J. Clin. Invest.* **130**, 4423–4439 (2020).

20. Goetz, S. C., Bangs, F., Barrington, C. L., Katsanis, N. & Anderson, K. V. The Meckel syndrome- associated protein MKS1 functionally interacts with components of the BBSome and IFT complexes to mediate ciliary trafficking and hedgehog signaling. *PloS One* **12**, e0173399 (2017).
21. Putoux, A. *et al.* KIF7 mutations cause fetal hydrolethalus and acrocallosal syndromes. *Nat. Genet.* **43**, 601–606 (2011).
22. Vierkotten, J., Dildrop, R., Peters, T., Wang, B. & Rüther, U. Ftm is a novel basal body protein of cilia involved in Shh signalling. *Dev. Camb. Engl.* **134**, 2569–2577 (2007).
23. Cheung, H. O.-L. *et al.* The kinesin protein Kif7 is a critical regulator of Gli transcription factors in mammalian hedgehog signaling. *Sci. Signal.* **2**, ra29 (2009).
24. Guo, J. *et al.* Primary Cilia Signaling Promotes Axonal Tract Development and Is Disrupted in Joubert Syndrome-Related Disorders Models. *Dev. Cell* **51**, 759-774.e5 (2019).
25. Suciu, S. K., Long, A. B. & Caspary, T. Smoothened and ARL13B are critical in mouse for superior cerebellar peduncle targeting. *Genetics* **218**, iyab084 (2021).
26. Ferent, J. *et al.* The Ciliary Protein Arl13b Functions Outside of the Primary Cilium in Shh-Mediated Axon Guidance. *Cell Rep.* **29**, 3356-3366.e3 (2019).
27. Mariani, L. E. *et al.* Arl13b regulates Shh signaling from both inside and outside the cilium. *Mol. Biol. Cell* mbc.E16-03-0189 (2016) doi:10.1091/mbc.E16-03-0189.
28. Jacoby, M. *et al.* INPP5E mutations cause primary cilium signaling defects, ciliary instability and ciliopathies in human and mouse. *Nat. Genet.* **41**, 1027–1031 (2009).
29. Niswander, L., Jeffrey, S., Martin, G. R. & Tickle, C. A positive feedback loop coordinates growth and patterning in the vertebrate limb. *Nature* **371**, 609–612 (1994).
30. Huangfu, D. *et al.* Hedgehog signalling in the mouse requires intraflagellar transport proteins. *Nature* **426**, 83–87 (2003).
31. Frikstad, K.-A. M. *et al.* A CEP104-CSPP1 Complex Is Required for Formation of Primary Cilia Competent in Hedgehog Signaling. *Cell Rep.* **28**, 1907-1922.e6 (2019).
32. Chen, C. *et al.* Ciliopathy protein HYLS1 coordinates the biogenesis and signaling of primary cilia by activating the ciliary lipid kinase PIPKIγ. *Sci. Adv.* **7**, eabe3401 (2021).
33. Breslow, D. K. *et al.* A CRISPR-based screen for Hedgehog signaling provides insights into ciliary function and ciliopathies. *Nat. Genet.* **50**, 460–471 (2018).
34. Liu, Y. C. *et al.* The PPFIA1-PP2A protein complex promotes trafficking of Kif7 to the ciliary tip and Hedgehog signaling. *Sci. Signal.* **7**, ra117 (2014).
35. Endoh-Yamagami, S. *et al.* The mammalian Cos2 homolog Kif7 plays an essential role in modulating Hh signal transduction during development. *Curr. Biol. CB* **19**, 1320–1326 (2009).
36. Liem, K. F., He, M., Ocbina, P. J. R. & Anderson, K. V. Mouse Kif7/Costal2 is a cilia-associated protein that regulates Sonic hedgehog signaling. *Proc. Natl. Acad. Sci. U. S. A.* **106**, 13377–13382 (2009).

37. Li, Z. J. *et al.* Kif7 regulates Gli2 through Sufu-dependent and -independent functions during skin development and tumorigenesis. *Dev. Camb. Engl.* **139**, 4152–4161 (2012).
38. Terhune, E. A. *et al.* Mutations in KIF7 implicated in idiopathic scoliosis in humans and axial curvatures in zebrafish. *Hum. Mutat.* **42**, 392–407 (2021).
39. Garcia-Gonzalo, F. R. *et al.* Phosphoinositides Regulate Ciliary Protein Trafficking to Modulate Hedgehog Signaling. *Dev. Cell* **34**, 400–409 (2015).
40. Chávez, M. *et al.* Modulation of Ciliary Phosphoinositide Content Regulates Trafficking and Sonic Hedgehog Signaling Output. *Dev. Cell* **34**, 338–350 (2015).
41. Caspary, T., Larkins, C. E. & Anderson, K. V. The graded response to Sonic Hedgehog depends on cilia architecture. *Dev. Cell* **12**, 767–778 (2007).
42. Su, C.-Y., Bay, S. N., Mariani, L. E., Hillman, M. J. & Caspary, T. Temporal deletion of Arl13b reveals that a mispatterned neural tube corrects cell fate over time. *Dev. Camb. Engl.* **139**, 4062–4071 (2012).
43. Nozaki, S. *et al.* Regulation of ciliary retrograde protein trafficking by the Joubert syndrome proteins ARL13B and INPP5E. *J. Cell Sci.* **130**, 563–576 (2017).
44. Larkins, C. E., Aviles, G. D. G., East, M. P., Kahn, R. A. & Caspary, T. Arl13b regulates ciliogenesis and the dynamic localization of Shh signaling proteins. *Mol. Biol. Cell* **22**, 4694–4703 (2011).
45. Gigante, E. D., Taylor, M. R., Ivanova, A. A., Kahn, R. A. & Caspary, T. ARL13B regulates Sonic hedgehog signaling from outside primary cilia. *eLife* **9**, e50434 (2020).
46. Bay, S. N., Long, A. B. & Caspary, T. Disruption of the ciliary GTPase Arl13b suppresses Sonic hedgehog overactivation and inhibits medulloblastoma formation. *Proc. Natl. Acad. Sci. U. S. A.* **115**, 1570–1575 (2018).
47. Chih, B. *et al.* A ciliopathy complex at the transition zone protects the cilia as a privileged membrane domain. *Nat. Cell Biol.* **14**, 61–72 (2011).
48. Garcia-Gonzalo, F. R. *et al.* A transition zone complex regulates mammalian ciliogenesis and ciliary membrane composition. *Nat. Genet.* **43**, 776–784 (2011).
49. Asadollahi, R. *et al.* Clinical and experimental evidence suggest a link between KIF7 and C5orf42-related ciliopathies through Sonic Hedgehog signaling. *Eur. J. Hum. Genet. EJHG* **26**, 197–209 (2018).
50. Burke, M. C. *et al.* Chibby promotes ciliary vesicle formation and basal body docking during airway cell differentiation. *J. Cell Biol.* **207**, 123–137 (2014).
51. Slaats, G. G. *et al.* MKS1 regulates ciliary INPP5E levels in Joubert syndrome. *J. Med. Genet.* **53**, 62–72 (2016).
52. Schindelin, J. *et al.* Fiji: an open-source platform for biological-image analysis. *Nat. Methods* **9**, 676–682 (2012).
53. Goedhart, J. SuperPlotsOfData—a web app for the transparent display and quantitative comparison of continuous data from different conditions. *Mol. Biol. Cell* **32**, 470–474 (2021).
54. Postma, M. & Goedhart, J. PlotsOfData—A web app for visualizing data together with their summaries. *PLOS Biol.* **17**, e3000202 (2019).
55. Liao, Y., Smyth, G. K. & Shi, W. The R package Rsubread is easier, faster, cheaper and better for alignment and quantification of RNA sequencing reads. *Nucleic Acids Res.* **47**, e47 (2019).

Chapter 4: Assay validation and modifications

Authors: Arianna Gomez[1] and Dan Doherty[1]
[1]Department of Pediatrics, University of Washington

Introduction

Our literature review demonstrated that Hedgehog (Hh) response is perturbed in different JS-associated gene models. These perturbations have been measured using a range of assays in a variety of cells and tissues, making it difficult to make conclusions about how Hh signaling is disrupted in the JS disease. We wanted to address this knowledge gap by performing the same assays in a single model system to determine whether Hh signaling is disrupted similarly across genetic causes of JS. Based on assays commonly used to measure differences in Hh response, we decided to evaluate the response to pathway stimulation at several steps: 1) localization of Hh signaling components using quantitative immunofluorescence of cilia, 2) proteolytic processing of GLI3 transcription factors using western blots, and 3) target gene expression using qPCR (Chapter 2) and RNA-seq (Chapter 3). Adapting these assays for use across multiple cell types (retinal pigment epithelial cells, murine fibroblasts, embryonic kidney cells) and a library of mutant hTERT RPE-1 cell lines required the optimization described in this Chapter.

Quantitative immunofluorescence

We and others have used immunofluorescence to evaluate differences in pathway protein localization in cell lines, tissues, and patient-derived cells[1–3]. Our lab uses a quantitative measurement of fluorescence intensity (qIF described in [4]) to determine changes in protein localization at baseline and in stimulated cells. In Chapter 2, we used this technique to determine SMO and GPR161 localization, using *ARL13B* as a cilium marker. We encountered two challenges when performing qIF in our library of mutant lines described in Chapter 3: 1) inability to use ARL13B antibody as a cilium marker for *ARL13B* mutant lines due to lack of ARL13B expression, and 2) lack of GPR161 staining in control and mutant cell lines. In this section, I will describe how we identified a cilium marker in *ARL13B* mutants and present troubleshooting experiments to determine whether we detect a cilium-specific GPR161 signal.

Selection of a cilium marker for *ARL13B* mutants

Chapter 3 described our use of an hTERT RPE-1 library of JS-gene mutant lines. Typically, we use ARL13B, INPP5E, or acetylated tubulin antibodies to mark cilia for qIF experiments. Not surprisingly, our *ARL13B* mutants did not express ARL13B by IF or western blot (Figure 4.1), so we had to identify a different cilium marker to determine the

proportion of ciliated cells and for qIF experiments. All other mutant lines showed robust ARL13B signal, so we could use that antibody for the rest of our experiments. The SMO and GPR161 antibodies we use were generated in mouse and rabbit, respectively; therefore, we identified cilium marker antibodies generated in different animals for further testing in hTERT RPE-1 cells. While AC3, gamma tubulin, and SSTR3 did not give a robust ciliary signal, detyrosinated tubulin and glutamylated tubulin marked cilia well enough to use for qIF (Figure 4.2A). To ensure that detyrosinated tubulin and glutamylated tubulin would work with and without stimulation, we tested them in *ARL13B* mutant lines under these conditions (Figure 4.2B, C). Rabbit detyrosinated tubulin antibody gave the best signal, so we used it for our SMO qIF experiments. We intend to use the mouse GT335 antibody for future GPR161 experiments in our *ARL13B* mutants.

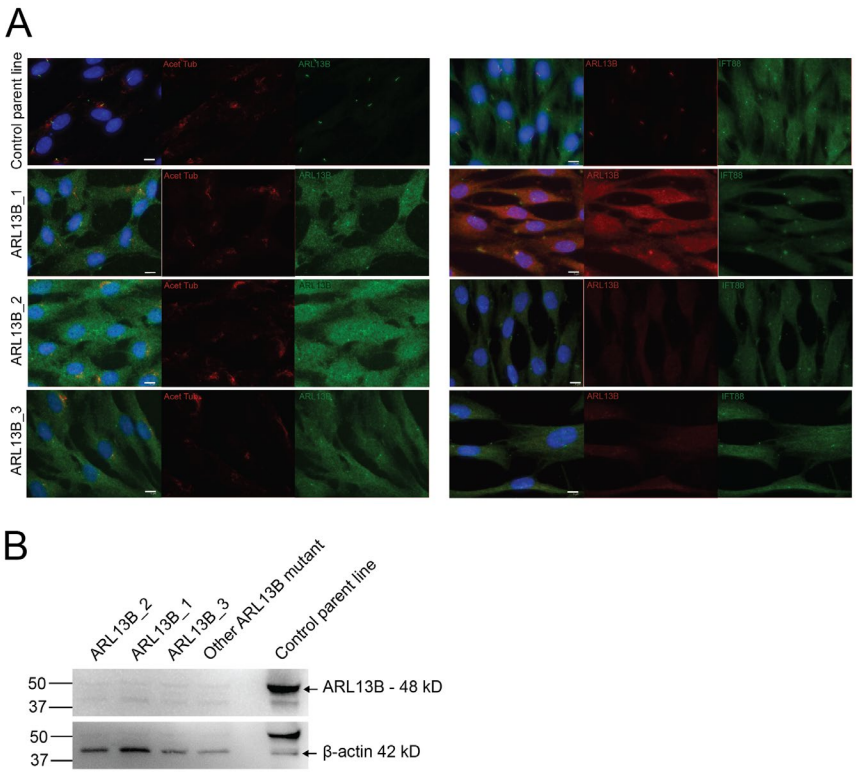

Figure 4.1. ARL13B mutant validation. (A) Immunofluorescence staining of *ARL13B* mutants and a control parent line with anti-acetylated tubulin and anti-ARL13B (left) and anti-ARL13B and anti-IFT88 (right). The mutant lines are the same lines used in Chapter 3. (B) Western blot of ARL13B and a control line. An *ARL13B* mutant that was not used in Chapter 3 was included in this western blot as part of the validation process. Scale bars are 10μm.

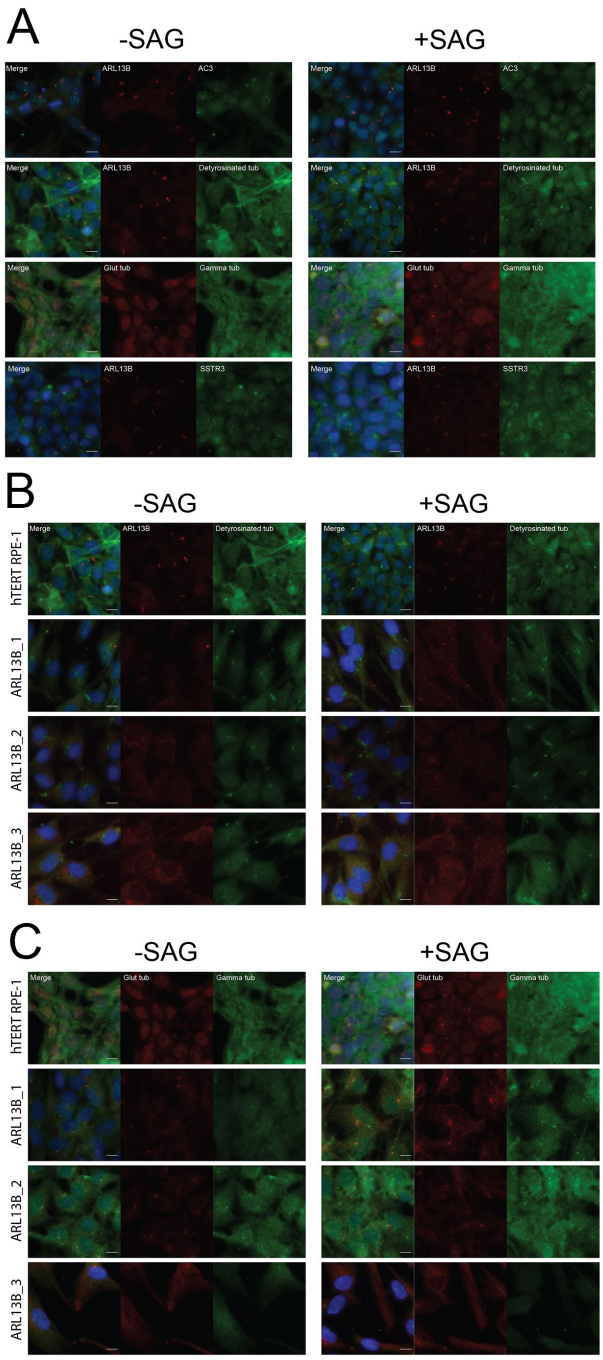

Figure 4.2. Cilium markers in ARL13B mutants. (A) Control hTERT RPE-1 cells stained with anti-ARL13B, anti-AC3, anti-detyrosinated tubulin, anti-glutamylated tubulin, anti-gamma tubulin, and anti-SSTR3. Images from cells at baseline are shown on the left and stimulated cells are on the right. (B) Staining of control and *ARL13B* mutant hTERT RPE-1 cell lines stained with anti-ARL13B and anti-detyrosinated tubulin. (C) Staining of control and *ARL13B* mutant hTERT RPE-1 cell lines stained with anti-glutamylated tubulin and anti-gamma tubulin.

Variability of GPR161 fluorescence intensity

While identifying cilium markers for *ARL13B* mutants, we moved forward with staining the other mutants for SMO and GPR161. We performed preliminary experiments with GPR161 in controls and mutants and detected a faint ciliary signal (Figure 4.3, "Preliminary GPR161 data"). As we compared our qIF results to the images, it was difficult to see any cilium-specific GPR161 signal. The cells had been fixed ~3 months prior to immunofluorescence staining, so we hypothesized that the protein had degraded. To determine whether this was true, we stained other hTERT RPE-1 cells that had been fixed from 1 week to 9 months prior to staining (Figure 4.3). Comparing the images, we detected GPR161 signal, but the intensity of the signal was low.

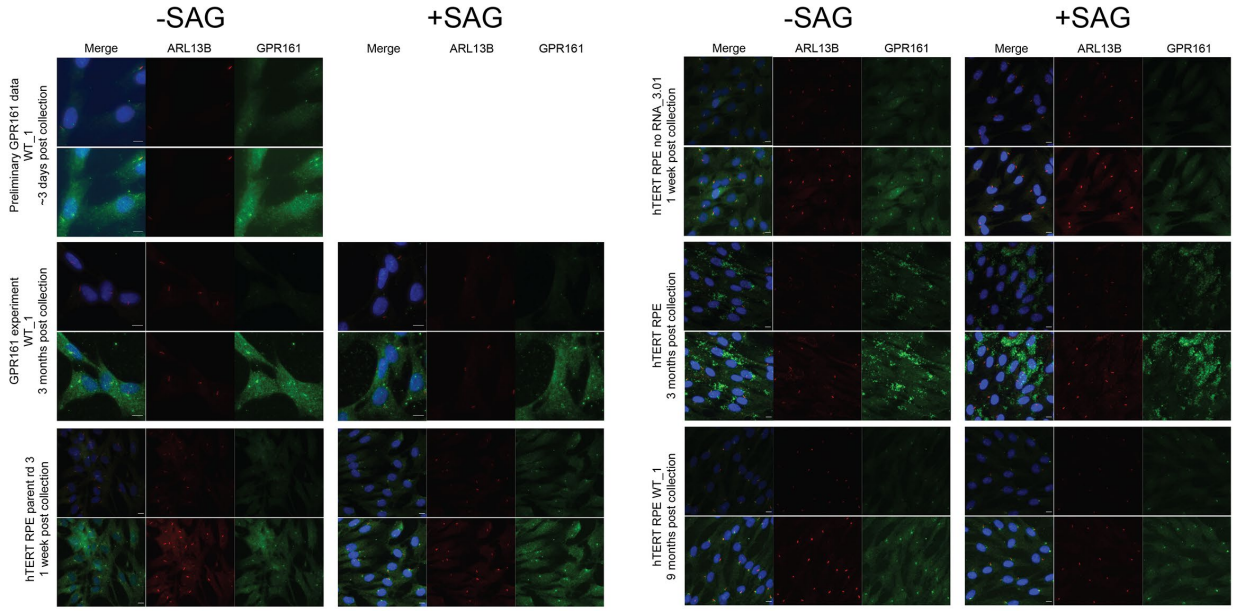

Figure 4.3. GPR161 staining in hTERT RPE-1 lines at different time points after fixation. Different hTERT RPE-1 control lines stained with anti-ARL13B and anti-GPR161. Upper panels for each line are images with no adjustment to brightness and lower panels have the brightness increased. Preliminary GPR161 data were collected when the JS mutant library was initially generated, and we did not treat these cells with SAG. Other cell lines have representative images of unstimulated cells on the left and stimulated cells on the right. Labels to the left indicate how long prior to staining the cells were fixed. Scale bars are 10μm.

Our goal is to determine whether GPR161 localization is different between control cell lines and JS mutants. In controls, we expect GPR161 signal to be lower in stimulated cells compared to baseline. Since we are only achieving low fluorescence intensity at baseline, we are reaching the lower level of detection for this assay,

therefore we will look for ways to adjust our protocol and have a brighter baseline GPR161 signal. Some parameters we can adjust include the concentration of the antibodies, using a different GPR161 antibody, trying different fixation methods, and performing these experiments using a tagged construct. Another direction we could take is changing cell culture parameters, including performing a time-course experiment to determine whether GPR161 signal is stronger at earlier or later time points and using a different pathway activator, such as recombinant SHH.

GLI3 processing

Without Hh pathway stimulation, the GLI3 transcription factor is preferentially cleaved into its repressor form (GLI3R), while pathway stimulation leads to a higher proportion of GLI3 activator form (GLI3A).[5,6] We intended to evaluate GLI3 processing in JS gene mutants by measuring the ratio between GLI3A and GLI3R bands with and without pathway stimulation. Since upstream and downstream steps in the Hh pathway responded to stimulation, we postulated that we would be able to measure the intermediate step (GLI3 processing). We used a GLI3 antibody that detects the GLI3A and GLI3R isoforms and were going to measure densitometry of the bands to calculate normalized ratios of GLI3A/GLI3R (Figure 4.4).

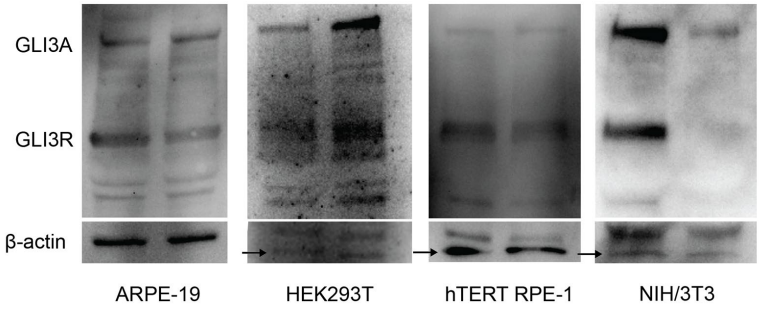

Figure 4.4. GLI3 processing in immortal cell lines. Representative western blots for ARPE-19, HEK293T, hTERT RPE-1, and NIH/3T3 cell lines probed with anti-GLI3 and anti-β-actin. GLI3 activator (GLI3A), GLI3 repressor (GLI3R), and β-actin bands are labeled on the left of the image. β-actin was used as a loading control. The arrows in HEK293T, hTERT RPE-1, and NIH/3T3 β-actin blots point to the band that is at the predicted molecular weight of β-actin. The band above is a non-specific band from the GLI3 antibody.

GLI3 processing with Hh pathway stimulation in control hTERT RPE-1 lysates

We wanted to measure differences in GLI3A/R ratios from our hTERT RPE-1 JS-gene library. We probed control lysates for GLI3 and did not observe substantial

differences in GLI3A/GLI3R normalized ratios in control cell lines (Figure 4.5). In the 7 control lines we used, we only measured slight differences in the normalized ratio between baseline and stimulated cells. This would make it challenging to determine whether differences between baseline and stimulated cells in mutants were due to assay variation or whether mutant lines differed in their GLI3 processing compared to controls.

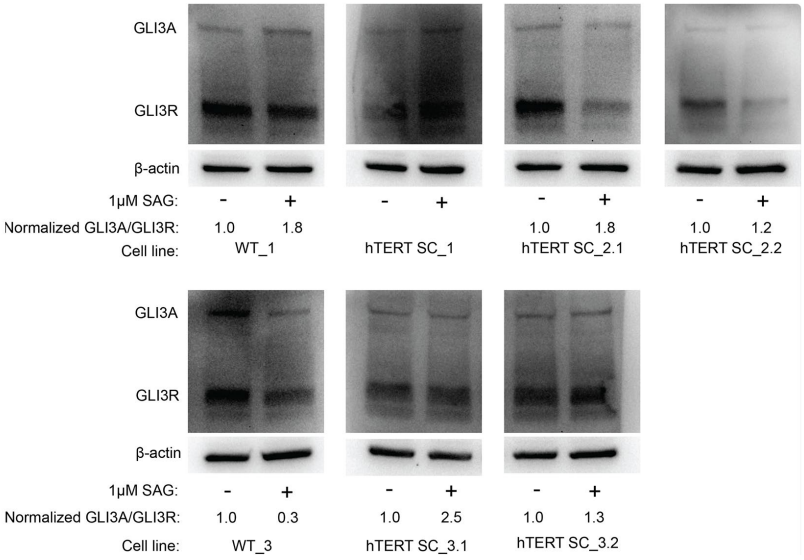

Figure 4.5. GLI3 processing in control hTERT RPE-1 cells. GLI3 western blots in control cell lines from the JS-gene mutant library. GLI3 activator (GLI3A) and GLI3 repressor (GLI3R) isoforms are labeled on the left of the image. β-actin was used as a loading control. Normalized GLI3A/GLI3R is listed below each blot except for hTERT SC_1 where the background was too high in the stimulated lane.

Since we could not demonstrate a robust GLI3 processing response to pathway stimulation, we decided to evaluate whether baseline GLI3 processing differed between JS gene mutant lines and controls (Figure 4.6A). We performed GLI3 western blots on unstimulated cell lines of controls and mutants. Baseline GLI3A/GLI3R ratios in *CSPP1, INPP5E, CC2D2A,* and *BBS1* were similar to controls. *KIF7, ARL13B, CPLANE1, TMEM67,* and *TOG1* mutants were variable within each gene, making it challenging to determine whether these differences were due to the mutations or an unknown factor

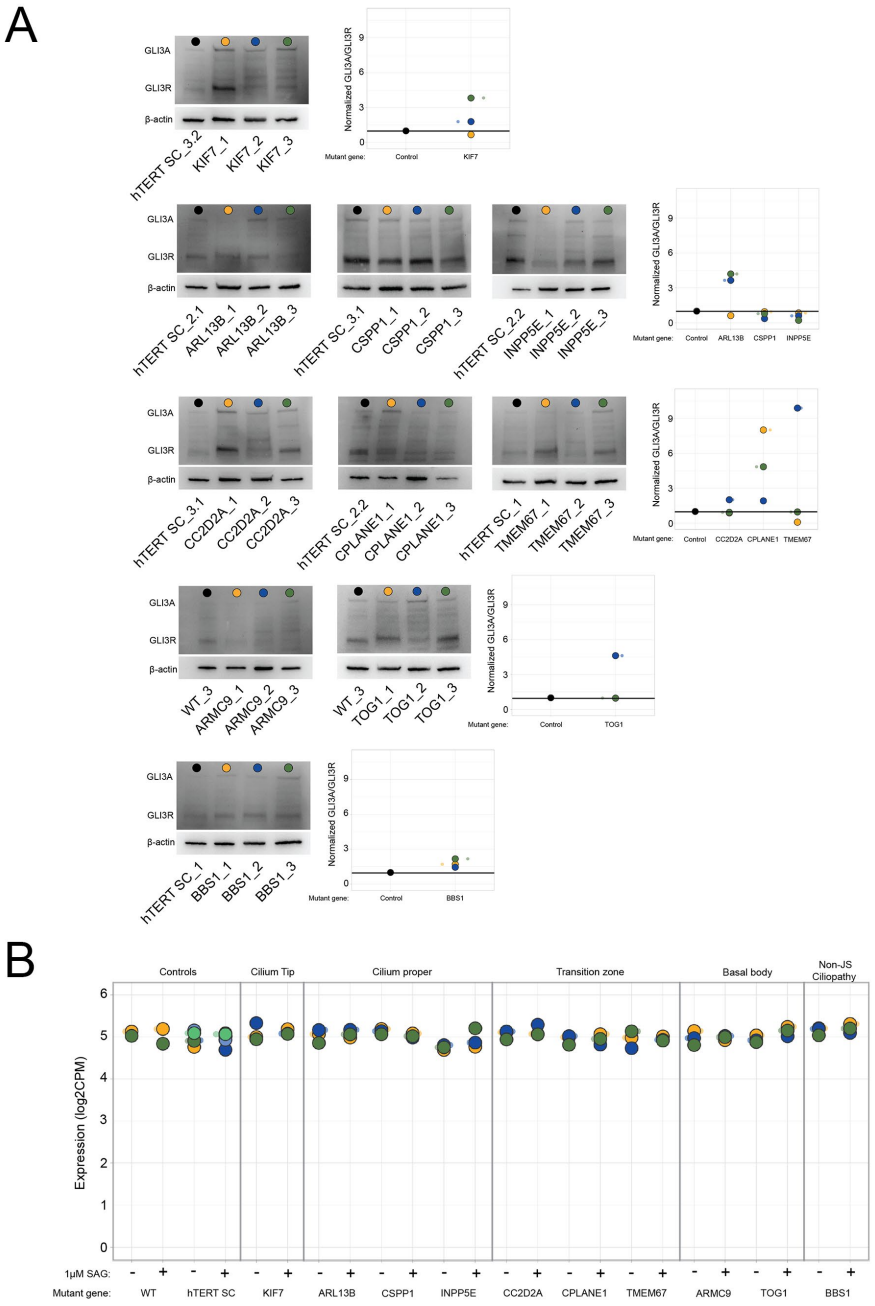

Figure 4.6. GLI3 processing in JS-gene mutants. (A) GLI3 western blots were performed using baseline control and JS-gene mutant protein lysates. Normalized GLI3A/GLI3R was calculated based on the western blot and plotted on the graphs to the right of each row. Dots above each lane correspond to the data points in the graphs. GLI3A and GLI3R are labeled on the left of each row. (B) Expression of GLI3 across controls and JS-library mutant lines. The graph was generated using data from Chapter 3 RNA-seq experiments.

affecting the results. Using the RNA-seq data generated in Chapter 3, there were no striking differences in GLI3 expression across controls and mutants (Figure 4.6B).

We are still interested in determining GLI3A/R ratios in our mutants and are considering adjusting our protocol. One proposal is to perform time-course assays to determine whether measurable changes in GLI3 isoform bands occur at a different time point than what we used. We only found two studies that used human cells to perform GLI3 western blots with pathway stimulation in JS-associated gene models, with SAG treatment time being the major difference.[7,8] The first study used S12 human keratinocyte cells in knockdowns of *Arl3.* The knockdown model had more GLI3A in baseline and stimulated cells, and a visible decrease in the GLI3R band with stimulation. Only baseline blots were shown in the study that used patient-derived cells and differences in band intensity were visible.[9–11] The predominant difference in methods between these studies and ours was the pathway stimulation length, which ranged from 12-16 hours in the publications. This supports our plan to perform time-course experiments to determine differences in GLI3 processing. Other parameters we could change are using different agonists or a different SAG concentration.

***GLI1* and *PTCH1* qPCR**

Hh pathway target genes are induced by stimulation and can be measured using qPCR and RNA-seq. Reference genes are utilized for data normalization in qPCR and their cycle threshold (CT) values should not change in response to the parameter being tested. In chapter 2, we measured the expression of *GLI1* and *PTCH1* using qPCR. Early in our validation, we identified changes in reference gene expression with pathway stimulation that would interfere with accurate measurement of *GLI1* and *PTCH1* and potentially result in erroneous results. In human fibroblasts, the reference gene, *GAPDH*, was expressed 2-4-fold lower in stimulated versus unstimulated cells, indicating that *GAPDH* is influenced by Hh signaling (Figure 4.7A). As described in the MIQE guidelines for qPCR, “[the reference gene] utility must be experimentally validated for particular tissues or cell types and specific experimental designs,” which led us to evaluate 10 reference genes for our Hh experiments[12] (Methods table 4.3).

We built a list of common reference genes used in the literature and started by testing the proposed reference genes in the four immortal cell lines at baseline and with

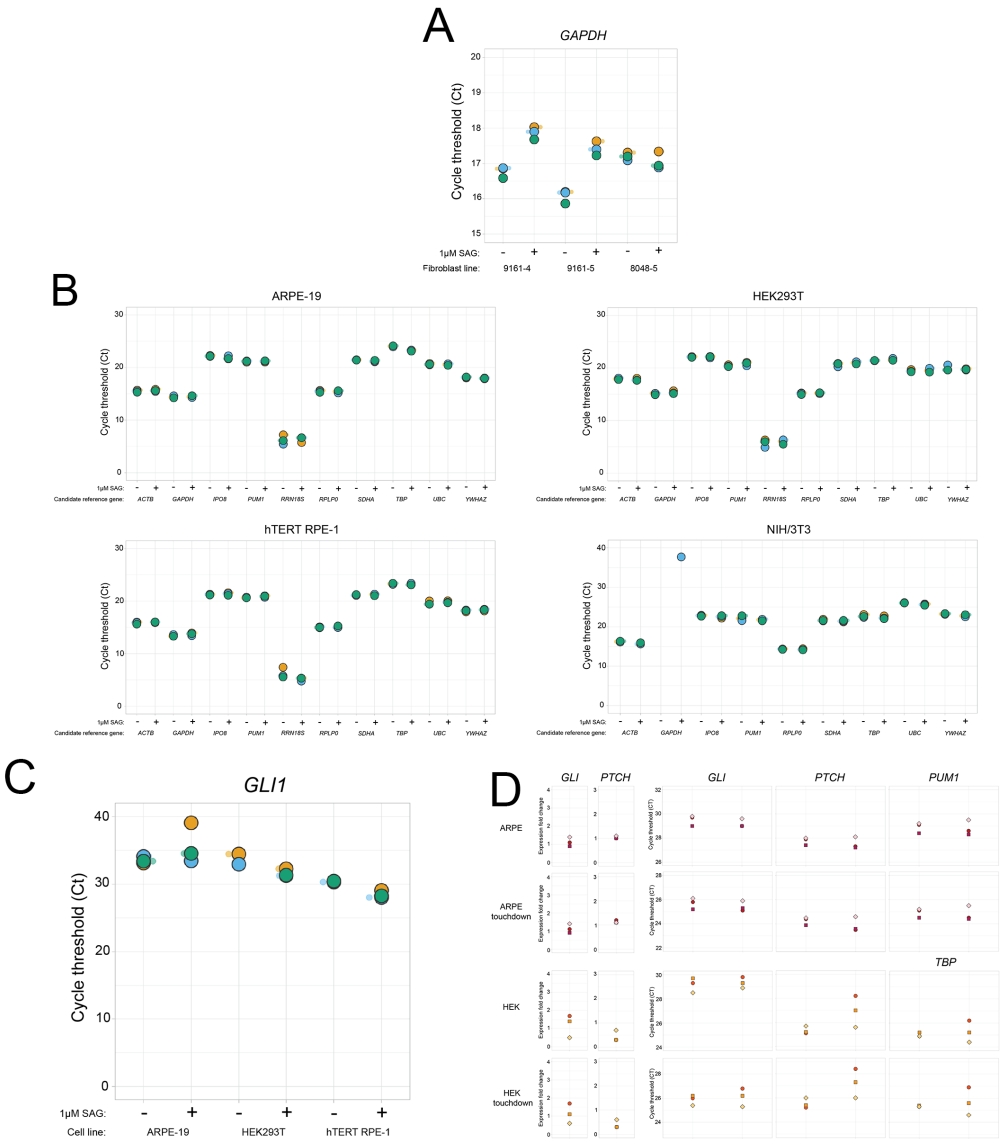

Figure 4.7. *GLI1* and *PTCH1* expression via qPCR. (A) Data from fibroblasts showing cycle threshold (CT) of the reference gene, GAPDH in unstimulated and stimulated cells. Each dot represents a technical replicate. Higher CT values normally translate to lower gene expression, while lower CT values will normally translate to higher gene expression. (B) CT of reference genes in ARPE-19, HEK293T, hTERT RPE-1, and NIH/3T3. Each dot represents a technical replicate. For GAPDH in NIH/3T3 lines, there was no measurable signal in the unstimulated replicates and only one measurable signal in the stimulated replicates. (C) CT values of GLI1 from ARPE-19, HEK293T, and hTERT RPE-1 prior to any modifications in qPCR protocol. cDNA from unstimulated and stimulated cells were used. (D) Normalized *GLI1* and *PTCH1* expression fold change for ARPE-19 and HEK293T cells in the left two columns. Raw CT values are shown for technical replicates in the right panels. Each line has data using the recommended qPCR protocol and the touchdown qPCR protocol to show differences in CT between the two protocols.

stimulation (Figure 4.7B). For our Hh experiments, we were interested in a reference gene with a Ct >20 and <30, similar to *GLI1* and *PTCH1.* We determined that the cell lines required different reference genes. After identification of a stable reference gene for each cell line, we moved on to test different primer concentrations, primer temperature gradients, and dilution curves of the cDNA template to ensure we were reliably measuring expression.

Once the parameters for our *GLI1/PTCH1* and reference gene primers were determined, we moved into experiments for the four immortal cell lines. Ct values >30 often indicate a low level of starting template, which increases variability within an experiment.[13] Early experiments with *GLI1* had Ct's >30 (Figure 4.7C), therefore we wanted to modify our protocol to lower the CT values in samples where we had a low starting template. Our first attempt at lowering the CT of *GLI1* was to elongate the primers to allow for higher fluorescence substrate binding and increase cDNA input concentration. The increased cDNA input remained within the parameters of the dilution curve with an R^2 ≥0.99 and efficiency between 80-120%. This lowered Ct's in hTERT RPE-1 and NIH/3T3 cells, but ARPE-19 and HEK293T cells continued to have CT's close to 30, so we added the touchdown qPCR protocol for these samples (Figure 4.7D). This helped lower CT's an additional 2-3 cycles and we found that the results were more reliable when repeating the experiments.

Discussion

Here, I described preliminary results from assays that need further troubleshooting, validation/modification to our protocols, and potential next steps for determining differences in Hh response related to JS. Even reliable parameters need to be adjusted based on the experiment, for example, changing a cilium marker if the protein is disrupted in a model. From our experiments, we learned the importance of validating assays for different cell types and model systems. While translating assays from one cell type or model system to another would ideally be easy, taking the time to determine how your assay is working improves the reliability of the assays and gives us more confidence in our results.

Methods

Cell culture

Cell line name and catalog number	ARPE-19 (CRL-2302)	HEK293T (CRL- 3216)	hTERT RPE-1 (CRL-4000)	NIH/3T3 (CRL-1658)	SH-SY5Y (CRL-2266)
Growth medium	DMEM:F12 with 10% FBS and 1% Pen-strep	DMEM with 10% FBS and 1% Pen-strep	DMEM:F12 with 10% FBS and 1% Pen-strep	DMEM with 10% Bovine calf serum and 1% Pen-strep	1:1 Eagle's Minimum Essential Medium: F12 with 10% FBS and 1% Pen-Strep
Cell dissociation	0.05% Trypsin				

Methods Table 1. Immortal cell line media composition. Composition of growth medium and cell dissociation method used for each cell line. All cell lines were purchased from ATCC, with catalog numbers included above.

Cells were seeded on pairs of coverslips coated with 0.3mg/mL poly-D-lysine and allowed to grow for 2-3 days, until they reach 60-80% confluency. Cells in the same batch were seeded at the same cell density and starved for 48 hours starting at the same time. Cells were serum starved for a total of 48 hours. After the initial 24 hours of serum starvation, we replaced the media on half of the coverslips with DMEM only + 1uM Smoothened Agonist (Millipore, 566661). After 24 hours of starvation, we fixed coverslips using 4% paraformaldehyde for 5 minutes, followed by permeabilization using cold Methanol for 3 minutes and stored in PBS at 4°C until ready to stain.

Cells for RNA collection were grown at the same time as coverslips. T-75 flasks were grown in pairs, and allowed to grow for 2-3 days, until cell lines reached 60-80% confluency. Cells were starved for a total of 48 hours. Half the flasks had their media replaced after the initial 24 hours with DMEM only + 1uM SAG. We lysed cells for RNA extraction using Trizol (Thermo Fisher Scientific #15596018). Trizol was added directly to cells and collected in a 15ml conical. Lysates were stored at -80°C until ready for extraction.

Immunofluorescence and microscopy

Antibody Name	Species	Concentration	Supplier	Product number
SMO	Mouse Monoclonal	1:200	Santa Cruz Biotechnology	sc-166685
ARL13B	Mouse	1:200	NeuroMab	75-287
GPR161	Rabbit polyclonal	1:200	Proteintech	13398-1-AP
Anti-tubulin, detyrosinated	Rabbit polyclonal	1:200	Sigma Aldrich	AB3201
Adenylate cyclase 3	Rabbit polyclonal	1:500	Thermo Fisher	PA5-35382
SSTR3	Rabbit polyclonal	1:2500	Thermo Fisher	PA3-207
GT335	Mouse monoclonal	1:1000	Adipogen Life Sciences	AG-20B-0020-C100
Gamma tubulin	Rabbit polyclonal	1:1000	Sigma Aldrich	T3559

Methods table 2. Antibodies used for immunofluorescence staining.

We blocked coverslips in 2% BSA in PBS for 20 minutes at room temperature. GPR161, SMO, and ARL13B antibodies were diluted as shown in the chart above. We incubated coverslips with primary antibodies at either 4°C overnight or for 1 hour at room temperature, then washed three times in PBS for 5 minutes. We incubated coverslips with the following secondary antibodies at 1:400 dilution for 1 hour at room temperature: Goat anti-Rabbit IgG, Alexa Fluor 488 (Thermo Fisher Scientific #A11008) and Donkey anti-Mouse IgG, Alexa Fluor 568 (Thermo Fisher Scientific, #A10037). After incubation, we washed coverslips three times in PBS for 5 minutes. Coverslips were mounted on slides using a Fluoromount with DAPI (Invitrogen, #00-4959-52), then sealed with nail polish after sitting for at least 1 hour.

Quantitative immunofluorescence

We quantified ciliary protein localization using a validated protocol previously established in the laboratory.[4] We acquired z-stack images for >20 cells for each condition using identical microscope settings. We converted z-stack images to sum-projections and randomized these images using the FIJI[14] script, Filename_randomizer (https://imagej.nih.gov/ij/macros/Filename_Randomizer.txt) to minimize bias. We

created cilium masks using the cilia marker (ARL13B) channel. We used this mask to measure the signal intensity for the protein of interest and measured the signal intensity of an adjacent region to subtract background signal.

All figures and graphs were generated using Plots Of Data and Super Plots Of Data.[15,16]

Western Blot

Cells were grown in pairs of T-75 cell culture flasks until ~50-75% confluent. Cells were starved for a total of 48 hours. Half the flasks had their media replaced after the initial 24 hours with DMEM only + 1uM SAG. After 24 hours, protein lysate was collected using NP-40 buffer (Thermo Fisher Scientific, FNN0021) with Halt Protease and Phosphatase Inhibitor (1:100, Thermo Fisher Scientific 78442) and PMSF (1:100, Fisher Scientific, ICN19538101). Cell lysates were reduced in 4x Laemmeli Buffer (BioRad, 1610747), 2-mercaptoethanol, and 2-3uL of DNase I. After being reduced, samples were stored at -80C. We then followed standard western blot methods[35] to probe for GLI3 (R&D Systems, AF3690-SP) using an anti-goat HRP secondary (Santa Cruz Biotech, #sc-2354). For ARPE-19, HEK293T, and hTERT RPE-1, we used β-actin as the loading control. For NIH/3T3, we used SDHA as a loading control. GLI3 isoform ratios are measured using band densitometry on a BioRad ChemiDoc.

RNA isolation and qPCR

Cells were grown in pairs of T-75 cell culture flasks until ~50-75% confluent. Cells were starved for a total of 48 hours. Half the flasks had their media replaced after the initial 24 hours with DMEM only + 1uM SAG. We dissociated the cells and extracted RNA using the Aurum Total RNA mini kit (Biorad, 7326820). We measured RNA concentration using a spectrophotometer (brand) and only included RNA that had an A260/280 >1.8. cDNA was generated using the BioRad iScript cDNA Synthesis kit. We set up qPCR reactions using the PowerUp SYBR Green Master Mix (Thermo Fisher Scientific, #A25741). For cell lines that required the touchdown qPCR protocol, we followed the protocol outlined in Zhang et al.[18] Briefly, our protocol went as follows: 50ºC (2 min), 95ºC (2 min), 4x [95ºC (20 sec), 65ºC (10 sec, decrease

Gene symbol	Gene name	Forward and Reverse Primer
ACTB	Actin Beta	5'-GAGCACAGAGCCTCGCCTTT-3' 5'-TCATCATCCATGGTGAGCTGG-3'
GAPDH	Glyceraldehyde 3-phosphate dehydrogenase	5'-AGGTGAAGGTCGGAGTCAAC-3' 5'-TTCACACCCATGACGAACAT-3'
IPO8	Importin 8	5'-TGCAGTCCGGCCTACTGTTC-3' 5'-TGTAGGACTGGTTGAGCTCGTTC-3'
PUM1	Pumillio RNA Binding Family Member	5'-AAGGACAGCAGCAGGTTCTC-3' 5'-CCTTGTCCAAATGCAAGGGC-3'
RPLP0	Ribosomal Protein Lateral Stalk Subunit P0	5'-CGTCCTCGTGGAAGTGACAT-3' 5'-TAGTTGGACTTCCAGGTCGC-3'
SDHA	Succinate dehydrogenase complex flavoprotein subunit A	5'-GCATTTGGCCTTTCTGAGGC-3' 5'-TTGATTCCTCCCTGTGCTGC-3'
TBP	TATA Binding Protein	5'-GTGACCCAGCATCACTGTTTC-3' 5'-AGAGCATCTCCAGCACACTC-3'
UBC	Ubiquitin C	5'-CCGGGATTTGGGTCGCAG-3' 5'-TCACGAAGATCTGCATTGTCAAG-3'
YWHAZ	Tryosine 3-Monooygenase.Tryptophan 5-Monooygenase Activation Protein Zeta	5'-GACACAGAACATCCAGTCATGG-3' 5'-TCATATCGCTCAGCCTGCTC-3'
18S[97]	18S rRNA	5'-AGAAACGGCTACCACATCCA-3' 5'-CACCAGACTTGCCCTCCA-3'
Actb	Actin Beta	5'-TAGGCACCAGGGTGTGATG-3' 5'-TCTCCATGTCGTCCCAGTTG-3'
Gapdh	Glyceraldehyde 3-phosphate dehydrogenase	5'-AATGTGTCCGTCGTGGATCT-3' 5'-ATACGGCTACAGCAACAGGG-3'
Ipo8	Importin 8	5'-ACAAGCTCTGCTGACTGTGC-3' 5'-CAGTGTCCTTCGGTGCTCTG-3'
Pum1	Pumillio RNA Binding Family Member	5'-GAAAGGTAAGGGGGAGCGAG-3' 5'-CTCATTCCACCAACACGGGC-3'
Rplp0	Ribosomal Protein Lateral Stalk Subunit P0	5'-TCCTCGTTGGAGTGACATCG-3' 5'-AGTTGGACTTCCAGGTCGC-3'
Sdha	Succinate dehydrogenase complex flavoprotein subunit A	5'-ACTGTTATTGCTACTGGGGGC-3' 5'-CCCTAGTGACCATGGCTGTG-3'
Tbp	TATA Binding Protein	5'-GGTATCTGCTGGCGGTTTGG-3' 5'-GAAATAGTGATGCTGGGCACTG-3'
Ubc	Ubiquitin C	5'-CCCACACAAAGCCCCTCAAT-3' 5'-AAGATCTGCATCGTCTCTCTCACG-3'
Ywhaz	Tryosine 3-Monooygenase.Tryptophan 5-Monooygenase Activation Protein Zeta	5'-GGTATCTGCTGGCGGTTTGG-3' 5'-GAAATAGTGATGCTGGGCACTG-3'

Methods Table 3. Candidate qPCR reference gene names and primer sequences. We included 10 candidate reference genes for human-derived cell lines and 9 candidate gene reference genes for the NIH/3T3 murine-derived cell line.

3ºC/cycle, 72ºC (1 min)], 40x [95ºC (15 sec), 55ºC (15 sec), 72ºC (1 min)], ending with a melt temperature curve. qPCR data acquisition was performed on the Bio-Rad CFX96 Touch Real-Time PCR Detection System.

Human *GLI1* primers
Forward 5'-GATGACCCCACCACCAATCAGTAG-3'
Reverse 5'-AGACAGTCCTTCTGTCCCCACA-3'
Human *PTCH1 primers*
Forward 5'-GAGCACTTCAAGGGGTACGA-3'
Reverse 5'-GGAAAGCACCTTTTGAGTGG-3'
Mouse *Gli1* primers
Forward 5'-CCGACGGAGGTCTCTTTGTC-3'
Reverse 5'-GCGTCTCAGGGAAGGATGAG-3'
Human *Ptch1 primers*
Forward 5'-GAGCAGATTTCCAAGGGGAAG -3'
Reverse 5'-CCACAACCAAAAACTTGCCG -3'

RNA isolation and RNA-seq

When ready to extract, frozen lysates were thawed and chloroform was added (Millipore #C2432), with the aqueous phase being used for RNA cleanup (RNA Clean and Concentrator kit, Zymo research, #R1013). Following RNA cleanup, RNA concentration and purity were determined using a spectrophotometer. RIN RNA purity was determined using the Agilent 2100 Bioanalyzer (#G2939BA). Total RNA samples were submitted to Novogene for Eukaryotic RNA-seq (cDNA library). Only samples with a RIN score ≥4 with smooth baseline, A260/280 >1.8-2.2, and A260/230 ≥1.8, as outlined by the company. Sample submission included RNA sample QC, mRNA library prep (poly A enrichment), Sequencing (Illumina – PE150 – 30M paired reads), data quality control, and raw data. Sequence data was generated in a single run in the same lane.

Sequencing quality was assessed using FASTQC results. Read alignment was performed using GRCh38.p12 with reference genome GENCODE human release 30 using STAR (v2.7.9a). The aligned BAM files were used for analysis and the number of reads that overlap each gene were counted using the featureCounts function in Bioconducted Rsubread[125] package and gene definitions were used from the

GENCODE human release 30 GTF files. Read counts are used to compare the expression of each gene in different samples.

References

1. Frikstad, K.-A. M. *et al.* A CEP104-CSPP1 Complex Is Required for Formation of Primary Cilia Competent in Hedgehog Signaling. *Cell Rep.* **28**, 1907-1922.e6 (2019).
2. Constable, S., Long, A. B., Floyd, K. A., Schurmans, S. & Caspary, T. The ciliary phosphatidylinositol phosphatase Inpp5e plays positive and negative regulatory roles in Shh signaling. *Dev. Camb. Engl.* **147**, dev183301 (2020).
3. Shimada, H. *et al.* In Vitro Modeling Using Ciliopathy-Patient-Derived Cells Reveals Distinct Cilia Dysfunctions Caused by CEP290 Mutations. *Cell Rep.* **20**, 384–396 (2017).
4. Slaats, G. G. *et al.* MKS1 regulates ciliary INPP5E levels in Joubert syndrome. *J. Med. Genet.* **53**, 62–72 (2016).
5. Belgacem, Y. H. & Borodinsky, L. N. Sonic hedgehog signaling is decoded by calcium spike activity in the developing spinal cord. *Proc. Natl. Acad. Sci. U. S. A.* **108**, 4482–4487 (2011).
6. Mukhopadhyay, S. *et al.* The Ciliary G-Protein-Coupled Receptor GPR161 Negatively Regulates the Sonic Hedeghog Pathway via cAMP Signaling. https://reader.elsevier.com/reader/sd/pii/S0092867412015486?token=8218DA8606404AD9458BFEABA8432B12E0931F47C9C6427A380F88C0BF5C947C622B40E7336E249D34CE916D497FFDBD&originRegion=us-east-1&originCreation=20210404205857 doi:10.1016/j.cell.2012.12.026.
7. Lai, C. K. *et al.* Functional characterization of putative cilia genes by high-content analysis. *Mol. Biol. Cell* **22**, 1104–1119 (2011).
8. De Mori, R. *et al.* Hypomorphic Recessive Variants in SUFU Impair the Sonic Hedgehog Pathway and Cause Joubert Syndrome with Cranio-facial and Skeletal Defects. *Am. J. Hum. Genet.* **101**, 552–563 (2017).
9. Alby, C. *et al.* Mutations in KIAA0586 Cause Lethal Ciliopathies Ranging from a Hydrolethalus Phenotype to Short-Rib Polydactyly Syndrome. *Am. J. Hum. Genet.* **97**, 311–318 (2015).
10. Putoux, A. *et al.* KIF7 mutations cause fetal hydrolethalus and acrocallosal syndromes. *Nat. Genet.* **43**, 601–606 (2011).
11. Thomas, S. *et al.* TCTN3 mutations cause Mohr-Majewski syndrome. *Am. J. Hum. Genet.* **91**, 372–378 (2012).
12. Bustin, S. A. *et al.* The MIQE guidelines: minimum information for publication of quantitative real-time PCR experiments. *Clin. Chem.* **55**, 611–622 (2009).
13. Taylor, S. C. *et al.* The Ultimate qPCR Experiment: Producing Publication Quality, Reproducible Data the First Time. *Trends Biotechnol.* **37**, 761–774 (2019).
14. Schindelin, J. *et al.* Fiji: an open-source platform for biological-image analysis. *Nat. Methods* **9**, 676–682 (2012).
15. Goedhart, J. SuperPlotsOfData—a web app for the transparent display and quantitative comparison of continuous data from different conditions. *Mol. Biol. Cell* **32**, 470–474 (2021).
16. Postma, M. & Goedhart, J. PlotsOfData—A web app for visualizing data together with their summaries. *PLOS Biol.* **17**, e3000202 (2019).

17. Jacob, F. *et al.* Careful selection of reference genes is required for reliable performance of RT-qPCR in human normal and cancer cell lines. *PloS One* **8**, e59180 (2013).
18. Zhang, Q. *et al.* TqPCR: A Touchdown qPCR Assay with Significantly Improved Detection Sensitivity and Amplification Efficiency of SYBR Green qPCR. *PLOS ONE* **10**, e0132666 (2015).
19. Liao, Y., Smyth, G. K. & Shi, W. The R package Rsubread is easier, faster, cheaper and better for alignment and quantification of RNA sequencing reads. *Nucleic Acids Res.* **47**, e47 (2019).

Chapter 5: Concluding Remarks

Our ability to identify genetic causes in individuals with Joubert syndrome (JS) has improved greatly over time, but we know less about how the genetic defects impact cellular function and result in the JS brain malformation and progressive characteristics seen in patients. Animal, cell, and human-derived cell models are providing clues for the function of JS-associated genes, and potential cellular defects that contribute to JS. JS is defined by a brain malformation unique among ciliopathies, so we hypothesize that ll of the genetic causes converge on a single cellular defect that results in the abnormal brain development central to JS. This shared defect or other cellular defects may contribute to the progressive organ features experienced by Individuals with JS and other ciliopathies. Identifying the mechanism(s) underlying JS will identify potential therapeutic targets for the variable features that will help individuals with JS live longer, healthier lives. Our understanding of the cellular mechanisms will also help us better understand the role of cilia during hindbrain development and how cilium dysfunction leads to the molar tooth sign.

To determine whether aberrant Hh signaling could be a unifying mechanism present across genetic causes of JS, I first evaluated immortal cell lines to identify the most suitable for modeling Hh with JS gene dysfunction. hTERT RPE-1 cells met our criteria: human-derived, immortal, adherent, increased ciliation with serum starvation, genetically tractable, and were responsive to Hh signaling by relocalizing pathway proteins and upregulating pathway target genes. I then performed Hh pathway assays in a library of genome-engineered JS mutant lines, and while SMO localization and Hh target gene expression are frequently abnormal, we did not identify a shared Hh pathway dysfunction across 9 causes of JS. While our experiments cannot fully exclude a role for Hh dysfunction in the JS-related brain phenotype, and substantial evidence supports a role for Hh dysfunction in JS-related kidney disease.[1]

In the short term, we will continue using our library of mutant cell lines to evaluate other aspects of Hh signaling. We would like to evaluate GPR161 in the mutant library and use this data to complement our SMO data. Recently, a manufactured rat ARL13B antibody became available, which offers an opportunity to co-stain SMO, GPR161, and ARL13B. This would allow us to measure differences in localization within the same cilia, making for more efficient data generation and help us better understand the

dynamic process of protein localization in response to pathway stimulation. Other parameters in our Hh assays that we are interested in adjusting are measuring Hh response at different SAG exposure time points and using different pathway activators (Shh-N and recombinant SHH). These experiments will add to our understanding of differences between control and mutant response to pathway stimulation.

Another route we plan to take in the short term is using our RNA-seq data to generate new hypothesis-based questions and identify genes with changes in expression with pathway stimulation. This includes looking at expression of known pathway-related genes (i.e. GPR161, TULP3, KIF7), identifying genes that change expression with pathway stimulation in controls, and identifying genes that change expression in mutants but not controls. In a broader sense, we also want to determine how other signaling pathways respond to Hh pathway stimulation. In Chapter 3, there was a pattern of blunted Hh signaling in a subset of mutants, but there were instances of downstream target gene expression having minimal perturbation when upstream SMO localization was perturbed. This could suggest other cilium-mediated signaling pathways could be affecting downstream pathway signaling in mutants. For example, WNT, PDGFα, Notch, and mTOR signaling are mediated by the primary cilium.[2–4] Evidence of crosstalk between some of these pathways with Hh signaling is already known and breakdown of this crosstalk leads to disease states (i.e. cancer, diabetes).[5–7] A deep dive into this data set will help us determine whether multiple pathways are perturbed in JS and contribute to the underlying mechanism.

In the medium term, I'd like to see our lab expand the mutant library and incorporate additional tools to help us understand whether Hh signaling is abnormal across genetic causes of JS. I would like to see the library expand by number of genes represented and by the cell types used to generate the mutants. We started with 9 JS-associated genes that span the different ciliary subdomains, but there were limitations in some of the genes we selected. For example, *CPLANE1* and *TMEM67* mutants did not ciliate at high proportions, which did not allow us to measure SMO fluorescence intensity, while *CC2D2A* mutants ciliated at moderate proportions and were the only data we had for transition zone mutants in our SMO data set. We would want to include more transition zone mutants to determine any shared SMO localization patterns and

expanding the number of genes represented in other ciliary subdomains will help us better identify any shared patterns in response to Hh stimulation. JS affects multiple organs, including the brain, eye, kidney, and liver. We selected hTERT RPE-1 cells based on their response to Hh signaling *in vitro*, but incorporating other cell types that represent organ systems affect by JS will help us better understand the broader disease mechanism(s) of JS. Human renal cortical tubular epithelial cells (RCTE) have been used to determine differences in GLI3 processing in a model of *HYLS1*[8] and could be a useful cell type to generate mutants in.

At the experimental level, I'd want to incorporate other means of measuring changes in Hh response. Our current experiments look at response to pathway at one time point in fixed cells. We could consider incorporating the GLI luciferase assay, which measures the activity of GLI transcription factors over time by expressing a GLI-8x plasmid.[9] We determined *GLI1* expression in cilium proper and transition zone mutants was lower 24-hours after SAG exposure. Being able to measure changes in GLI activity across time points using the GLI-8x plasmid could determine if mutants responded faster or slower to pathway stimulation, and if the blunted response is consistent.

In the long term, we would want to pair our experiments in immortal cell models with the library of patient-derived JS cell lines available in our library. Once we identify a potential JS mechanism, we would use our patient cell lines to validate our findings. Validating any potential mechanism in patient-derived cells will allow for the possibility to identify therapeutic targets to dampen the severity of the variable features of JS. If time and money were not a factor, we would expand our cell library to include induced pluripotent stem cells (iPSC) and potentially move towards non-human primates. This would bring us closer to understanding what neural types are affected by JS-variants and how different cell types, derived from the same iPSC parent line or in the same animal, are affected by the same variant/mutation.

While we did not identify a shared difference in Hh signaling response, we took an approach that differed from what is typically done. Instead of focusing deeply on a single gene, we looked broadly across genetic causes of JS using the same assays, which helped us determine that in SMO localization and target gene induction are not

consistently perturbed across genetic causes of JS. My work has generated mutant cell lines and data sets to use to further explore Hh signaling and other candidate mechanisms for JS. My results will help guide future work to evaluate other aspects of Hh signaling in cell-based and animal-based models for JS and other ciliopathies.

References

1. Hynes, A. M. *et al.* Murine Joubert syndrome reveals Hedgehog signaling defects as a potential therapeutic target for nephronophthisis. *Proc. Natl. Acad. Sci. U. S. A.* **111**, 9893–9898 (2014).
2. Cano, D. A., Murcia, N. S., Pazour, G. J. & Hebrok, M. Orpk mouse model of polycystic kidney disease reveals essential role of primary cilia in pancreatic tissue organization. *Dev. Camb. Engl.* **131**, 3457–3467 (2004).
3. Schneider, L. *et al.* PDGFRalphaalpha signaling is regulated through the primary cilium in fibroblasts. *Curr. Biol. CB* **15**, 1861–1866 (2005).
4. Boehlke, C. *et al.* Primary cilia regulate mTORC1 activity and cell size through Lkb1. *Nat. Cell Biol.* **12**, 1115–1122 (2010).
5. Larsen, L. J. & Møller, L. B. Crosstalk of Hedgehog and mTORC1 Pathways. *Cells* **9**, E2316 (2020).
6. Pelullo, M. *et al.* Wnt, Notch, and TGF-β Pathways Impinge on Hedgehog Signaling Complexity: An Open Window on Cancer. *Front. Genet.* **10**, 711 (2019).
7. Benchoula, K., Parhar, I. S. & Wong, E. H. The crosstalk of hedgehog, PI3K and Wnt pathways in diabetes. *Arch. Biochem. Biophys.* **698**, 108743 (2021).
8. Chen, C. *et al.* Ciliopathy protein HYLS1 coordinates the biogenesis and signaling of primary cilia by activating the ciliary lipid kinase PIPKIγ. *Sci. Adv.* **7**, eabe3401 (2021).
9. Hyman, J. M. *et al.* Small-molecule inhibitors reveal multiple strategies for Hedgehog pathway blockade. *Proc. Natl. Acad. Sci. U. S. A.* **106**, 14132–14137 (2009).

Appendix A

	Abnormal SMO localization	Abnormal GLI2 localization	Abnormal GLI3 localization	Abnormal GPR161 localization	Abnormal GLI2 WB	Abnormal GLI3 WB	Abnormal *GLI1* mRNA	Abnormal *PTCH1* mRNA	Abnormal *SHH* mRNA	Abnormal *GLI1* in situ	Abnormal *PTCH1* in situ	Abnormal neural tube (in situ/IF)	Polydactyly
AHI1 KO[1]	NL						AB	NL					
ARL13B KO/null[2–9]	AB NL	NL	AB			NL	AB	AB	AB			AB	AB
ARL13B KD[5,6,10]	AB	NL	AB				AB	AB NL					
ARL3 KD[11,12]	AB		AB			AB							
ARMC9 KO/null[13]	NL	AB	AB										
B9D1 KO/null[14]	AB					AB	AB	AB				AB	AB
B9D1 KD[15]	AB												
B9D2 KD[15]													AB
C2CD3 KD[16–18]					AB	AB		AB	AB	AB	AB	AB	AB
CC2D2A KO/null[14,19,20]	AB											AB	AB
CC2D2A KD[14,19,20]	AB												
CEP41													
CEP83													
CEP104 KD[21,22]	AB		AB	AB									
CEP120													
CEP290 KO/null[23–26]	AB	AB		AB			AB	AB					
CEP290 KD[23–26]	AB NL					AB	AB NL		NL				
CPLANE1 KD[27]							AB	AB					
CSPP1 KO/null[22,28]	AB												
CSPP1 KD[22,28]							AB						
FAM149B1 KD[29]							AB	AB					AB
HYLS1 KD[30]			AB	AB			AB	AB					
IFT7172 KO/null[31–37]	AB					AB	AB				AB	AB	
IFT7172 KD[31–37]							AB			AB	AB		AB
INPP5E KO/null[38–41]	AB	AB	AB	AB	AB	AB	AB	AB				AB	AB

KATNIP													
KIAA0586 KO/null[42–46]					AB		AB	AB		AB	AB	AB	AB
KIAA0586 KD[42–46]						AB	AB	AB				AB	AB
KIAA0753 KD[47]							AB	AB	AB				
KIF7 KO/null[48–55]	NL	AB	AB		AB	AB	AB NL	AB		AB	AB	AB	AB
KIF7 KD[11,27,52,56–61]	NL	AB	AB		AB	AB	NL	AB NL			AB	AB	AB
MKS1 KO/null[37,62–64]	AB			AB						AB	AB	AB	AB
MKS1 KD[37,62–64]										AB	AB	AB	AB
NPHP1													
NPHP4													
OFD1 KD[65]						AB	AB	AB	AB				
PDE6D													
PIBF1													
RPGRIP1L KO/null[66–68]						AB	AB	AB			AB	AB	AB
RPGRIP1L KD[66–68]	AB						AB	AB					
SUFU KO/null[55,69–79]		AB	AB	AB	AB	AB	AB NL	AB	AB	AB	AB	AB	AB
SUFU KD[55,73,75,76,80–83]	AB				AB NL	AB	AB	AB	AB		AB	AB	AB
TCTN1 KO/null[19]	AB					AB				AB	AB		AB
TCTN2 KO/null[19,84–86]	AB					AB	AB	AB				AB	AB
TCTN2 KD[19,84–86]													AB
TCTN3 KO/null[87,88]	AB											AB	AB
TCTN3 KD[87,88]					AB	AB	AB	AB					AB
TMEM67 KO/null[19,89]	NL								AB			AB	
TMEM67 KD[19,89]							NL	NL		NL	AB		
TMEM107 KO/null[90,91]													AB
TMEM107 KD[90,91]							AB			AB	AB	AB	AB

TMEM138													
TMEM216[92] KD													AB
TMEM218													
TMEM231 KO/null[14]							AB					AB	AB
TMEM231 KD[14]	AB												
TMEM237													
TOGARAM1 KD[93]	AB												

Appendix Table 1. Overview of Hedgehog readouts from the literature divided by knockout/null and knockdown models. Readouts of Hedgehog assays were categorized as normal (NL) if there was no statistical difference between controls and mutants or if authors categorized the results as normal. If there was a statistical difference between controls and mutants or if authors categorized results as different between control and mutants, than results were categorized as abnormal (AB). Models were categorized as knockout/null based on available functional assays, whereas all other models were categorized as knockdown. Human cell lines that did not have any functional data available were categorized as knockdowns. References are the same as Table 1.2.

	Abnormal SMO localization	Abnormal GLI2 localization	Abnormal GLI3 localization	Abnormal GPR161 localization	Abnormal GLI2 WB	Abnormal GLI3 WB	Abnormal *GLI1* mRNA	Abnormal *PTCH1* mRNA	Abnormal *SHH* mRNA	Abnormal *GLI1* in situ	Abnormal *PTCH1* in situ	Abnormal neural tube (in situ/IF)	Polydactyly
AHI1[1]	NL: M cells						M cells	NL: M cells					
ARL13B KO/null[2–9]	M, H cells NL: M cells	NL: M cells	M cells	H cells		NL: M cells	M cells M tissue	M cells M tissue	M tissue			M	M
ARL13B KD[5,6,10]	M cells	NL: M cells	M cells				M, H cells	H cells NL: M cells					
ARL3[11,12]	M cells		M, H cells			H cells							
ARMC9[13]	NL: M cells	M cells	M cells										
B9D1[14,15]	M cells					M tissue	M cells M tissue	M cells				M	M
B9D2[15]													H
C2CD3 KD[16–18]					C tissue	M, C tissue		C tissue	C tissue	M, C tissue	M tissue	M	M, C
CC2D2A[14,19,20]	M cells											M	M, C
CEP41													
CEP83													
CEP104[21,22]	H cells		H cells	H cells									
CEP120													
CEP290 KO/null[24,25]	PT cells	PT cells		PT cells			PT cells	PT cells					
CEP290 KD[23,26]	M cells NL: M cells					M tissue	M tissue M cells NL: M, H cells		NL: H cells				
CPLANE1[27]							PT cells	PT cells					
CSPP1[22,65]	H cells						PT cells						
FAM149B1[29]							PT cells	PT cells					H
HYLS1 KD[30]			H cells	H cells			H cells	H cells					
IFT7172 KO/null[31–37]	M cells					M tissue	M cells			M tissue	M tissue	M	M

INPP5E KO/null[38–41]	M cells	M cells	M cells	M cells M tissue	M tissue	M tissue	M tissue M cells	M cells				M	M
KATNIP													
KIAA0586 KO/null[42–46]					M tissue	PT cells C tissue	M tissue PT cells	M tissue PT cells		M tissue	M tissue	M, C	M, C
KIAA0753[47]							PT cells	PT cells	H cells				
KIF7 KO/null[48–55]	NL: M cells	M cells	M cells		M tissue	M tissue	M cells NL: M cells	M cells		M cells	M tissue	M	M
KIF7 KD[11,27,52,56–61]	NL: M cells	M cells	M H cells		M tissue	M, H tissue	NL: Z tissue	H tissue NL: Z tissue		M, Z tissue		M	M, H
MKS1[37,62–64]	M cells			M cells						M tissue	M tissue	M	M
NPHP1													
NPHP4													
OFD1[65]						M tissue	M tissue	M tissue	M tissue				
PDE6D													
PIBF1													
RPGRIP1L[66–68]	PT cells					M tissue	M cells, PT cells	M cells, PT cells		M tissue		M	M
SUFU KO/null[55,69–79]		M cells	M cells	M cells	M cells M tissue	M cells M tissue	M cells M tissue NL: M tissue	M tissue	M tissue	M tissue	M tissue	M	M
SUFU KD[55,73,75,76,80–83]	PT cells				M tissue NL: M tissue	M cells M tissue	M cells M tissue	M cell M tissue	M tissue	M tissue		M	M
TCTN1[19]	M cells					M tissue				M tissue	M tissue		M
TCTN2[19,84–86]	M, H cells					M tissue	M cells	M cells				M	M, H
TCTN3[87,88]	M cells				M tissue	PT cell M tissue	M cells M tissue	H cells M tissue				M	M, H
TMEM67 KO/null[19,89]	NL: M cells								M tissue			M	
TMEM67 KD[94]							NL: Z tissue	NL: Z tissue		NL: Z tissue	Z tissue		
TMEM107 KO/null[90,91]							PT cells			M tissue	M tissue	M	M, H
TMEM138													

TMEM216[92]													H
TMEM218													
TMEM231[14]	M cells						M tissue					M	M
TMEM237													
TOGARAM1[93]	H cells												

Appendix Table 2. Overview of model systems used to determine Hedgehog assay readout. Different model systems were categorized by their origin: Human (H), Patient (PT), Mouse (M), Chick (C), Zebrafish (Z). References are the same as Table 1.2.

References

1. Muñoz-Estrada, J. & Ferland, R. J. Ahi1 promotes Arl13b ciliary recruitment, regulates Arl13b stability and is required for normal cell migration. *J. Cell Sci.* **132**, jcs230680 (2019).
2. Larkins, C. E., Aviles, G. D. G., East, M. P., Kahn, R. A. & Caspary, T. Arl13b regulates ciliogenesis and the dynamic localization of Shh signaling proteins. *Mol. Biol. Cell* **22**, 4694–4703 (2011).
3. Su, C.-Y., Bay, S. N., Mariani, L. E., Hillman, M. J. & Caspary, T. Temporal deletion of Arl13b reveals that a mispatterned neural tube corrects cell fate over time. *Dev. Camb. Engl.* **139**, 4062–4071 (2012).
4. Nozaki, S. *et al.* Regulation of ciliary retrograde protein trafficking by the Joubert syndrome proteins ARL13B and INPP5E. *J. Cell Sci.* **130**, 563–576 (2017).
5. Mariani, L. E. *et al.* Arl13b regulates Shh signaling from both inside and outside the cilium. *Mol. Biol. Cell* mbc.E16-03-0189 (2016) doi:10.1091/mbc.E16-03-0189.
6. Gigante, E. D., Taylor, M. R., Ivanova, A. A., Kahn, R. A. & Caspary, T. ARL13B regulates Sonic hedgehog signaling from outside primary cilia. *eLife* **9**, e50434 (2020).
7. Caspary, T., Larkins, C. E. & Anderson, K. V. The graded response to Sonic Hedgehog depends on cilia architecture. *Dev. Cell* **12**, 767–778 (2007).
8. Li, Y. *et al.* Deletion of ADP Ribosylation Factor-Like GTPase 13B Leads to Kidney Cysts. *J. Am. Soc. Nephrol. JASN* **27**, 3628–3638 (2016).
9. Ferent, J. *et al.* The Ciliary Protein Arl13b Functions Outside of the Primary Cilium in Shh-Mediated Axon Guidance. *Cell Rep.* **29**, 3356-3366.e3 (2019).
10. Bay, S. N., Long, A. B. & Caspary, T. Disruption of the ciliary GTPase Arl13b suppresses Sonic hedgehog overactivation and inhibits medulloblastoma formation. *Proc. Natl. Acad. Sci. U. S. A.* **115**, 1570–1575 (2018).
11. Schwarz, N. *et al.* Arl3 and RP2 regulate the trafficking of ciliary tip kinesins. *Hum. Mol. Genet.* **26**, 2480–2492 (2017).
12. Lai, C. K. *et al.* Functional characterization of putative cilia genes by high-content analysis. *Mol. Biol. Cell* **22**, 1104–1119 (2011).
13. Breslow, D. K. *et al.* A CRISPR-based screen for Hedgehog signaling provides insights into ciliary function and ciliopathies. *Nat. Genet.* **50**, 460–471 (2018).
14. Chih, B. *et al.* A ciliopathy complex at the transition zone protects the cilia as a privileged membrane domain. *Nat. Cell Biol.* **14**, 61–72 (2011).
15. Dowdle, W. E. *et al.* Disruption of a ciliary B9 protein complex causes Meckel syndrome. *Am. J. Hum. Genet.* **89**, 94–110 (2011).
16. Hoover, A. N. *et al.* C2cd3 is required for cilia formation and Hedgehog signaling in mouse. *Dev. Camb. Engl.* **135**, 4049–4058 (2008).
17. Chang, C.-F. *et al.* The cellular and molecular etiology of the craniofacial defects in the avian ciliopathic mutant talpid2. *Dev. Camb. Engl.* **141**, 3003–3012 (2014).
18. Brooks, E. C. *et al.* Mutation in the Ciliary Protein C2CD3 Reveals Organ-Specific Mechanisms of Hedgehog Signal Transduction in Avian Embryos. *J. Dev. Biol.* **9**, 12 (2021).
19. Garcia-Gonzalo, F. R. *et al.* A transition zone complex regulates mammalian ciliogenesis and ciliary membrane composition. *Nat. Genet.* **43**, 776–784 (2011).

20. Veleri, S. *et al.* Ciliopathy-associated gene Cc2d2a promotes assembly of subdistal appendages on the mother centriole during cilia biogenesis. *Nat. Commun.* **5**, 4207 (2014).
21. Yamazoe, T., Nagai, T., Umeda, S., Sugaya, Y. & Mizuno, K. Roles of TOG and jelly-roll domains of centrosomal protein CEP104 in its functions in cilium elongation and Hedgehog signaling. *J. Biol. Chem.* **295**, 14723–14736 (2020).
22. Frikstad, K.-A. M. *et al.* A CEP104-CSPP1 Complex Is Required for Formation of Primary Cilia Competent in Hedgehog Signaling. *Cell Rep.* **28**, 1907-1922.e6 (2019).
23. Shimada, H. *et al.* In Vitro Modeling Using Ciliopathy-Patient-Derived Cells Reveals Distinct Cilia Dysfunctions Caused by CEP290 Mutations. *Cell Rep.* **20**, 384–396 (2017).
24. Kilander, M. B. C. *et al.* A rare human CEP290 variant disrupts the molecular integrity of the primary cilium and impairs Sonic Hedgehog machinery. *Sci. Rep.* **8**, 17335 (2018).
25. Hynes, A. M. *et al.* Murine Joubert syndrome reveals Hedgehog signaling defects as a potential therapeutic target for nephronophthisis. *Proc. Natl. Acad. Sci. U. S. A.* **111**, 9893–9898 (2014).
26. Srivastava, S. *et al.* A human patient-derived cellular model of Joubert syndrome reveals ciliary defects which can be rescued with targeted therapies. *Hum. Mol. Genet.* **26**, 4657–4667 (2017).
27. Asadollahi, R. *et al.* Clinical and experimental evidence suggest a link between KIF7 and C5orf42-related ciliopathies through Sonic Hedgehog signaling. *Eur. J. Hum. Genet. EJHG* **26**, 197–209 (2018).
28. Shaheen, R. *et al.* Mutations in CSPP1, encoding a core centrosomal protein, cause a range of ciliopathy phenotypes in humans. *Am. J. Hum. Genet.* **94**, 73–79 (2014).
29. Shaheen, R. *et al.* Bi-allelic Mutations in FAM149B1 Cause Abnormal Primary Cilium and a Range of Ciliopathy Phenotypes in Humans. *Am. J. Hum. Genet.* **104**, 731–737 (2019).
30. Chen, C. *et al.* Ciliopathy protein HYLS1 coordinates the biogenesis and signaling of primary cilia by activating the ciliary lipid kinase PIPKIγ. *Sci. Adv.* **7**, eabe3401 (2021).
31. Huangfu, D. *et al.* Hedgehog signalling in the mouse requires intraflagellar transport proteins. *Nature* **426**, 83–87 (2003).
32. Huangfu, D. & Anderson, K. V. Cilia and Hedgehog responsiveness in the mouse. *Proc. Natl. Acad. Sci. U. S. A.* **102**, 11325–11330 (2005).
33. Gorivodsky, M. *et al.* Intraflagellar transport protein 172 is essential for primary cilia formation and plays a vital role in patterning the mammalian brain. *Dev. Biol.* **325**, 24–32 (2009).
34. Ocbina, P. J. R. & Anderson, K. V. Intraflagellar transport, cilia, and mammalian Hedgehog signaling: analysis in mouse embryonic fibroblasts. *Dev. Dyn. Off. Publ. Am. Assoc. Anat.* **237**, 2030–2038 (2008).
35. Ocbina, P. J. R., Tuson, M. & Anderson, K. V. Primary cilia are not required for normal canonical Wnt signaling in the mouse embryo. *PloS One* **4**, e6839 (2009).

36. Friedland-Little, J. M. *et al.* A novel murine allele of Intraflagellar Transport Protein 172 causes a syndrome including VACTERL-like features with hydrocephalus. *Hum. Mol. Genet.* **20**, 3725–3737 (2011).
37. Goetz, S. C., Bangs, F., Barrington, C. L., Katsanis, N. & Anderson, K. V. The Meckel syndrome- associated protein MKS1 functionally interacts with components of the BBSome and IFT complexes to mediate ciliary trafficking and hedgehog signaling. *PloS One* **12**, e0173399 (2017).
38. Chávez, M. *et al.* Modulation of Ciliary Phosphoinositide Content Regulates Trafficking and Sonic Hedgehog Signaling Output. *Dev. Cell* **34**, 338–350 (2015).
39. Garcia-Gonzalo, F. R. *et al.* Phosphoinositides Regulate Ciliary Protein Trafficking to Modulate Hedgehog Signaling. *Dev. Cell* **34**, 400–409 (2015).
40. Dyson, J. M. *et al.* INPP5E regulates phosphoinositide-dependent cilia transition zone function. *J. Cell Biol.* **216**, 247–263 (2017).
41. Constable, S., Long, A. B., Floyd, K. A., Schurmans, S. & Caspary, T. The ciliary phosphatidylinositol phosphatase Inpp5e plays positive and negative regulatory roles in Shh signaling. *Dev. Camb. Engl.* **147**, dev183301 (2020).
42. Bashford, A. L. & Subramanian, V. Mice with a conditional deletion of Talpid3 (KIAA0586) - a model for Joubert syndrome. *J. Pathol.* **248**, 396–408 (2019).
43. Alby, C. *et al.* Mutations in KIAA0586 Cause Lethal Ciliopathies Ranging from a Hydrolethalus Phenotype to Short-Rib Polydactyly Syndrome. *Am. J. Hum. Genet.* **97**, 311–318 (2015).
44. Davey, M. G. *et al.* The chicken talpid3 gene encodes a novel protein essential for Hedgehog signaling. *Genes Dev.* **20**, 1365–1377 (2006).
45. Davey, M. G., McTeir, L., Barrie, A. M., Freem, L. J. & Stephen, L. A. Loss of cilia causes embryonic lung hypoplasia, liver fibrosis, and cholestasis in the talpid3 ciliopathy mutant. *Organogenesis* **10**, 177–185 (2014).
46. Bangs, F. *et al.* Generation of mice with functional inactivation of talpid3, a gene first identified in chicken. *Dev. Camb. Engl.* **138**, 3261–3272 (2011).
47. Inskeep, K. A. *et al.* Genetic and phenotypic heterogeneity in KIAA0753-related ciliopathies. *Am. J. Med. Genet. A.* **188**, 104–115 (2022).
48. Liu, Y. C. *et al.* The PPFIA1-PP2A protein complex promotes trafficking of Kif7 to the ciliary tip and Hedgehog signaling. *Sci. Signal.* **7**, ra117 (2014).
49. Hsu, S.-H. C. *et al.* Kif7 promotes hedgehog signaling in growth plate chondrocytes by restricting the inhibitory function of Sufu. *Dev. Camb. Engl.* **138**, 3791–3801 (2011).
50. Endoh-Yamagami, S. *et al.* The mammalian Cos2 homolog Kif7 plays an essential role in modulating Hh signal transduction during development. *Curr. Biol. CB* **19**, 1320–1326 (2009).
51. Cheung, H. O.-L. *et al.* The kinesin protein Kif7 is a critical regulator of Gli transcription factors in mammalian hedgehog signaling. *Sci. Signal.* **2**, ra29 (2009).
52. Li, Z. J. *et al.* Kif7 regulates Gli2 through Sufu-dependent and -independent functions during skin development and tumorigenesis. *Dev. Camb. Engl.* **139**, 4152–4161 (2012).
53. Law, K. K. L. *et al.* Antagonistic and cooperative actions of Kif7 and Sufu define graded intracellular Gli activities in Hedgehog signaling. *PloS One* **7**, e50193 (2012).

54. Putoux, A. *et al.* Altered GLI3 and FGF8 signaling underlies acrocallosal syndrome phenotypes in Kif7 depleted mice. *Hum. Mol. Genet.* **28**, 877–887 (2019).
55. Zhulyn, O. & Hui, C.-C. Sufu and Kif7 in limb patterning and development. *Dev. Dyn. Off. Publ. Am. Assoc. Anat.* **244**, 468–478 (2015).
56. He, M. *et al.* The kinesin-4 protein Kif7 regulates mammalian Hedgehog signalling by organizing the cilium tip compartment. *Nat. Cell Biol.* **16**, 663–672 (2014).
57. Yue, Y., Engelke, M. F., Blasius, T. L. & Verhey, K. J. Hedgehog-induced ciliary trafficking of kinesin-4 motor KIF7 requires intraflagellar transport but not KIF7's microtubule binding. *Mol. Biol. Cell* **33**, br1 (2022).
58. Liem, K. F., He, M., Ocbina, P. J. R. & Anderson, K. V. Mouse Kif7/Costal2 is a cilia-associated protein that regulates Sonic hedgehog signaling. *Proc. Natl. Acad. Sci. U. S. A.* **106**, 13377–13382 (2009).
59. Putoux, A. *et al.* KIF7 mutations cause fetal hydrolethalus and acrocallosal syndromes. *Nat. Genet.* **43**, 601–606 (2011).
60. Terhune, E. A. *et al.* Mutations in KIF7 implicated in idiopathic scoliosis in humans and axial curvatures in zebrafish. *Hum. Mutat.* **42**, 392–407 (2021).
61. Tay, S. Y., Ingham, P. W. & Roy, S. A homologue of the Drosophila kinesin-like protein Costal2 regulates Hedgehog signal transduction in the vertebrate embryo. *Dev. Camb. Engl.* **132**, 625–634 (2005).
62. Cui, C. *et al.* Disruption of Mks1 localization to the mother centriole causes cilia defects and developmental malformations in Meckel-Gruber syndrome. *Dis. Model. Mech.* **4**, 43–56 (2011).
63. Weatherbee, S. D., Niswander, L. A. & Anderson, K. V. A mouse model for Meckel syndrome reveals Mks1 is required for ciliogenesis and Hedgehog signaling. *Hum. Mol. Genet.* **18**, 4565–4575 (2009).
64. Burnicka-Turek, O. *et al.* Cilia gene mutations cause atrioventricular septal defects by multiple mechanisms. *Hum. Mol. Genet.* **25**, 3011–3028 (2016).
65. D'Angelo, A. *et al.* Ofd1 controls dorso-ventral patterning and axoneme elongation during embryonic brain development. *PloS One* **7**, e52937 (2012).
66. Wang, L. *et al.* Ciliary gene RPGRIP1L is required for hypothalamic arcuate neuron development. *JCI Insight* **4**, 123337 (2019).
67. Vierkotten, J., Dildrop, R., Peters, T., Wang, B. & Rüther, U. Ftm is a novel basal body protein of cilia involved in Shh signalling. *Dev. Camb. Engl.* **134**, 2569–2577 (2007).
68. Chen, J. *et al.* The ciliopathy gene Rpgrip1l is essential for hair follicle development. *J. Invest. Dermatol.* **135**, 701–709 (2015).
69. Pal, K. *et al.* Smoothened determines β-arrestin–mediated removal of the G protein–coupled receptor Gpr161 from the primary cilium. *J. Cell Biol.* **212**, 861–875 (2016).
70. Chen, M.-H. *et al.* Cilium-independent regulation of Gli protein function by Sufu in Hedgehog signaling is evolutionarily conserved. *Genes Dev.* **23**, 1910–1928 (2009).
71. Yabut, O. R., Fernandez, G., Huynh, T., Yoon, K. & Pleasure, S. J. Suppressor of Fused Is Critical for Maintenance of Neuronal Progenitor Identity during Corticogenesis. *Cell Rep.* **12**, 2021–2034 (2015).

72. Lin, C. *et al.* Differential regulation of Gli proteins by Sufu in the lung affects PDGF signaling and myofibroblast development. *Dev. Biol.* **392**, 324–333 (2014).
73. Hoelzl, M. A. *et al.* Differential requirement of SUFU in tissue development discovered in a hypomorphic mouse model. *Dev. Biol.* **429**, 132–146 (2017).
74. Yin, W.-C. *et al.* Dual Regulatory Functions of SUFU and Targetome of GLI2 in SHH Subgroup Medulloblastoma. *Dev. Cell* **48**, 167-183.e5 (2019).
75. Li, J. *et al.* Suppressor of Fused Is Required for Determining Digit Number and Identity via Gli3/Fgfs/Gremlin. *PloS One* **10**, e0128006 (2015).
76. Makino, S. *et al.* T396I mutation of mouse Sufu reduces the stability and activity of Gli3 repressor. *PloS One* **10**, e0119455 (2015).
77. Svärd, J. *et al.* Genetic elimination of Suppressor of fused reveals an essential repressor function in the mammalian Hedgehog signaling pathway. *Dev. Cell* **10**, 187–197 (2006).
78. Noguchi, H., Castillo, J. G., Nakashima, K. & Pleasure, S. J. Suppressor of fused controls perinatal expansion and quiescence of future dentate adult neural stem cells. *eLife* **8**, e42918 (2019).
79. Hoelzl, M. A. *et al.* Suppressor of Fused Plays an Important Role in Regulating Mesodermal Differentiation of Murine Embryonic Stem Cells In Vivo. *Stem Cells Dev.* **24**, 2547–2560 (2015).
80. Schröder, S. *et al.* Heterozygous truncating variants in SUFU cause congenital ocular motor apraxia. *Genet. Med. Off. J. Am. Coll. Med. Genet.* **23**, 341–351 (2021).
81. Kim, J. J. *et al.* Suppressor of fused controls mid-hindbrain patterning and cerebellar morphogenesis via GLI3 repressor. *J. Neurosci. Off. J. Soc. Neurosci.* **31**, 1825–1836 (2011).
82. De Mori, R. *et al.* Hypomorphic Recessive Variants in SUFU Impair the Sonic Hedgehog Pathway and Cause Joubert Syndrome with Cranio-facial and Skeletal Defects. *Am. J. Hum. Genet.* **101**, 552–563 (2017).
83. Svärd, J., Rozell, B., Toftgård, R. & Teglund, S. Tumor suppressor gene co-operativity in compound Patched1 and suppressor of fused heterozygous mutant mice. *Mol. Carcinog.* **48**, 408–419 (2009).
84. Weng, R. R. *et al.* Super-Resolution Imaging Reveals TCTN2 Depletion-Induced IFT88 Lumen Leakage and Ciliary Weakening. *Biophys. J.* **115**, 263–275 (2018).
85. Sang, L. *et al.* Mapping the NPHP-JBTS-MKS protein network reveals ciliopathy disease genes and pathways. *Cell* **145**, 513–528 (2011).
86. Shaheen, R. *et al.* A TCTN2 mutation defines a novel Meckel Gruber syndrome locus. *Hum. Mutat.* **32**, 573–578 (2011).
87. Wang, C., Li, J., Meng, Q. & Wang, B. Three Tctn proteins are functionally conserved in the regulation of neural tube patterning and Gli3 processing but not ciliogenesis and Hedgehog signaling in the mouse. *Dev. Biol.* **430**, 156–165 (2017).
88. Thomas, S. *et al.* TCTN3 mutations cause Mohr-Majewski syndrome. *Am. J. Hum. Genet.* **91**, 372–378 (2012).
89. Abdelhamed, Z. A. *et al.* Variable expressivity of ciliopathy neurological phenotypes that encompass Meckel-Gruber syndrome and Joubert syndrome is caused by

complex de-regulated ciliogenesis, Shh and Wnt signalling defects. *Hum. Mol. Genet.* **22**, 1358–1372 (2013).
90. Shaheen, R. *et al.* Identification of a novel MKS locus defined by TMEM107 mutation. *Hum. Mol. Genet.* **24**, 5211–5218 (2015).
91. Christopher, K. J., Wang, B., Kong, Y. & Weatherbee, S. D. Forward genetics uncovers Transmembrane protein 107 as a novel factor required for ciliogenesis and Sonic hedgehog signaling. *Dev. Biol.* **368**, 382–392 (2012).
92. Valente, E. M. *et al.* Mutations in TMEM216 perturb ciliogenesis and cause Joubert, Meckel and related syndromes. *Nat. Genet.* **42**, 619–625 (2010).
93. Latour, B. L. *et al.* Dysfunction of the ciliary ARMC9/TOGARAM1 protein module causes Joubert syndrome. *J. Clin. Invest.* **130**, 4423–4439 (2020).
94. Lee, S.-H. *et al.* Functional validation of novel MKS3/TMEM67 mutations in COACH syndrome. *Sci. Rep.* **7**, 10222 (2017).